Published for SISSA by Springer

Received: *June 23, 2015*
Accepted: *July 15, 2015*
Published: *August 27, 2015*

Study of $(W/Z)H$ production and Higgs boson couplings using $H \to WW^*$ decays with the ATLAS detector

The ATLAS collaboration

E-mail: atlas.publications@cern.ch

Abstract: A search for Higgs boson production in association with a W or Z boson, in the $H \to WW^*$ decay channel, is performed with a data sample collected with the ATLAS detector at the LHC in proton-proton collisions at centre-of-mass energies $\sqrt{s} = 7\,\text{TeV}$ and 8 TeV, corresponding to integrated luminosities of $4.5\,\text{fb}^{-1}$ and $20.3\,\text{fb}^{-1}$, respectively. The WH production mode is studied in two-lepton and three-lepton final states, while two-lepton and four-lepton final states are used to search for the ZH production mode. The observed significance, for the combined WH and ZH production, is 2.5 standard deviations while a significance of 0.9 standard deviations is expected in the Standard Model Higgs boson hypothesis. The ratio of the combined WH and ZH signal yield to the Standard Model expectation, μ_{VH}, is found to be $\mu_{VH} = 3.0^{+1.3}_{-1.1}\,(\text{stat.})^{+1.0}_{-0.7}\,(\text{sys.})$ for the Higgs boson mass of 125.36 GeV. The WH and ZH production modes are also combined with the gluon fusion and vector boson fusion production modes studied in the $H \to WW^* \to \ell\nu\ell\nu$ decay channel, resulting in an overall observed significance of 6.5 standard deviations and $\mu_{\text{ggF+VBF+VH}} = 1.16^{+0.16}_{-0.15}(\text{stat.})^{+0.18}_{-0.15}(\text{sys.})$. The results are interpreted in terms of scaling factors of the Higgs boson couplings to vector bosons (κ_V) and fermions (κ_F); the combined results are: $|\kappa_V| = 1.06^{+0.10}_{-0.10}$, $|\kappa_F| = 0.85^{+0.26}_{-0.20}$.

Keywords: Hadron-Hadron Scattering, Higgs physics

ArXiv ePrint: 1506.06641

doi:10.1007/JHEP08(2015)137

JHEP08(2015)137

Contents

JHEP08(2015)137

1 Introduction

In the Standard Model (SM) of fundamental interactions, the Brout-Englert-Higgs [1–3] mechanism induces the electroweak symmetry breaking that provides mass to elementary particles. The mechanism postulates the existence of an elementary scalar particle, the Higgs boson. The ATLAS and CMS collaborations at the CERN Large Hadron Collider (LHC) have observed the Higgs boson with a mass (m_H) of about 125 GeV [4, 5]. The measurements of the Higgs boson couplings to SM particles, and its spin and CP quantum numbers, are essential tests of the SM [6–12]. Higgs boson production in association with a W or Z (weak) boson, which are respectively denoted by WH and ZH, and collectively referred to as VH associated production in the following, provides direct access to the Higgs boson couplings to weak bosons. In particular, in the WH mode with subsequent $H\to WW^*$ decay, the Higgs boson couples only to W bosons, at both the production and decay vertices.

Searches for VH production have been performed at both the Tevatron and LHC colliders, in events with leptons, b-jets and either missing transverse momentum or two central jets. Evidence for VH production has been recently reported in the Tevatron combination [13] while no VH production has been observed so far at the LHC [14–20].

In this paper, a search for Higgs boson production in association with a weak boson, followed by $H\to WW^*$ decay, is presented. The data were collected in 2011 and 2012 by the ATLAS experiment at centre-of-mass energies of $\sqrt{s} = 7$ TeV and 8 TeV, respectively. In the SM, for $m_H = 125$ GeV, the cross sections of the WH and ZH associated production modes, followed by the $H\to WW^*$ decay, are 0.12 pb and 0.07 pb at $\sqrt{s} = 7$ TeV and 0.15 pb and 0.09 pb at $\sqrt{s} = 8$ TeV [21], respectively. Four topologies are considered, with two, three or four charged leptons in the final state (only electrons or muons are considered). The analyses are optimised to search for both the WH and ZH production modes; a combined result for VH is also presented. The VH results are then further combined with the $H\to WW^*\to \ell\nu\ell\nu$ analysis of gluon fusion (ggF) and vector boson fusion (VBF) production, for which the ATLAS Collaboration has reported the observation of the Higgs boson in the $H\to WW^*$ decay channel with a significance of 6.1 standard deviations [22].

The combination of the ggF, VBF and VH analyses, presented in this paper, is used to determine the couplings of the Higgs boson to vector bosons and, indirectly, to fermions, providing further constraints on the Higgs boson couplings.

2 Analysis overview

Higgs boson production in association with a W or Z boson, followed by $H\to WW^*$ decay, is sought using events with two, three or four charged leptons in the final state. Leptonic decays of τ leptons from $H\to WW^*\to\tau\nu\tau\nu$ are considered as signal, while no specific selection is performed for events with hadronically decaying τ leptons in the final state. In the present analysis events from $VH(H\to\tau\tau)$ are considered as background. The analysis is designed to select events which are kinematically consistent with the $VH(H\to WW^*)$ process, in order to enhance the signal-to-background ratio. Figure 1 illustrates the relevant

JHEP08(2015)137

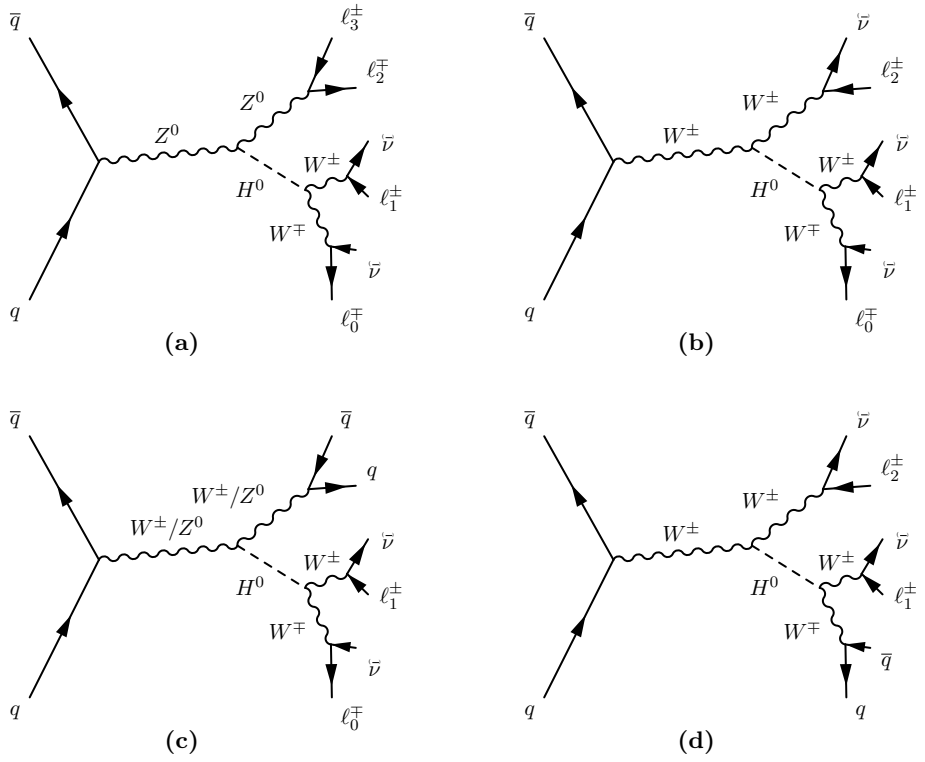

Figure 1. Tree-level Feynman diagrams of the $VH(H\to WW^*)$ topologies studied in this analysis: (a) 4ℓ channel (b) 3ℓ channel (c) opposite-sign 2ℓ channel and (d) same-sign 2ℓ channel. For charged lepton external lines, the directions of arrows refer to the superscripted sign. Relevant arrows are assigned to the associated neutrino external lines.

tree-level Feynman diagrams of the studied processes, in which a Higgs boson is produced in association with a weak boson.

Four channels are analysed, defined as follows:

(a) **4ℓ channel** (figure 1(a)): the leading contribution consists of a process in which a virtual Z boson radiates a Higgs boson, which in turn decays to a W boson pair. The decays of the weak bosons produce four charged leptons and two neutrinos in the final state. The lepton pair with an invariant mass closest to the Z boson mass is labelled as (ℓ_2, ℓ_3), while the remaining leptons are labelled as ℓ_0 and ℓ_1 and are assumed to originate in the $H\to WW^*$ decay. The main backgrounds to this channel are non-resonant ZZ^* and ZWW^* production.

(b) **3ℓ channel** (figure 1(b)): the leading contribution consists of a process in which a virtual W boson radiates a Higgs boson, and the Higgs boson decays to a W boson pair. All the weak bosons decay leptonically producing three charged leptons and three neutrinos in the final state. The lepton with unique charge is labelled as ℓ_0, the lepton closest to ℓ_0 in angle is labelled as ℓ_1, and the remaining lepton is labelled as ℓ_2. Leptons ℓ_0 and ℓ_1 are assumed to originate from the $H\to WW^*$ decay. The

JHEP08(2015)137

most prominent background to this channel is $WZ/W\gamma^*$ production; non-resonant WWW^* production is also a significant background having the same final state as the signal. Other important backgrounds are ZZ^*, $Z\gamma$, Z+jets, $t\bar{t}$ and Wt production, as they pass the signal selection if a lepton is undetected or because of a misidentified or non-prompt lepton from a jet.

(c) **Opposite-sign 2ℓ channel** (figure 1(c)): the leading contribution consists of a process in which the weak boson V, which radiates the Higgs boson, decays hadronically and produces two energetic jets, while W bosons from the $H\to WW^*$ decay produce two oppositely charged leptons, labelled as ℓ_0 and ℓ_1, and two neutrinos. The WH process is expected to account for 70% of the signal yield, while the ZH process accounts for the remaining 30%. After requiring two leptons of different flavour, the leading backgrounds for this channel are $t\bar{t}$ and Wt processes. Other major components are $Z\to\tau\tau$ and WW production with two associated jets. Final states including W+jets and multijets may produce misidentified leptons, contaminating the signal region. Other background sources include $WZ/W\gamma^*$ production and other Higgs boson production and decay modes, especially ggF production.

(d) **Same-sign 2ℓ channel** (figure 1(d)): the leading contribution consists of a process in which a W boson radiates the Higgs boson, and then decays leptonically. The radiated Higgs boson decays to two W bosons, one decaying hadronically and the other, with the same charge as the first lepton, decaying leptonically. The final state therefore contains two leptons with same charge, labelled as ℓ_1 and ℓ_2, two neutrinos and two energetic jets. Significant backgrounds in this channel are $WZ/W\gamma^*$, $W\gamma$ and W+jets production; WW, Z+jets and top-quark processes also contribute to this final state. Due to the overwhelming background from $t\bar{t}$ production, the selection is not optimised for events in which the lepton from the Higgs boson decay and the lepton from the associated W boson have opposite charges.

All the channels described above are mutually exclusive due to the respective number of leptons with transverse momentum, p_{T}, greater than 15 GeV. To maximise the analysis sensitivity to the $VH(H\to WW^*)$ process in each of these decay modes, the data samples for each topology, except for the opposite-sign 2ℓ channel, are further subdivided into several signal regions (SRs). Additional kinematic regions, with orthogonal selection criteria, designated as control regions (CRs), are used to normalise the major backgrounds in each SR by extracting normalisation factors.

The final results are extracted from a fit that simultaneously considers all SRs and CRs. The 4ℓ channel is split into two samples according to the number of same-flavour opposite-sign (SFOS) lepton pairs, namely 4ℓ-2SFOS and 4ℓ-1SFOS. The sample containing two SFOS pairs suffers from a higher background contamination than the sample with one SFOS pair. The 3ℓ analysis requires at least one opposite-charge lepton pair, therefore the 3ℓ system must have total charge of ±1. This analysis separates events with three same-flavour (SF) leptons, one SFOS lepton pair and zero SFOS lepton pairs, which have different signal-to-background ratios. For the 3ℓ-3SF and 3ℓ-1SFOS channels a multivariate analysis

JHEP08(2015)137

is performed. The same-sign 2ℓ sample is divided into two sub-channels with one or two selected jets in the final state, namely 2ℓ-SS1jet and 2ℓ-SS2jet. The channel with two leptons of different flavour and opposite sign is denoted by 2ℓ-DFOS in the following sections.

3 The ATLAS detector

ATLAS [23] is a multi-purpose particle physics detector with a forward-backward symmetric cylindrical geometry[1] and close to 4π coverage in solid angle. It consists of an inner tracking detector (ID) surrounded by a thin 2 T superconducting solenoid, electromagnetic and hadronic calorimeters, and a muon spectrometer (MS) incorporating three large superconducting toroid magnets, each with eight coils.

The ID covers the pseudorapidity range $|\eta| < 2.5$ and consists of multiple layers of silicon pixel and microstrip detectors, and a straw-tube transition radiation tracker. The calorimeter system covers the pseudorapidity range $|\eta| < 4.9$. Within the region $|\eta| < 3.2$, electromagnetic calorimetry is provided by barrel and endcap high-granularity lead/liquid-argon (LAr) calorimeters. An additional thin LAr presampler covering $|\eta| < 1.8$ is used to correct for energy loss in the material upstream of the calorimeters. Hadronic calorimetry is provided by a steel/scintillator-tile calorimeter, covering $|\eta| < 1.7$, and two copper/LAr hadronic endcap calorimeters. The solid angle coverage is completed with forward copper/LAr and tungsten/LAr calorimeter modules optimised for electromagnetic and hadronic measurements, respectively. The MS consists of separate trigger and high-precision tracking chambers that measure the deflection of muons in the magnetic field generated by superconducting air-core toroids. The precision chamber system covers the region $|\eta| < 2.7$ with three stations of monitored drift-tube layers, except for the forward region where the innermost station is equipped with cathode strip chambers. The muon trigger system covers the range $|\eta| < 2.4$ with resistive plate chambers in the barrel and thin gap chambers in the endcap regions. A three-level trigger system is used. The first-level trigger is hardware-based, using a subset of the detector information, and reduces the event rate to less than 75 kHz. This is followed by two software-based trigger levels, which together reduce the event rate to about 400 Hz.

4 Data samples

The data were recorded using inclusive single-lepton and dilepton triggers. Overall quality criteria were applied in order to suppress non-collision backgrounds such as cosmic-ray muons, beam-related backgrounds, or noise in the calorimeters. The datasets used in the 8 TeV and 7 TeV analyses correspond to an integrated luminosity of $20.3\,\text{fb}^{-1}$ and $4.5\,\text{fb}^{-1}$ respectively. The analysis of the 2ℓ-SS channel was performed only on the 8 TeV

[1] ATLAS uses a right-handed coordinate system with its origin at the nominal interaction point (IP) in the centre of the detector and the z-axis along the beam pipe. The x-axis points from the IP to the centre of the LHC ring, and the y axis points upward. Cylindrical coordinates (r, ϕ) are used in the transverse plane, ϕ being the azimuthal angle around the beam pipe. The pseudorapidity is defined in terms of the polar angle θ as $\eta = -\ln\tan(\theta/2)$.

JHEP08(2015)137

data sample, due to the low sensitivity of this channel. The 8 TeV data were taken at a higher instantaneous luminosity ($\mathcal{L} \simeq 7 \times 10^{33}$ cm^{-2}s^{-1}) than that for the 7 TeV data ($\mathcal{L} \simeq 3 \times 10^{33}$ cm^{-2}s^{-1}) and with a higher number ($\simeq 21$ versus $\simeq 9$) of overlapping proton-proton collisions, producing higher out-of-time and in-time pile-up [24]. The increased pile-up rate, rather than the increased centre-of-mass energy, is the main reason for the differences between 8 TeV and 7 TeV analysis selections.

Table 1 lists the Monte Carlo (MC) generators used to model the signal and background processes. For the Higgs production processes the production cross section multiplied by the branching fraction of the $H \to WW^*$ decay is shown, while for the background processes the production cross section, including effects of cuts applied at the event generation, is presented. The samples were simulated and normalised for a Higgs boson of mass $m_H = 125$ GeV. The VH samples were simulated with Pythia and normalised to the next-to-next-to-leading-order (NNLO) QCD calculations [21, 44–47] with additional next-to-leading-order (NLO) electroweak (EW) corrections computed with Hawk [48] and applied as a function of the transverse momentum of the associated vector boson. The $gg \to ZH$ samples were simulated with Powheg-Box1.0 interfaced with pythia8 and normalised to the NNLO QCD calculations [45]. Associated Higgs boson production with a $t\bar{t}$ pair ($t\bar{t}H$) is simulated with Pythia8 and normalised to the NLO QCD estimation [21, 44, 45].

The matrix-element-level calculations are interfaced to generators that model the parton shower, the hadronisation and the underlying event, using either Pythia6, Pythia8, Herwig with the underlying event modelled by Jimmy [49], or Sherpa. The CT10 parton distribution function (PDF) set [50] is used for the Powheg-Box and Sherpa samples while the CTEQ6L1 PDF set [51] is used for Alpgen and AcerMC samples. The Z/γ^* sample is reweighted to the MRSTMCal [52] PDF set. The simulated samples are described in detail in ref. [22] with a few exceptions that are reported in the following.

The Z/γ^* processes associated with light- and heavy-flavour (HF) jets are modelled by Alpgen+Herwig with merged leading-order (LO) calculations. The simulation includes processes with up to five additional partons in the matrix element, or three additional partons in processes with b- or c-quarks. An overlap-removal procedure is applied to avoid double counting of HF in the light-jet samples. The sum of the two samples is normalised to the NNLO calculation of Dynnlo [53, 54]. The $t\bar{t}W/Z$ and tZ backgrounds are simulated using Madgraph at LO interfaced with Pythia6. The production of four leptons from a pair of virtual Z or γ bosons, indicated by ZZ^* in the following, contributes to the background in the 3ℓ channel when one low-p_{T} lepton is not detected. Since this background is more prominent when one lepton pair has a very low mass, a dedicated sample which requires at least one SFOS pair with $m_{\ell\ell} < 4$ GeV, generated with Sherpa and normalised to the NLO QCD cross section from the parton-level MC program MCFM [55], is included. Production of triboson processes is a major source of background, in particular WWW^* in the 3ℓ channel and ZWW^* in the 4ℓ channel. They are modelled by Madgraph interfaced with Pythia6 and normalised to the NLO cross section from ref. [56]. All samples are processed using the full ATLAS detector simulation [57] based on Geant4 [58], except for WH, $WZ/W\gamma^*$ with $m_{\ell\ell} > 7$ GeV, $q\bar{q}/qg \to WW$, $WW\gamma^*$, $t\bar{t}$ and single top, which are instead simulated with Atlfast-II [59], a parameterisation of the response

JHEP08(2015)137

Process	Generator	$\sigma(\times\text{Br})$ [pb]	Cross-section normalisation
Higgs boson			
VH ($H\to WW^*$)	Pythia [25, 26] v8.165, v6.428	0.24, 0.20	NNLO QCD + NLO EW
VH ($H\to\tau\tau$)	Pythia v8.165, v6.428	0.07, 0.06	NNLO QCD + NLO EW
$gg\to H$ ($H\to WW^*$)	Powheg-Box [27–30] v1.0 (r1655)+ Pythia v8.165, v6.428	4.1, 3.3	NNLO+NNLL QCD + NLO EW
VBF ($H\to WW^*$)	Powheg-Box [31] v1.0 (r1655)+ Pythia v8.165, v6.428	0.34, 0.26	NNLO QCD + NLO EW
$t\bar{t}$H ($H\to WW^*$)	Pythia v8.165	0.028, 0.019	NLO
Single boson			
$Z/\gamma^*(\to\ell\ell)$+jets ($m_{\ell\ell}>10$ GeV)	Alpgen [32] v2.14 + Herwig [33] v6.52	16540, 12930	NNLO
HF $Z/\gamma^*(\to\ell\ell)$+jets ($m_{\ell\ell}>30$ GeV)	Alpgen v2.14 + Herwig v6.52	126, 57	NNLO
VBF $Z/\gamma^*(\to\ell\ell)$ ($m_{\ell\ell}>7$ GeV)	Sherpa [34] v1.4.1	5.3, 2.8	LO
Top-quark			
$t\bar{t}$	Powheg-Box [35] v1.0 (r2129)+Pythia v6.428 MC@NLO [36] v4.03	250, 180	NNLO+NNLL
$t\bar{t}W/Z$	MadGraph [37] v5.1.5.2, v5.1.3.28 +Pythia v6.428	0.35, 0.25	LO
tqb	AcerMC [38] v3.8 +Pythia v6.428	88, 65	NNLL
tb, tW	Powheg-Box [39, 40] v1.0 (r2092)+ Pythia v6.428	28, 20	NNLL
tZ	MadGraph v5.1.5.2, v5.1.5.11 +Pythia v6.428	0.035, 0.025	LO
Dibosons			
$WZ/W\gamma^*(\to\ell\ell\ell\nu)(m_{\ell\ell}>7$ GeV)	Powheg-Box [41] v1.0 (r1508)+Pythia v8.165, v6.428	12.7, 10.7	NLO
$WZ/W\gamma^*(\to\ell\ell\ell\nu)$(min. $m_{\ell\ell}<7$ GeV)	Sherpa v1.4.1	12.2, 10.5	NLO
other WZ	Powheg-Box [41] v1.0 (r1508) + Pythia v8.165	21.2, 17.2	NLO
$q\bar{q}/qg\to Z^{(*)}Z^{(*)}(\to\ell\ell\ell\ell,\ell\ell\nu\nu)$ ($m_{\ell\ell}>4$ GeV)	Powheg-Box [41] v1.0 (r1556) +Pythia v8.165, v6.428	1.24, 0.79	NLO
$q\bar{q}/qg\to Z^{(*)}Z^{(*)}(\to\ell\ell\ell\ell,\ell\ell\nu\nu)$ (min. $m_{\ell\ell}<4$ GeV)	Sherpa v1.4.1	7.3, 5.9	NLO
other $q\bar{q}/qg\to ZZ$	Powheg-Box [41] v1.0 (r1556) + Pythia v8.165	6.9, 5.7	NLO
$gg\to Z^{(*)}Z^{(*)}$	gg2ZZ [42] v3.1.2 + Herwig v6.52 (8 TeV only)	0.59	LO
$q\bar{q}/qg\to WW$	Powheg-Box [41] v1.0 (r1556) + Pythia v6.428	54, 45	NLO
	Sherpa v1.4.1 (for 2ℓ-DFOS 8 TeV only)	54	NLO
$gg\to WW$	gg2WW [43] v3.1.2 + Herwig v6.52	1.9, 1.1	LO
VBS WZ, $ZZ(\to\ell\ell\ell\ell,\ell\ell\nu\nu)$ ($m_{\ell\ell}>7$ GeV), WW	Sherpa v1.4.1	1.2, 0.88	LO
$W\gamma$ ($p_{\mathrm{T}}^{\gamma}>8$ GeV)	Alpgen v2.14 +Herwig v6.52	1140, 970	NLO
$Z\gamma$ ($p_{\mathrm{T}}^{\gamma}>8$ GeV)	Sherpa v1.4.3	960, 810	NLO
Tribosons			
$WWW^*, ZWW^*, ZZZ^*, WW\gamma^*$	MadGraph v5.1.3.33, v5.1.5.10 + Pythia v6.428	0.44, 0.18	NLO

Table 1. MC generators used to model the signal and background processes. The Higgs boson samples are normalised using the production cross section and the decay branching fraction computed for $m_H = 125$ GeV. The values reported for the VH ($H\to WW^*$) process include the NNLO contribution from the $gg\to ZH$ ($H\to WW^*$) process. For generators and cross sections, wherever two comma-separated values are given, the first value refers to $\sqrt{s}=8$ TeV and the second to $\sqrt{s}=7$ TeV. When a single value is given, it refers to $\sqrt{s}=8$ TeV. The corresponding cross section times branching fraction of the $H\to WW^*$ decay, $\sigma\times$ Br, are shown for the Higgs production processes, while for background processes the production cross section, including the effect of the leptonic branching fraction, and the $m_{\ell\ell}$ and p_T^{γ} cuts, as specified in the "Process" column, is presented. 'HF' refers to heavy-flavour jet production, and 'VBS' refers to vector boson scattering. When a lower cut on $m_{\ell\ell}$ is specified, it is applied to all SFOS lepton pairs, while when an upper cut is indicated it is applied to the SFOS pair of lowest mass in the event. For the Sherpa1.1 $Z^{(*)}Z^{(*)}$ sample a lower cut of 4 GeV is applied, in addition, to the SFOS lepton pair of higher mass. Cross sections are computed to different levels of accuracy (LO, NLO, NNLO or next-to-next-to-leading-logarithm, NNLL), as specified by the last column.

of the electromagnetic and hadronic calorimeters, and with GEANT4 for other detector components. The events are reweighted to ensure that the distribution of pile-up observed in the data is correctly reproduced.

5 Event reconstruction and selection

5.1 Event reconstruction

The primary vertex of each event is selected as the vertex with the largest value of $\sum(p_{\mathrm{T}})^2$, where the sum is over all the tracks associated with that particular vertex. Furthermore, it is required to have at least three tracks with $p_{\mathrm{T}} > 400\,\mathrm{MeV}$.

Muons are reconstructed in the region $|\eta| < 2.5$ by combining tracks reconstructed in the MS and ID [60]. This analysis uses muon candidates referred to as "Chain 1, CB muons" in ref. [60]. Electrons are identified within the region $|\eta| < 2.47$, except in the transition region between barrel and endcap calorimeters ($1.37 < |\eta| < 1.52$), through the association of an ID track to a calorimeter cluster whose shower profile is consistent with an electromagnetic shower [61]. Electron identification uses information from both the calorimetric and tracking system. In the 7 TeV analysis a cut-based approach is adopted while in the 8 TeV analysis a likelihood-based selection is also exploited as described in [62]. Following that reference, in the 4ℓ and 3ℓ channels, electrons with $p_{\mathrm{T}} < 20$ GeV are required to satisfy the "very tight" likelihood requirement, while electrons with $p_{\mathrm{T}} > 20$ GeV are required to satisfy the "loose" likelihood requirement. In the 2ℓ channels, electrons with $p_{\mathrm{T}} < 25$ GeV are required to satisfy the "very tight" likelihood requirement, while electrons with $p_{\mathrm{T}} > 25$ GeV are required to satisfy the "medium" likelihood requirement.

Both a track-based and a calorimeter-based isolation selection are applied to leptons. The isolation criteria are chosen to maximise the sensitivity to the $VH(H\to WW^*)$ process at $m_H = 125$ GeV. The track-based isolation is built on the computation of the scalar sum of the p_{T} of tracks associated with the primary vertex and inside a cone, constructed around the candidate lepton, of size $\Delta R = 0.2$[2] and excluding the track of the candidate lepton. The calorimeter-based isolation uses the scalar sum of the transverse energies measured within a cone of $\Delta R = 0.2$, excluding the energy of the calorimeter cluster associated with the lepton itself. For the 8 TeV data the electron calorimeter-based isolation algorithm uses topological clusters [62], while for the 7 TeV data it uses calorimeter cells. Cell-based isolation is used for muons in the calorimeter in both the 8 TeV and 7 TeV analyses. The calorimeter and track isolation criteria differ between the 8 TeV and 7 TeV data samples and are not the same for all the channels. The upper bound of the calorimeter-based isolation energy varies from 7% to 30% of the lepton p_{T}, while the sum of the p_{T} of the tracks in the cone is required to be smaller than 4% to 12% of the lepton p_{T}, where tighter cuts are applied at low p_{T}. Less stringent isolation criteria on energy and p_{T} are required for the 7 TeV data sample, due to the lower level of pile-up compared to the 8 TeV data sample.

Jets are reconstructed from three-dimensional topological clusters [63] over the region $|\eta| < 4.5$ using the anti-k_t algorithm [64] with radius parameter $R = 0.4$. Jets are required

[2] $\Delta R = \sqrt{(\Delta\eta)^2 + (\Delta\phi)^2}$.

JHEP08(2015)137

to have p_{T} larger than 25 GeV except for the forward region, $|\eta| > 2.4$, in which the threshold is raised to 30 GeV. In order to suppress the contamination of jets from pile-up, the following selection is applied: the sum of the p_{T} of all tracks within $\Delta R = 0.4$ of the jet axis and that of the subset of these associated with the primary vertex is computed. The ratio of the latter to the former is required to be larger than 0.5 (0.75) for the 8 (7) TeV data samples, for all jets with $p_{\mathrm{T}} < 50$ GeV and $|\eta| < 2.4$.

The MV1 b-jet identification algorithm is used to tag jets containing a b-hadron [65]. For b-jets with $|\eta| < 2.5$ and $p_{\mathrm{T}} > 20$ (25) GeV in the 8 (7) TeV data analysis, the selection has an efficiency of 85%, estimated using simulated $t\bar{t}$ events. It corresponds to a rejection of a factor of 10 against jets originating from light quarks or gluons [66, 67].

When two leptons are reconstructed within a cone of $\Delta R = 0.1$, or a lepton and a jet are reconstructed within $\Delta R = 0.3$, they are considered to be the same physical object and one of the two is removed. In the rare occurrence of an overlap between two leptons of the same flavour, the higher-p_{T} lepton is kept while the lower-p_{T} lepton is discarded. The muon is retained in the presence of an overlap with an electron, the electron is retained in the presence of an overlap with a jet, and the jet is retained in the presence of an overlap with a muon.

Two variables describing the missing transverse momentum are employed in this study: one is calorimeter-based and the other is track-based. The former, which benefits from the large rapidity coverage of the calorimeter and its sensitivity to neutral particles, is referenced as $\mathbf{E}_{\mathrm{T}}^{\mathrm{miss}}$ [68]. The $\mathbf{E}_{\mathrm{T}}^{\mathrm{miss}}$ magnitude, $E_{\mathrm{T}}^{\mathrm{miss}}$, is used in the analysis selection. The quantity $\mathbf{E}_{\mathrm{T}}^{\mathrm{miss}}$ is calculated as the negative vector sum of the momenta of muons, electrons, τ leptons, photons, jets and clusters of calorimeter cells that are not associated with these objects (the "soft term"). In the 8 TeV analysis, to suppress the pile-up effect, the ratio of the scalar p_{T} sum of all soft term tracks associated with the primary vertex to the scalar p_{T} sum of all soft term tracks from all vertices is employed. This ratio is used to scale all soft-event contributions to $E_{\mathrm{T}}^{\mathrm{miss}}$ [69]. The track-based missing transverse momentum measurement is used to reduce the effects of pile-up on the resolution of the calorimeter-based variant [70]. It is calculated as the vector sum of the transverse momenta of tracks with $p_{\mathrm{T}} > 500$ MeV that originate from the primary vertex. This quantity is called $\mathbf{p}_{\mathrm{T}}^{\mathrm{miss}}$, and the analysis selections are applied to its magnitude, $p_{\mathrm{T}}^{\mathrm{miss}}$. In order to include neutral components in the calculation of $p_{\mathrm{T}}^{\mathrm{miss}}$ in final states with jets, the sum of track momenta in jets is replaced by their energy measured in the calorimeter.

5.2 Event selection

Events are required to contain a primary vertex. The four channels are further split into eight signal regions, designed to optimise the sensitivity to the $VH(H \to WW^*)$ process, with a specific set of selections applied to define each signal region. The selection criteria rely on the number of leptons and their properties such as charge, flavour, p_{T}, and on the number of jets and b-tagged jets and on the magnitude of the missing transverse momentum. Leptons with $p_{\mathrm{T}} > 15$ GeV are selected and their number is used to divide the analysis in the various channels. Similarly the analysis channels are subdivided in categories according the number of selected jets. Of particular importance are the invariant masses and opening angles among the selected objects, most notably those of opposite-sign lepton

JHEP08(2015)137

pairs. The spin-0 property of the Higgs boson, in conjunction with the V-A structure of the weak interaction, results in a preference for a small opening angle of lepton pairs from the $H \to WW^* \to \ell\nu\ell\nu$ decays. On the other hand, as described in section 2, major backgrounds often contain Z boson production or $t\bar{t}$ production which give rise to opposite-sign lepton pairs with a large opening angle. In the 2ℓ-SS channel, the lepton originating from the Higgs boson decay is selected by minimising the invariant mass of the lepton and jet(s); cuts are then applied to the opening angle between this lepton and the closest jet in the transverse plane. The definitions of the signal regions used for each channel are summarised in table 2 and further detailed in sections 5.2.1–5.2.4.

In all the 4ℓ and 3ℓ signal regions, events are recorded using inclusive single-lepton triggers, which are fully efficient for high lepton multiplicity signatures. For the 2ℓ channels in 8 TeV data taking, dilepton triggers are also used. In all channels at least one lepton must match a candidate reconstructed at trigger level. This requires the leading lepton in an event to have p_{T} greater than 24 GeV in the 8 TeV data sample, and greater than 18 GeV and 20 GeV for muons and electrons respectively in the 7 TeV data sample. Single lepton trigger efficiencies are measured with respect to offline reconstructed leptons using leptonic Z decays. The measured values are approximately 95% for electrons, 90% for muons in the endcap and 70% for muons in the barrel.

5.2.1 Four-lepton channel

Events in the 4ℓ channel are required to have exactly four leptons. The p_{T} of leading and sub-leading leptons must be above 25 GeV and 20 GeV, respectively, and the p_{T} of each of the remaining two leptons must exceed 15 GeV. The total charge of the four leptons is required to be zero. Only events with at least one SFOS lepton pair are accepted, and events are assigned to the 4ℓ-2SFOS and 4ℓ-1SFOS SRs according to the number of such pairs.

In order to select final states with neutrinos, $E_{\mathrm{T}}^{\mathrm{miss}}$ and $p_{\mathrm{T}}^{\mathrm{miss}}$ are required to be above 20 GeV and above 15 GeV, respectively. In order to reduce the $t\bar{t}Z$ background, events are vetoed if they contain more than one jet. Top-quark production is further suppressed by vetoing events with any b-tagged jet with p_{T} above 20 GeV. The invariant mass of ℓ_2 and ℓ_3, $m_{\ell_2\ell_3}$, is required to satisfy $|m_{\ell_2\ell_3} - m_Z| < 10$ GeV (where m_Z is the mass of the Z boson), and the invariant mass of ℓ_0 and ℓ_1, $m_{\ell_0\ell_1}$, is required to be between 10 GeV and 65 GeV. This requirement on $m_{\ell_0\ell_1}$ greatly reduces the contamination from $ZZ^{(*)}$ production in events with two pairs of SFOS leptons.

The sensitivity is improved by exploiting two additional variables. The variable $\Delta\phi_{\ell_0\ell_1}^{\mathrm{boost}}$ denotes the difference in azimuthal angle between the two leptons from the Higgs boson candidate in the frame where the Higgs boson's p_{T} is zero. The Higgs boson transverse momentum is approximated with $\mathbf{p}_{\mathrm{T}}^{H} \sim -\mathbf{p}_{\mathrm{T}}^{Z} - \mathbf{p}_{\mathrm{T}}^{\mathrm{jet}}$, or with $\mathbf{p}_{\mathrm{T}}^{H} \sim -\mathbf{p}_{\mathrm{T}}^{Z}$ if no jet is present. The angular separation $\Delta\phi_{\ell_0\ell_1}^{\mathrm{boost}}$ is required to be below 2.5 rad. The magnitude of the vector sum of the lepton transverse momenta, $p_{\mathrm{T}4\ell}$, can discriminate against the main background, $ZZ^{(*)}$, which has no neutrinos. A cut requiring $p_{\mathrm{T}4\ell} > 30$ GeV is introduced for the 4ℓ-2SFOS SR. In this signal region the invariant mass of the four leptons is required to be above 140 GeV to remove events from the $H \to ZZ^* \to 4\ell$ decay, which are the target of another analysis [17]. In the signal extraction through the fit explained in section 8.4, the 4ℓ-2SFOS and 4ℓ-1SFOS SRs enter as two separate signal regions.

JHEP08(2015)137

Channel	4ℓ		3ℓ			2ℓ		
Category	2SFOS	1SFOS	3SF	1SFOS	0SFOS	DFOS	SS2jet	SS1jet
Trigger	single-lepton triggers		single-lepton triggers			single-lepton & dilepton triggers		
Num. of leptons	4	4	3	3	3	2	2	2
$p_{\mathrm{T,leptons}}$ [GeV]	$> 25, 20, 15$	$> 25, 20, 15$	> 15	> 15	> 15	$> 22, 15$	$> 22, 15$	$> 22, 15$
Total lepton charge	0	0	± 1	± 1	± 1	0	± 2	± 2
Num. of SFOS pairs	2	1	2	1	0	0	0	0
Num. of jets	≤ 1	≤ 1	≤ 1	≤ 1	≤ 1	≥ 2	2	1
$p_{\mathrm{T,jets}}$ [GeV]	> 25 (30)	> 25 (30)	> 25 (30)	> 25 (30)	> 25 (30)	> 25 (30)	> 25 (30)	> 25 (30)
Num. of b-tagged jets	0	0	0	0	0	0	0	0
$E_{\mathrm{T}}^{\mathrm{miss}}$ [GeV]	> 20	> 20	> 30	> 30	—	> 20	> 50	> 45
$p_{\mathrm{T}}^{\mathrm{miss}}$ [GeV]	> 15	> 15	> 20	> 20	—	—	—	—
$\lvert m_{\ell\ell} - m_Z \rvert$ [GeV]	< 10 ($m_{\ell_2\ell_3}$)	< 10 ($m_{\ell_2\ell_3}$)	> 25	> 25	—	—	> 15	> 15
Min. $m_{\ell\ell}$ [GeV]	> 10 ($m_{\ell_0\ell_1}$)	> 10 ($m_{\ell_0\ell_1}$)	> 12	> 12	> 6	> 10	> 12 ($ee, \mu\mu$) > 10 ($e\mu$)	> 12 ($ee, \mu\mu$) > 10 ($e\mu$)
Max. $m_{\ell\ell}$ [GeV]	< 65 ($m_{\ell_0\ell_1}$)	< 65 ($m_{\ell_0\ell_1}$)	< 200	< 200	< 200	< 50	—	—
$m_{4\ell}$ [GeV]	> 140	—	—	—	—	—	—	—
$p_{\mathrm{T},4\ell}$ [GeV]	> 30	—	—	—	—	—	—	—
$m_{\tau\tau}$ [GeV]	—	—	—	—	—	$< (m_Z - 25)$	—	—
$\Delta R_{\ell_0\ell_1}$	—	—	< 2.0	< 2.0	—	—	—	—
$\Delta\phi_{\ell_0\ell_1}$ [rad]	< 2.5 ($\Delta\phi_{\ell_0\ell_1}^{\mathrm{boost}}$)	< 2.5 ($\Delta\phi_{\ell_0\ell_1}^{\mathrm{boost}}$)	—	—	—	< 1.8	—	—
m_{T} [GeV]	—	—	—	—	—	< 125	—	> 105 ($m_{\mathrm{T}}^{\mathrm{lead}}$)
Min. $m_{\ell ij(j)}$ [GeV]	—	—	—	—	—	—	< 115	< 70
Min. $\phi_{\ell_i j}$ [rad]	—	—	—	—	—	—	< 1.5	< 1.5
Δy_{jj}	—	—	—	—	—	< 1.2	—	—
$\lvert m_{jj} - 85 \rvert$ [GeV]	—	—	—	—	—	< 15	—	—

Table 2. Definition of each signal region in this analysis. $m_{\mathrm{T}}^{\mathrm{lead}}$ is the transverse mass of the leading lepton and the $\mathbf{E}_{\mathrm{T}}^{\mathrm{miss}}$ (see section 5.2.4 for the definition of $m_{\mathrm{T}}^{\mathrm{lead}}$). For $p_{\mathrm{T,leptons}}$ in the 4ℓ channel the three values listed above refer to the leading, sub-leading, and to the two remaining leptons, respectively. For $p_{\mathrm{T,leptons}}$ in the 2ℓ channel the two values listed above refer to the leading and sub-leading leptons, respectively. For $p_{\mathrm{T,jets}}$ the value in parentheses refers to forward jets ($|\eta| > 2.4$).

5.2.2 Three-lepton channel

For the 3ℓ channel, exactly three leptons with $p_{\mathrm{T}} > 15$ GeV are required with a total charge of ± 1. After this requirement, contributions from background processes that include more than one misidentified lepton, such as W+jet production and inclusive $b\bar{b}$ pair production, are negligible. Events are then separated into the 3ℓ-3SF, 3ℓ-1SFOS and 3ℓ-0SFOS SRs, requiring three SF leptons, one SFOS lepton pair and zero SFOS lepton pairs, respectively.

In order to reduce the background from $t\bar{t}$ production, events are vetoed if they contain more than one jet. The background from top-quark production is further suppressed by vetoing events if they contain any b-tagged jet with $p_{\mathrm{T}} > 20$ GeV. In order to select final states with neutrinos, $E_{\mathrm{T}}^{\mathrm{miss}}$ is required to be above 30 GeV and $p_{\mathrm{T}}^{\mathrm{miss}}$ above 20 GeV in the 3ℓ-3SF and 3ℓ-1SFOS SRs. In the 3ℓ-0SFOS SR, $E_{\mathrm{T}}^{\mathrm{miss}}$ or $p_{\mathrm{T}}^{\mathrm{miss}}$ selections are not imposed because the main backgrounds also contain neutrinos. The invariant mass of all SFOS pairs in the 3ℓ-3SF and 3ℓ-1SFOS SRs is required to satisfy $|m_{\ell\ell} - m_Z| > 25$ GeV. This requirement suppresses WZ and ZZ^* events, and increases the Z+jets rejection.

A lower bound is set on the smallest invariant mass of pairs of oppositely charged leptons at 12 GeV in the 3ℓ-3SF and 3ℓ-1SFOS SRs, and at 6 GeV in the 3ℓ-0SFOS SR. In addition, an upper bound on the invariant mass of oppositely charged leptons is set at 200 GeV in the three signal regions. These selections reject backgrounds from HF and reduce the number of combinatorial lepton pairs from the $WZ/W\gamma^*$ process. The latter could indeed give larger mass values with respect to the WH process since it can proceed through the t- and u-channels, in addition to the s-channel, which is also present in WH production.

The angular separation $\Delta R_{\ell_0\ell_1}$ is required to be smaller than 2 in the 3ℓ-3SF and 3ℓ-1SFOS SRs. This cut favours the Higgs boson decay topology relative to that of $WZ/W\gamma^*$ events.

In the 3ℓ-3SF and 3ℓ-1SFOS SRs, the shape of a multivariate discriminant based on a Boosted Decision Trees (BDT) [71], which produces a multivariate classifier ("BDT Score"), is used to achieve a further separation between signal and background. The main purpose of the multivariate classifier is to distinguish between the signal and the dominant $WZ/W\gamma^*$ and ZZ^* backgrounds, and the BDT is trained against these two background processes. The BDT parameters are chosen in order to ensure that there is no overtraining, i.e. that the BDT is robust against statistical fluctuations in the training samples. The BDT input discriminating variables which provide the best separation between signal and background are the p_{T} of each lepton, the magnitude of their vector sum, the invariant masses of the two opposite-sign lepton pairs ($m_{\ell_0\ell_1}$, $m_{\ell_0\ell_2}$), $\Delta R_{\ell_0\ell_1}$, $E_{\mathrm{T}}^{\mathrm{miss}}$, and $p_{\mathrm{T}}^{\mathrm{miss}}$. In the fit, the shape of the distribution of the "BDT Score", divided into six bins, is used to extract the number of observed events in the 3ℓ-3SF and 3ℓ-1SFOS SRs, while the shape of the distribution of $\Delta R_{\ell_0\ell_1}$, divided into four bins, is used to extract the number of observed events in the 3ℓ-0SFOS SR. In the other channels only the event yield in each signal and control region is used without shape information.

JHEP08(2015)137

5.2.3 Opposite-sign two-lepton channel

In the 2ℓ-DFOS channel, exactly two leptons with p_{T} larger than 22 GeV and 15 GeV are required. Only opposite-sign $e\mu$ final states are considered in order to reduce the background from Z+jets, WZ and ZZ events. A cut on the invariant mass of the lepton pair, $m_{\ell_0\ell_1} > 10$ GeV, is applied to reject combinatorial dilepton backgrounds. In order to select final states with neutrinos, $E_{\mathrm{T}}^{\mathrm{miss}}$ is required to be above 20 GeV. These selections reduce the background processes that contain jets faking leptons. The presence of at least two jets with $p_{\mathrm{T}} > 25$ GeV is required. The background from top-quark production is reduced by vetoing events if they contain any b-tagged jets with $p_{\mathrm{T}} > 20$ GeV. To reject the Z+jets production that leads to $e\mu$ final states through $Z \to \tau\tau$ decay, a requirement of $m_{\tau\tau} < (m_Z - 25$ GeV) is applied, where $m_{\tau\tau}$ is the dilepton invariant mass reconstructed using the collinear approximation [22], namely under the assumptions that the lepton pair originates from τ lepton decays, the neutrinos are the only source of $E_{\mathrm{T}}^{\mathrm{miss}}$ and they are collinear with the charged leptons.

Upper bounds on the invariant mass of the lepton pair, $m_{\ell_0\ell_1} < 50$ GeV, and the azimuthal angular separation of the lepton pair, $\Delta\phi_{\ell_0\ell_1} < 1.8$ rad, are applied to enhance the Higgs boson signal relative to the WW, $t\bar{t}$ and W+jets backgrounds. Requirements on the rapidity separation between the two leading jets, $\Delta y_{jj} < 1.2$, and the invariant mass of the two leading jets, $|m_{jj} - 85\ \mathrm{GeV}| < 15$ GeV, are introduced to select jets from the associated W/Z bosons. The central value of the m_{jj} selection interval is larger than the W boson mass in order to retain the acceptance for ZH production with $Z \to q\bar{q}$ decay.

The selection $m_{\mathrm{T}} < 125$ GeV is applied, where m_{T} is the transverse mass of the dilepton system and $E_{\mathrm{T}}^{\mathrm{miss}}$, defined as $m_{\mathrm{T}} = \sqrt{(E_{\mathrm{T}}^{\ell\ell} + E_{\mathrm{T}}^{\mathrm{miss}})^2 - |\mathbf{p}_{\mathrm{T}}^{\ell\ell} + \mathbf{E}_{\mathrm{T}}^{\mathrm{miss}}|^2}$, where $E_{\mathrm{T}}^{\ell\ell} = \sqrt{|\mathbf{p}_{\mathrm{T}}^{\ell\ell}|^2 + m_{\ell\ell}^2}$. The selections on Δy_{jj} and m_{jj} make this channel orthogonal to the ggF-enriched $n_j \geq 2$ category in ref. [22], while orthogonality with respect to the VBF category is ensured by explicitly vetoing the BDT signal region of the VBF analysis [22]. In the fit the 2ℓ-DFOS channel enters as a single signal region.

5.2.4 Same-sign two-lepton channel

In the 2ℓ-SS channel, exactly two leptons with the same charge are required. Lower bounds on lepton p_{T} are set to 22 GeV and 15 GeV and both the same-flavour and different-flavour combinations are considered. A lower bound on $m_{\ell_1\ell_2}$ is applied at 12 GeV for same-flavour lepton pairs and at 10 GeV for different-flavour lepton pairs. Despite the same-charge requirement, a wrong-charge assignment may allow background contributions from Z boson decays. Therefore a veto on same-flavour lepton pairs with $|m_{\ell_1\ell_2} - m_Z| < 15$ GeV is introduced.

The 2ℓ-SS2jet and 2ℓ-SS1jet SRs require the number of jets to be exactly two or exactly one, respectively. Events with b-tagged jets having $p_{\mathrm{T}} > 20$ GeV are discarded. The $E_{\mathrm{T}}^{\mathrm{miss}}$ is required to be larger than 50 GeV in the 2ℓ-SS2jet SR and larger than 45 GeV in the 2ℓ-SS1jet SR. Additional cuts are applied to events in the 2ℓ-SS2jet and 2ℓ-SS1jet SRs, on the following variables (see table 2 for details): the minimum invariant mass of a lepton and the jet(s) in the event, $m_{\ell_i\mathrm{j}}^{\mathrm{min}}$ ($m_{\ell_i\mathrm{jj}}^{\mathrm{min}}$); the smallest opening angle between the lepton which

JHEP08(2015)137

minimises the above variable and a jet, $\Delta\phi^{\min}_{\ell_i \mathrm{j}}$; the transverse mass of the leading lepton and the $\mathbf{E}_{\mathrm{T}}^{\mathrm{miss}}$, $m_{\mathrm{T}}^{\mathrm{lead}} = \sqrt{2 \times p_{\mathrm{T,lead}} \times E_{\mathrm{T}}^{\mathrm{miss}} \times (1 - \cos(\phi_{\mathrm{lead}} - \phi_{E_{\mathrm{T}}^{\mathrm{miss}}}))}$, where $p_{\mathrm{T,lead}}$ and ϕ_{lead} are respectively the transverse momentum and ϕ angle of the leading lepton. Lower values of $m^{\min}_{\ell_i \mathrm{j}}$ ($m^{\min}_{\ell_i \mathrm{jj}}$) and of $\Delta\phi^{\min}_{\ell_i \mathrm{j}}$ favour Higgs boson decays relative to the major backgrounds. High values of $m_{\mathrm{T}}^{\mathrm{lead}}$ help in reducing W+jets background. The p_{T} threshold for the sub-leading muon in the $\mu\mu$ channel is increased to 20 GeV in both the SRs to suppress misidentified muons from W+jets and multijet production.

In the fit, the 2ℓ-SS2jet and 2ℓ-SS1jet SRs are further split into four signal regions according to the combination of lepton flavours in each event: ee, $e\mu$, μe and $\mu\mu$, where $e\mu$ refers to the case in which the electron has leading p_{T} while μe refers to the case in which the muon has leading p_{T}. This splitting is motivated by the expected differences in the background contributions, for example $W\gamma$, which is expected to be zero in the $\mu\mu$ channel but not in the other channels.

5.2.5 Signal acceptance

The number of expected $VH(H \to WW^*)$ events surviving the event selections is presented for each channel in table 3. The total acceptance for $WH(H \to WW^* \to \ell\nu\ell\nu)$, $WH(H \to WW^* \to \ell\nu qq)$ and $ZH(H \to WW^* \to \ell\nu\ell\nu)$ is 3.7%, 0.3% and 1.9%, respectively. The analysis acceptance for the $ZH(H \to WW^* \to \ell\nu qq)$ process is negligible. The acceptance is defined as the ratio of the number of events in the SRs to the number of events expected according to the branching fractions for the various processes. Associated Higgs boson production followed by the decay $H \to \tau\tau$ cannot be completely isolated from the selected final states. Therefore the results presented in this paper, with the exception of section 8.5 for consistency of the analysed model, include this process as part of the background, with the production cross section (σ_{VH}) and $\mathrm{Br}(H \to \tau\tau)$ fixed to the SM value.

6 Background modelling

The background contamination in the signal regions results from various physics processes, each modelled by one of the following methods:

- Pure MC prediction: rates and differential distributions (shapes) are extracted from simulation and normalised to the cross sections in table 1;
- MC prediction normalised to data: rates are extracted from data in control regions but shapes are extracted from simulation;
- Pure data-driven prediction: rates and shapes are extracted from data.

Misidentified-lepton backgrounds (W+jets, multijets) in the 2ℓ channels are estimated by using a purely data-driven method, which utilises the rate at which a jet is misidentified as a lepton [22]. Table 4 summarises the method adopted for each process in each signal region. The labels "MC" and "Data" represent the pure MC prediction and the pure data-driven estimation. For backgrounds modelled by simulation with a normalisation factor

JHEP08(2015)137

(a) 8 TeV data sample

Channel	4ℓ		3ℓ			2ℓ		
Category	2SFOS	1SFOS	3SF	1SFOS	0SFOS	DFOS	SS2jet	SS1jet
WH ($H \to WW^*$)	—	—	0.56	1.4	1.3	1.5	1.0	1.8
ZH ($H \to WW^*$)	0.21	0.24	0.17	0.18	0.15	0.67	0.02	0.19
VH ($H \to WW^*$)	0.21	0.24	0.73	1.6	1.4	2.2	1.0	2.0
(all categories)	9.4							

(b) 7 TeV data sample

WH ($H \to WW^*$)	—	—	0.12	0.29	0.26	0.21
ZH ($H \to WW^*$)	0.023	0.021	0.013	0.033	0.028	0.075
VH ($H \to WW^*$)	0.023	0.021	0.13	0.32	0.29	0.29
(all categories)	1.1					

Table 3. Number of expected $VH(H \to WW^*)$ events in the signal regions, for $m_H = 125$ GeV, in the (a) 8 TeV and (b) 7 TeV data samples.

(NF) computed using data, the names of relevant control regions are shown as defined in tables 5 and 6. The ratio of $t\bar{t}$ yields to tW yields is found to be compatible between all the CRs and associated SRs, thus only one NF is computed per CR for the "Top" category. The ggF and VBF productions of Higgs bosons are treated as background as discussed in section 8.4.

Definitions of control regions in the 4ℓ and 3ℓ analyses are presented in table 5, and those defined in the 2ℓ analyses are shown in table 6. The CRs are made orthogonal to the corresponding SRs by inverting some selections with respect to the SR definitions. Such selections are in boldface font in the tables and are further explained in the following sections.

6.1 Background in the four-lepton channel

The main backgrounds that contribute to the 4ℓ-2SFOS and 4ℓ-1SFOS SRs are diboson processes, dominated by ZZ^* with $E_{\mathrm{T}}^{\mathrm{miss}}$ from $Z \to \tau\tau$ decay, and triboson processes, in particular ZWW^*, which has the same signature as the signal. These processes respectively account for about 85% and 15% of the total background contamination. To normalise ZZ^* a dedicated CR, the 4ℓ-ZZ CR, is defined by inverting the requirement on the invariant mass of dileptons from the Higgs boson candidate. All the other minor background processes, listed in table 4, are modelled by simulation.

6.2 Background in the three-lepton channel

Three classes of backgrounds contribute to the 3ℓ channel. The first class comprises diboson processes: $WZ/W\gamma^*$, ZZ^* with an undetected lepton mainly due to its low-p_{T}, and $Z\gamma$, in which the photon converts to electron-positron pairs. The ZZ^* contribution in this channel is mainly due to single-resonant ZZ^* production where the three-lepton invariant

JHEP08(2015)137

Channel	4ℓ	3ℓ	2ℓ	
Category	2SFOS, 1SFOS	3SF, 1SFOS, 0SFOS	DFOS	SS2jet, SS1jet
Process				
VVV	MC	MC	MC	MC
$WZ/W\gamma^*$	—	3ℓ-WZ CR, 3ℓ-Zjets CR	MC	2ℓ-WZ CR
ZZ^*	4ℓ-ZZ CR	3ℓ-ZZ CR, 3ℓ-Zjets CR	MC	MC
OS WW	—	MC	MC	2ℓ-WW CR
SS WW	—	MC	—	MC
$W\gamma$	—	—	—	2ℓ-$W\gamma$ CR
$Z\gamma$	—	3ℓ-$Z\gamma$ CR	MC	MC
Z/γ^*	—	3ℓ-Zjets CR, 3ℓ-ZZ CR	2ℓ-$Z\tau\tau$ CR	2ℓ-Zjets CR
W+jets	—	—	Data	Data
Multijets	—	—	Data	Data
Top	MC	3ℓ-Top CR	2ℓ-OSTop CR	2ℓ-SSTop CR

Table 4. Summary of background modelling."VVV" represents the triboson processes WWW^*, ZWW^*, ZZZ^* and $WW\gamma^*$. "Top" processes include $t\bar{t}$ and single-top production dominated by tW with $W \to \ell\nu$ decay, as well as $t\bar{t}W/Z$. Some backgrounds are normalised by rescaling the MC yields by the data-to-MC ratio measured in CRs. For these backgrounds the names of the most important CRs are listed. The symbol "—" denotes a negligible contribution to the total background in the signal region.

Channel	4ℓ	3ℓ			
CR	ZZ	WZ	ZZ	Zjets	Top	$Z\gamma$
Number of leptons	4	3	3	3	3	3
Total lepton charge	0	±1	±1	±1	±1	±1
Number of SFOS	2	2 or 1	2 or 1 ($ee\mu$ or $\mu\mu\mu$)	2 or 1	2 or 1	2 or 1 ($\mu\mu e$ or eee)
Number of jets	≤ 1	≤ 1	≤ 1	≤ 1	≥ 1	≤ 1
Number of b-jets	0	0	0	0	$\geq$ **1**	0
$E_{\mathrm{T}}^{\mathrm{miss}}$ (and/or) $p_{\mathrm{T}}^{\mathrm{miss}}$ [GeV]	—	> 30 and > 20	$<$ **30 or** $<$ **20**	$<$ **30 and** $<$ **20**	> 30 and > 20	$<$ **30 or** $<$ **20**
$\lvert m_{\ell\ell} - m_Z \rvert$ [GeV]	$< 10 (m_{\ell_2\ell_3})$	$<$ **25**	—	$<$ **25**	> 25	—
$\lvert m_{\ell\ell\ell} - m_Z \rvert$ [GeV]	—	—	< 15	> 15	—	$<$ **15**
Min. $m_{\ell\ell}$ [GeV]	$>$ **65**$(m_{\ell_0\ell_1})$	> 12	> 12	> 12	> 12	> 12
Max. $m_{\ell\ell}$ [GeV]	—	< 200	< 200	< 200	—	< 200
$\Delta R_{\ell_0\ell_1}$	—	< 2.0	< 2.0	< 2.0	—	< 2.0

Table 5. Definition of control regions in the 4ℓ and 3ℓ analyses. Selections indicated in boldface font are designed to retain the CR orthogonal to the relevant SR.

JHEP08(2015)137

Channel	DFOS 2ℓ		SS 2ℓ				
CR	OSTop	$Z \to \tau\tau$	Wγ	WZ	WW	SSTop	Zjets
Number of leptons	2	2	2	**3**	2	2	2
			$\geq$ 1 conversion e				
Total lepton charge	0	0	$\pm$2	$\pm$1	**0**	**0**	**0**
Number of SFOS	0	0	—	—	—	—	—
Number of jets	≥ 2	≥ 2	2 or 1	2 or 1	2 or 1	2 or 1	2 or 1
Number of b-jets	0	0	0	0	0	**$\geq$ 1**	0
$E_{\mathrm{T}}^{\mathrm{miss}}$ [GeV]	> 20	> 20	> 45 (1j)	> 45 (1j)	> 85 (1j)	> 45 (1j,$ee, \mu\mu$)	> 45 (1j)
						> 60 (1j,$e\mu$)	< 85 (1j,$e\mu$)
			> 50 (2j)	> 50 (2j)	> 80 (2j)	> 50 (2j,$ee, \mu\mu$)	> 50 (2j,$ee, \mu\mu$)
						> 60 (2j,$e\mu$)	< 80 (2j,$e\mu$)
$\lvert m_{\ell\ell} - m_Z \rvert$ [GeV]	—	—	—	< 15 (OS $ee, \mu\mu$)	> 15 ($ee, \mu\mu$)	> 15 ($ee, \mu\mu$)	$<$ **15** ($ee, \mu\mu$)
Min. $m_{\ell\ell}$ [GeV]	$>$ **90 (8 TeV)**	> 10	> 12 ($ee, \mu\mu$)	> 12 ($ee, \mu\mu$)	> 12 ($ee, \mu\mu$)	> 12 ($ee, \mu\mu$)	> 12 ($ee, \mu\mu$)
	$>$ **80 (7 TeV)**						
			> 10 ($e\mu$)	> 10 ($e\mu$)	> 10 ($e\mu$)	> 12 ($e\mu$)	> 55 ($e\mu$)
Max. $m_{\ell\ell}$ [GeV]	—	< 70	< 50	—	—	—	< 80 ($e\mu$)
$m_{\tau\tau}$ [GeV]	$< (m_Z - 25)$	—	—	—	—	—	
$\Delta\phi_{\ell_0\ell_1}$ [rad]	—	$>$ **2.8**	< 2.5	—	—	—	
m_{T} [GeV]	—	—	> 105 (1j)	> 105 (1j)	> 105 (1j)	> 105 (1j)	—
Min. $m_{\ell_i j}$ [GeV]	—	—	< 70	< 70	< 70	< 70	< 70
Min. $m_{\ell_i jj}$ [GeV]	—	—	< 115	< 115	< 115	< 115	< 115
Min. $\phi_{\ell_i j}$ [rad]	—	—	< 1.5	< 1.5	—	—	—
$p_{\mathrm{T}}^{\ell\ell}$ [GeV]	—	—	> 30	—	—	—	—

Table 6. Definition of control regions in the 2ℓ analyses. Selections indicated in boldface font are designed to keep the CR orthogonal to the relevant SR.

mass is just below the Z boson mass. The second class includes triboson processes, mainly WWW^*. The last class of backgrounds are processes with a misidentified lepton, mainly Z+jets and top-quark pair production.

In the 3ℓ-3SF and 3ℓ-1SFOS SRs, $WZ/W\gamma^*$ and ZZ^* represent the leading background contributions accounting for about 80% of the total background yields, with 65% from $WZ/W\gamma^*$ and 15% from ZZ^*. Production of $Z\gamma$, VVV, Z+jets and top-quarks share the remaining background fraction equally. The 3ℓ-0SFOS SR contains contributions of similar size from $WZ/W\gamma^*$, VVV and top-quark production. In this SR the total background event yield is about eight times lower than in the 3ℓ-3SF and 3ℓ-1SFOS SRs.

A 3ℓ-WZ CR is defined by reversing the Z-veto requirement, in order to select events with a Z boson decay. The 3ℓ-ZZ CR and 3ℓ-$Z\gamma$ CR are defined by requiring low $E_{\mathrm{T}}^{\mathrm{miss}}$ values to reflect the absence of final-state neutrinos in the background process under study. For these control regions, the invariant mass of the three leptons must be consistent with the Z boson mass. These regions are further distinguished according to the flavour combination of the three leptons, namely eee or $\mu\mu e$ for the 3ℓ-$Z\gamma$ CR, and $\mu\mu\mu$ or $ee\mu$ for the 3ℓ-ZZ CR.

The 3ℓ-Zjets CR is defined by reversing the $E_{\mathrm{T}}^{\mathrm{miss}}$ and the Z-veto selections. The properties of misidentified electrons and muons are different; therefore the 3ℓ-Zjets CR is further split into the misidentified-electron component ($eee+\mu\mu e$ events) and misidentified-muon component ($\mu\mu\mu + ee\mu$ events) and an NF is assigned to each component. In the 7 TeV data sample, the predicted Z+jets event yield with misidentified muons in the 3ℓ SRs is negligible. Furthermore, the number of events in the 3ℓ-Zjets CR with such a lepton

JHEP08(2015)137

flavour combination is too small to reliably extract the NF. Therefore the estimation of the misidentified-muon component is taken directly from simulation.

The 3ℓ-Top CR is defined by requiring at least one b-tagged jet. The Z+jets contribution is difficult to isolate from other processes that include Z bosons. Thus the NF for this process is constrained not only by the 3ℓ-Zjets CR, but also in part by the 3ℓ-WZ CR and the 3ℓ-ZZ CR, as indicated in table 4.

6.3 Background in the opposite-sign two-lepton channel

The dominant background in this channel is top-quark production, which accounts for about 50% of the total contamination. The 2ℓ-OSTop CR is defined by requiring a high invariant mass of the lepton pair in the final state. As the b-jet rejection criteria are the same in the CR and SR, the systematic uncertainties related to b-tagging largely cancel between the two regions. The second dominant background is $Z \to \tau\tau$, which accounts for 20% of the total background in the SR. A dedicated control region, 2ℓ-$Z\tau\tau$ CR, is defined by requiring a large opening angle between the two leptons. The WW process constitutes the third largest background, accounting for 10% of the total. Due to a difficulty in separating this process from $t\bar{t}$ events over a wide kinematic region, no dedicated CR is defined, and this process is modelled purely by MC simulation.

The contribution of backgrounds with misidentified leptons, W+jets and multijet, accounts for 10% of the total background. The misidentified-lepton background rate has an uncertainty of 40%. Due to this large uncertainty, the misidentified-lepton background contributes significantly to this channel. The $WZ/W\gamma^*$ production and the ggF production followed by $H \to WW^*$ decay, each representing 5% of the total background, are modelled with MC simulation.

6.4 Background in the same-sign two-lepton channel

The $WZ/W\gamma^*$ and W+jets processes each account for one third of the total background. Some of the $WZ/W\gamma^*$ events with three leptons enter the selection when one of the leptons escapes detection. To normalise this process, the 2ℓ-WZ CR is defined by selecting events with three leptons. The contamination from W+jets events with one misidentified lepton is estimated by using the same data-driven method used in the 2ℓ-DFOS channel.

The remaining background processes contribute at the 10% level or less. The normalisation of $W\gamma$ is based on the 2ℓ-$W\gamma$ CR, defined by requiring at least one electron consistent with a conversion, including a requirement that the electron does not have a hit in the innermost pixel layer. The background contribution to the 2ℓ-SS channel due to lepton charge misidentification, in otherwise charge-symmetric processes, is found to be relevant only for electrons and affects top-quark production, opposite-sign WW and Z+jets. It represents 10% of the total background in the 2ℓ-SS1jet SR and 3% of the total background in the 2ℓ-SS2jet SR. The 2ℓ-SSTop CR, 2ℓ-WW CR and 2ℓ-Zjets CR are defined selecting opposite-sign leptons to normalise these contributions. Moreover, in 2ℓ-SSTop CR at least one b-tagged jet is selected. Due to the small production rate, no control region is defined to normalise the WW events from vector boson scattering with same charge, whose rate is taken directly from simulation.

JHEP08(2015)137

(a) 8 TeV data sample

Channel	4ℓ	3ℓ	2ℓ	
Category	2SFOS, 1SFOS	3SF, 1SFOS, 0SFOS	DFOS	SS2jet, SS1jet
Process				
$WZ/W\gamma^*$	—	$1.08^{+0.08}_{-0.06}$	—	0.94 ± 0.10
ZZ^*	$1.03^{+0.11}_{-0.10}$	$1.28^{+0.22}_{-0.20}$	—	—
OS WW	—	—	—	0.80 ± 0.33
$W\gamma$	—	—	—	1.06 ± 0.12
$Z\gamma$	—	$0.62^{+0.15}_{-0.14}$	—	—
Z/γ^*	—	$0.80^{+0.68}_{-0.53}$ (μ-misid)	$0.90^{+0.18}_{-0.16}$	0.86 ± 0.30
		$0.33^{+0.12}_{-0.11}$ (e-misid)		
Top	—	$1.36^{+0.34}_{-0.30}$	$1.05^{+0.16}_{-0.14}$	1.04 ± 0.08

(b) 7 TeV data sample

Process			
$WZ/W\gamma^*$	—	$1.02^{+0.12}_{-0.11}$	—
ZZ^*	$1.59^{+0.36}_{-0.31}$	$1.78^{+0.51}_{-0.42}$	—
OS WW	—	—	—
$W\gamma$	—	—	—
$Z\gamma$	—	$0.45^{+0.09}_{-0.09}$	—
Z/γ^*	—	$0.68^{+0.16}_{-0.15}$ (e-misid)	$1.11^{+0.38}_{-0.34}$
Top	—	$1.25^{+0.66}_{-0.52}$	$0.93^{+0.16}_{-0.14}$

Table 7. Summary of background normalisation factors in the (a) 8 TeV and (b) 7 TeV data samples. The uncertainties include both the statistical and systematic components (see section 7). "—" denotes that the background process, when considered, is normalised by MC simulation.

JHEP08(2015)137

(a) 8 TeV data sample

Channel	4ℓ	3ℓ					DFOS 2ℓ	
CR	ZZ	WZ	ZZ	Zjets	Top	$Z\gamma$	$Z\tau\tau$	OSTop
Observed events	122	578	60	251	55	156	328	1169
MC prediction	121±16	576±63	60±10	249±46	55±12	155±31	326±55	1160±150
MC (no NFs)	118±10	543±50	48±4	351±40	48±6	188±17	354±56	1120±140
Composition (%)								
$WZ/W\gamma^*$	—	89.3±1.5	5.5±1.0	25.9±3.5	20±4	1.68±0.31	—	—
ZZ^*	99.49±0.17	6.7±1.2	90.1±2.1	38±5	3.6±1.2	47±6	—	—
$Z\gamma$	—	0.54±0.17	0.6±0.5	5.5±1.5	2.4±0.9	43±7	—	—
Z+jets	—	1.1±0.5	2.1±1.5	29±7	5.50±3.34	8.3±3.4	78.2±2.8	0.7±0.4
Top	0.019±0.012	0.66±0.18	0.27±0.13	0.081±0.034	64±6	0.13±0.06	10.5±1.6	71.3±3.3
Others	0.49±0.17	0.80±0.16	1.16±0.20	0.87±0.13	3.6±0.6	0.33±0.06	11.2±1.9	27.8±3.2
VH ($H \to WW^*$)	0.026±0.006	0.93±0.16	0.26±0.11	0.37±0.09	0.52±0.13	0.052±0.011	0.100±0.018	0.21±0.04

Channel	SS 2ℓ				
CR	$W\gamma$	WZ	WW	SSTop	Zjets
Observed events	228	331	769	5142	39731
MC prediction	229±41	311±66	742±63	5080±350	41000±14000
MC (no NFs)	218±35	335±68	787±58	4930±330	47000±16000
Composition (%)					
$W\gamma$	85.0±2.4	—	0.46±0.14	0.049±0.018	0.022±0.007
$WZ/W\gamma^*$	1.02±0.27	85±4	2.34±0.24	0.200±0.029	0.38±0.09
WW	0.37±0.08	0.028±0.014	23.9±2.3	1.43±0.21	0.57±0.15
Z+jets	4.2±1.6	7.0±3.5	7.0±2.0	2.2±0.7	97.7±0.5
Top	0.68±0.20	1.50±0.29	62.7±2.8	95.5±0.8	0.86±0.21
Others	8.7±1.2	5.3±1.2	3.2±0.4	0.63±0.11	0.44±0.11
VH ($H \to WW^*$)	—	0.77±0.17	0.32±0.04	0.036±0.005	0.0077±0.0020

(b) 7 TeV data sample

Channel	4ℓ	3ℓ					DFOS 2ℓ	
CR	ZZ	WZ	ZZ	Zjets	Top	$Z\gamma$	$Z\tau\tau$	OSTop
Observed events	24	101	18	68	9	123	55	137
MC prediction	24±8	101±16	18±5	67±15	8±4	123±26	55±15	137±20
MC (no NFs)	15±5	99±10	10.7±0.6	81±7	8.1±1.4	208±12	51±12	145±18
Composition (%)								
$WZ/W\gamma^*$	—	87.5±2.5	3.1±1.1	6.9±1.4	14±5	0.61±0.15	—	—
ZZ^*	99.71±0.12	7.4±2.1	92.7±2.3	26±6	4.2±2.5	32±7	—	—
$Z\gamma$	—	1.8±0.8	0.5±0.4	48±7	6±4	59±7	—	—
Z+jets	—	1.5±0.8	3.0±1.4	19±5	0.4±2.2	8.2±2.1	76±6	0.14±0.15
Top	0.031±0.015	0.7±0.4	0.01±0.20	0.07±0.13	71±10	0.03±0.04	13±5	75.2±3.2
Others	0.23±0.11	0.56±0.11	0.44±0.11	0.115±0.021	4.2±1.4	0.05±0.17	11±4	24.7±3.2
VH ($H \to WW^*$)	0.02±0.31	0.53±0.08	0.106±0.030	0.044±0.008	0.41±0.17	0.0154±0.0027	0.048±0.017	0.135±0.030

Table 8. Number of observed and predicted events and background composition in the CRs for the 4ℓ, 3ℓ and 2ℓ channels in the (a) 8 TeV and (b) 7 TeV data samples. Normalisation factors are taken into account in the calculation of the composition. The uncertainties on event yields include both the statistical and systematic components (see section 7).

JHEP08(2015)137

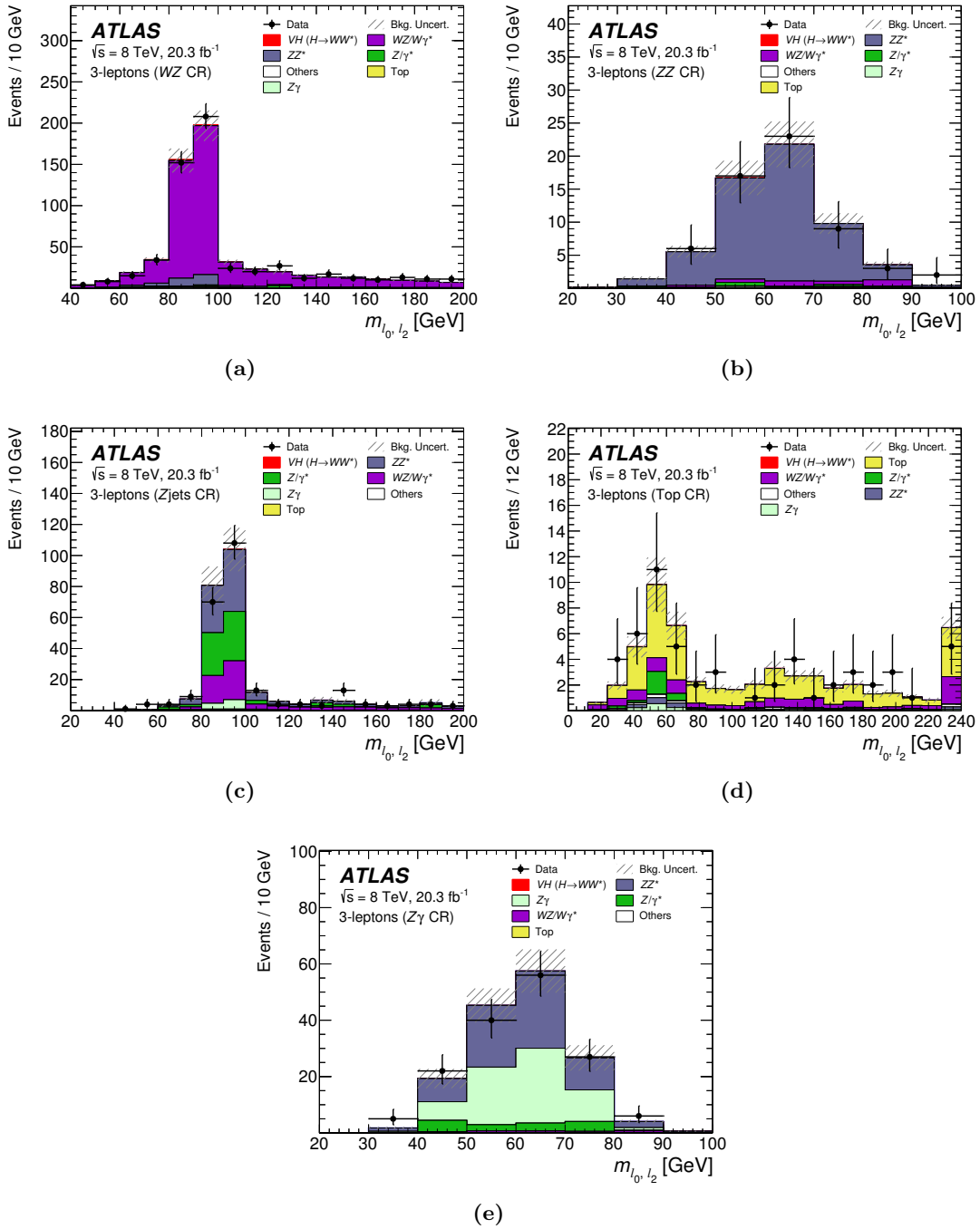

Figure 2. Distributions of the invariant mass of leptons ℓ_0 and ℓ_2, defined in secton 2, in the five CRs defined in the 3ℓ channel: (a) 3ℓ-WZ CR, (b) 3ℓ-ZZ CR, (c) 3ℓ-Zjets CR, (d) 3ℓ-Top CR and (e) 3ℓ-$Z\gamma$ CR. Data (points) are compared to the background plus $VH(H\rightarrow WW^*)$ (m_H=125 GeV) signal expectation (stacked filled histograms), where the background contributions are normalised by applying the normalisation factors shown in table 7. The hatched area on the histogram represents total uncertainty, both statistical and systematic (see section 7), on the total background estimate. The last bin includes overflows.

JHEP08(2015)137

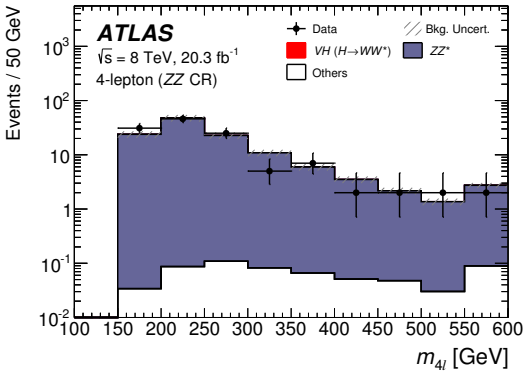

Figure 3. Distribution of the 4-lepton invariant mass $m_{4\ell}$ in the 4ℓ-ZZ CR control region. Data (points) are compared to the background plus $VH(H\to WW^*)$ (m_H=125 GeV) signal expectation (stacked filled histograms), where ZZ^* events are normalised by applying the normalisation factor shown in table 7. The hatched area on the histogram represents total uncertainty, both statistical and systematic (see section 7), on the total background estimate. The last bin includes overflows.

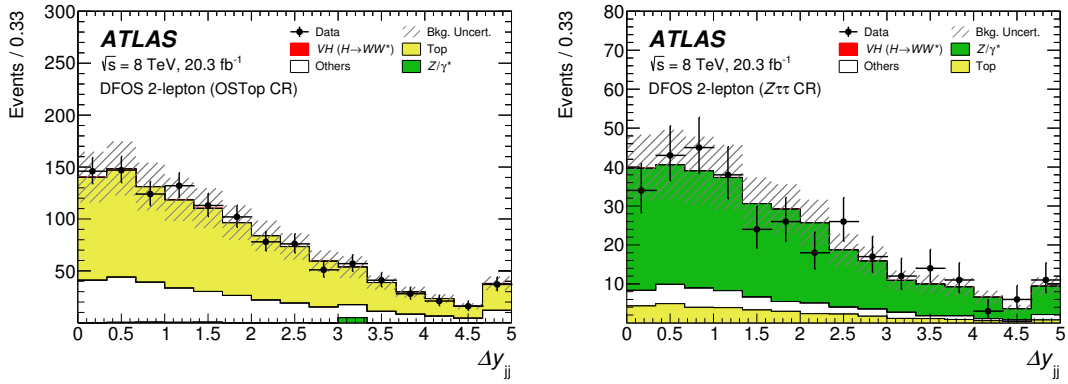

(a) **(b)**

Figure 4. Distributions of the difference in rapidity between the two leading jets Δy_{jj} (a) in the 2ℓ-OSTop CR and (b) in the 2ℓ-$Z\tau\tau$ CR. Data (points) are compared to the background plus $VH(H\to WW^*)$ (m_H=125 GeV) signal expectation (stacked filled histograms), where the background contributions are normalised by applying the normalisation factors shown in table 7. The hatched area on the histogram represents total uncertainty, both statistical and systematic (see section 7), on the total background estimate. The last bin includes overflows.

6.5 Normalisation factors and composition of control regions

NFs are computed through the signal extraction fit explained in section 8.4. Table 4 lists the main background processes, along with the CRs that contribute to the determination of their NFs. The NFs, which are specific to each signal region, are fitted taking into account only the total number of expected and observed events in each CR, separately for the 8 TeV and 7 TeV data samples, and are summarised in table 7. The numbers of observed and expected events from simulation in the 8 TeV and 7 TeV data analysis are summarised in table 8.

JHEP08(2015)137

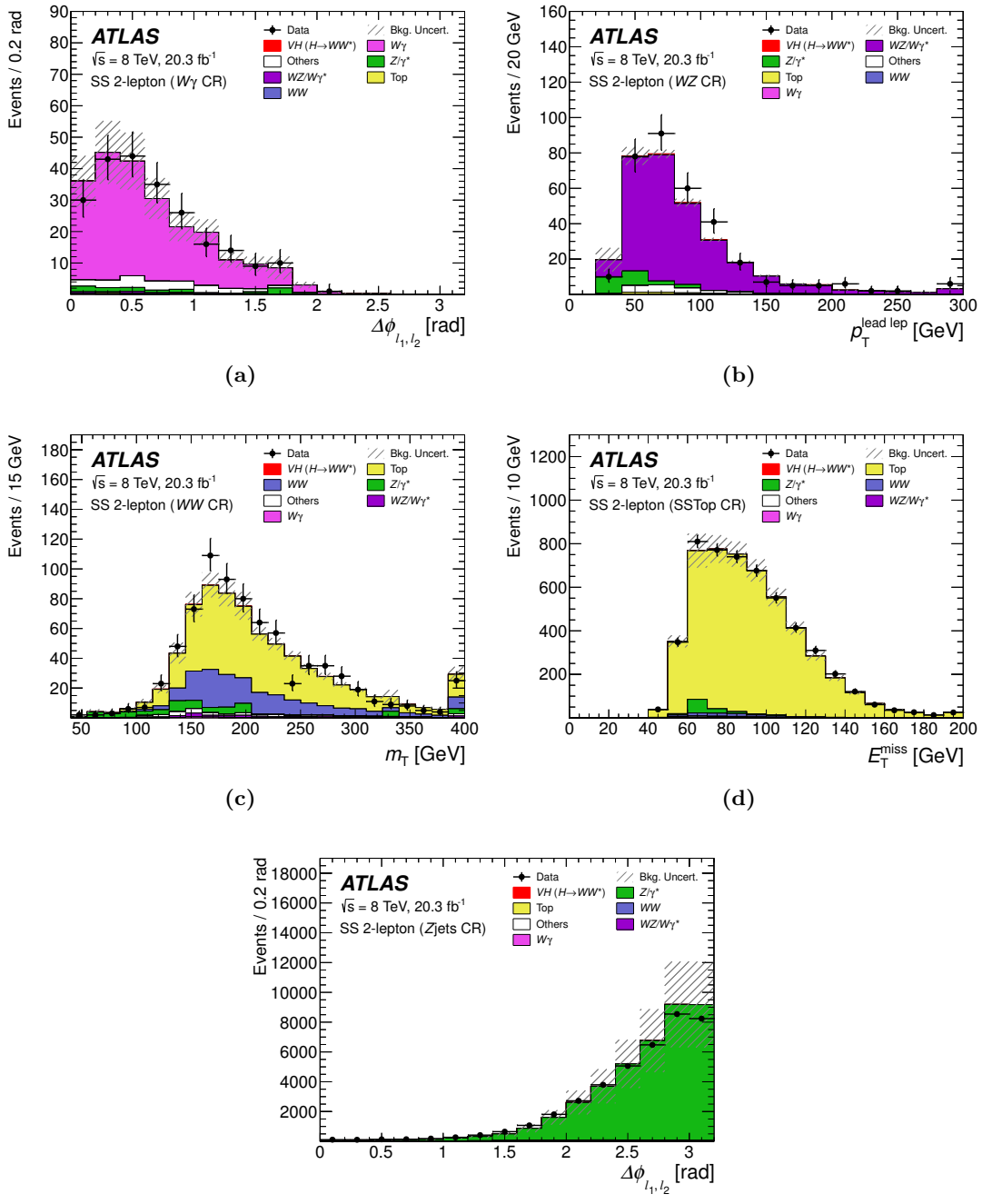

Figure 5. Distribution of relevant variables in the control regions in the 2ℓ-SS channel: (a) azimuthal angle between the two leptons $\Delta\phi_{\ell_1\ell_2}$ in the 2ℓ-$W\gamma$ CR, (b) transverse momentum of the leading lepton in the 2ℓ-WZ CR, (c) transverse mass m_{T} in the 2ℓ-WW CR, (d) missing transverse momentum $E_{\mathrm{T}}^{\mathrm{miss}}$ in the 2ℓ-SSTop CR and (e) $\Delta\phi_{\ell_1\ell_2}$, in the 2ℓ-Zjets CR. Data (points) are compared to the background plus $VH(H\rightarrow WW^*)$ (m_H=125 GeV) signal expectation (stacked filled histograms), where the background contributions are normalised by applying the normalisation factors shown in table 7. The hatched area on the histogram represents total uncertainty, both statistical and systematic (see section 7), on the total background estimate. The last bin includes overflows.

JHEP08(2015)137

Background spectra and the expected composition of the CRs in 8 TeV collisions are shown in figures 2–5. The $VH(H \to WW^*)$ component is shown on top of the background to demonstrate that there is no significant signal leakage in the CRs. The exact amount of signal leakage in each CR is presented in table 8.

In these tables and figures, each background process normalised using CRs is presented separately, while backgrounds that are not normalised using CRs are grouped together as "Others". The ggF and VBF production of Higgs bosons, and the $VH(H \to \tau\tau)$ process are included in the "Others" category, assuming $m_H = 125$ GeV and the SM value for the cross sections and for the branching fraction.

7 Systematic uncertainties

The sources of theoretical and experimental systematic uncertainty on the signal and background are described in this section, and summarised in table 9. The table shows the uncertainties on the estimated event yield after the fit in 8 TeV data samples. Similar values are obtained for the 7 TeV data analysis.

Systematic uncertainties have an impact on the estimates of the signal and background event yields in the SRs and CRs. The experimental uncertainties are applied to both the SRs and CRs. The extrapolation parameter from a SR to a CR is defined as the ratio of MC estimates in the SR and CR. The theoretical uncertainties are computed on the extrapolation parameters, and applied to SRs. Correlations between SRs and CRs are taken into account in the fit, and cancellation effects are expected for uncertainties correlated between SRs and CRs. The different uncertainty sources are treated according to their correlations across the data taking periods, among different analyses, between signal and background sources. Whenever an effect is expected to affect coherently the event yields in two event samples (SRs and/or CRs), for instance the muon reconstruction efficiency for both signal and background, a 100% correlation is assumed and the yields are varied coherently in the fit through the introduction of a single parameter (nuisance parameter). Alternatively when an uncertainty source is not expected to affect the event yields coherently, for instance trigger and luminosity uncertainties across different data taking years, different nuisance parameters are introduced to represent uncorrelated effects.

The "MC statistics" and "CR statistics" uncertainties in table 9 (b) arise from limited simulated events in the SRs and CRs and from the number of data events populating the CRs, respectively.

7.1 Theoretical uncertainties

The theoretical uncertainties on the total Higgs boson production cross section and branching fraction are evaluated by following the recommendation of the LHC Higgs cross-section working group [21, 44, 45]. Uncertainties concerning QCD renormalisation and factorisation scales, which are hereafter collectively referred to as QCD scales, PDF, the value of α_S and branching fraction are estimated.

JHEP08(2015)137

(a) Uncertainties on the $VH(H\to WW^*)$ process (%)

Channel	4ℓ		3ℓ			2ℓ		
Category	2SFOS	1SFOS	3SF	1SFOS	0SFOS	DFOS	SS2jet	SS1jet
Theoretical uncertainties								
VH acceptance	9.2	9.3	9.9	9.9	9.9	10	10	9.9
Higgs boson branching fraction	4.2	4.2	4.2	4.2	4.2	4.2	4.2	4.2
QCD scale	3.1	3.0	1.2	1.0	1.0	1.3	1.0	1.0
PDF and α_S	1.0	1.1	2.1	2.2	2.2	1.9	2.3	2.2
VH NLO EW corrections	1.7	1.8	1.9	1.9	1.9	1.9	1.9	1.9
Experimental uncertainties								
Jet	2.0	3.1	2.5	2.5	2.9	3.2	8.9	5.8
E_T^{miss} soft term	0.2	0.3	—	—	—	0.3	0.6	0.2
Electron	2.6	2.8	1.6	2.2	2.2	1.5	2.1	1.7
Muon	2.6	2.4	2.2	1.8	1.7	0.8	1.8	1.9
Trigger efficiency	0.2	—	0.4	0.3	0.3	0.5	0.6	0.5
b-tagging efficiency	0.9	0.9	0.9	0.8	0.8	2.9	3.5	2.4
Pile-up	1.9	0.7	2.0	1.4	0.8	1.7	1.0	2.4
Luminosity	2.8	2.8	2.8	2.8	2.8	2.8	2.8	2.8

(b) Uncertainties on the total background (%)

Theoretical uncertainties								
QCD scale	0.2	0.1	1.0	0.9	—	3.7	13	2.3
PDF and α_S	0.2	2.4	0.3	0.3	1.6	1.4	0.5	0.6
VVV K-factor	2.8	8.1	1.1	1.9	0.5	—	—	0.3
MC modelling	5.3	4.3	7.0	6.6	—	4.1	0.8	1.4
Experimental uncertainties								
Jet	3.1	2.4	3.2	1.8	4.1	7.2	5.0	3.4
E_T^{miss} soft term	2.3	0.6	1.8	1.9	0.5	1.1	0.2	0.7
Electron	1.0	1.4	1.0	0.4	1.1	0.7	1.1	0.8
Muon	1.1	1.2	0.4	0.7	0.2	0.2	0.4	0.8
Trigger efficiency	—	0.2	0.2	—	—	0.1	—	—
b-tagging efficiency	0.6	0.8	0.6	0.8	2.6	0.7	1.4	0.3
Fake factor	—	—	—	—	—	2.8	10	10
Charge mis-assignment	—	—	—	—	1.4	—	0.7	0.8
Photon conversion rate	—	—	—	—	—	—	1.1	0.9
Pile-up	1.2	1.1	1.4	0.3	1.2	0.9	1.0	1.0
Luminosity	0.4	0.8	0.1	0.2	0.7	—	0.7	0.3
MC statistics	5.3	8.0	3.8	3.2	5.5	3.1	7.3	3.9
CR statistics	8.1	6.6	4.2	3.9	8.8	2.5	2.8	3.5

Table 9. Theoretical and experimental uncertainties, in %, on the predictions of the (a) signal and (b) total background for each category. Fake factor refers to the data-driven estimates of the W+jets and multijet backgrounds in the 2ℓ channels. The dash symbol (–) indicates that the corresponding uncertainties either do not apply or are negligible. The values are obtained through the fit and given for the 8 TeV data sample. Similar values are obtained for the 7 TeV data sample.

JHEP08(2015)137

The main uncertainty on the VH ($H \to WW^*$) process, shown in the "VH Acceptance" row in table 9(a), accounts for the uncertainties in the acceptance of the signal processes and it is evaluated with MINLO-VHj Powheg-Box1.0 [72] simulation. The leading contributions are the missing next to leading order QCD contributions in $qq \to VH$ simulated with Pythia8 and the parton shower uncertainty. The first is evaluated by comparing the Pythia8 prediction with the MINLO-VHj interfaced with Pythia8 and amounts to 7%. The second is computed by comparing MINLO-VHj interfaced with Pythia8 with MINLO-VHj interfaced with Herwig and accounts for a further 7%.

The cuts on the number of jets are found to be the main source of such uncertainties. The uncertainty on the acceptance of the $gg \to ZH$ process is estimated to be 5% in the 4ℓ channel, the only channel where this process is relevant.

Uncertainty on the Higgs boson branching fraction to WW^*, which is particularly important for the VH and VBF production modes, amounts to 4%. The QCD scale uncertainty is 1% for WH production and 3% for ZH production. This uncertainty is larger for ZH production due to the $gg \to ZH$ contribution. The "VH NLO EW corrections" refers to additional uncertainties on the corrections [48] to the NLO differential cross section, applied as a function of the p_{T} of the associated weak bosons in the LO WH and ZH production modes generated by Pythia8. The size of this uncertainty is 2%.

The uncertainties on ggF production are due to the inclusive cross section dependence from QCD scales, the PDF choice and α_{S}, they range from 7% to 8%. In the 2ℓ-DFOS channel, an additional uncertainty due to the jet multiplicity cut is computed with MCFM [55] and amounts to about 12%.

The uncertainties from the QCD scales of backgrounds are estimated by varying the scales up and down independently by a factor of two. MCFM is used to estimate this uncertainty in the 4ℓ, 3ℓ and 2ℓ-SS channels. In the 4ℓ channel the uncertainty on ZZ^* is 4% in the SRs and CR. However, due to the cancellation between the SRs and CR, the resultant effect becomes negligible. In the 3ℓ-3SF and 3ℓ-1SFOS SRs the QCD scale uncertainty on $WZ/W\gamma^*$ is determined in each bin of the "BDT Score" and ranges between 3% and 6%. In the 2ℓ-SS channel, due to cancellations, the QCD scale uncertainties on $WZ/W\gamma^*$ and $W\gamma$ are found to be negligible with the exception of the 2ℓ-SS2jet SR, in which 100% uncertainty is assigned to $W\gamma$. The QCD scale uncertainty on the same-sign WW+2jet, estimated using VBF@NLO [73], is of the order of 40%. In the 2ℓ-DFOS channel, QCD scale uncertainties on top-quark and WW+2jet production with at least two QCD couplings, referred to as QCD WW in the following, are estimated as 9% and 17% by using MC@NLO and MadGraph, respectively.

The PDF uncertainties on backgrounds are calculated by following the PDF4LHC recipe [74] using the envelope of predictions from MSTW2008, CT10 and NNPDF2.3 PDF sets with the exception of top-quark production in the 2ℓ-DFOS channel, which is evaluated with the same technique used in the ggF-enriched $n_j \geq 2$ category in ref. [22]. The uncertainties range from 1% to 6%, depending on the background process and the categories. An uncertainty of 33% on the NLO K-factor for the triboson process is evaluated by using VBF@NLO; in the 3ℓ-0SFOS SR this uncertainty is estimated in bins of $\Delta R_{\ell_0,\ell_1}$ and ranges from 1% to 6%.

JHEP08(2015)137

The "MC modelling" row in table 9(b) takes the yield variation observed between predictions of different MC generators. In the 3ℓ and 2ℓ-SS channels, the uncertainties on the $WZ/W\gamma^*$ event yield due to the modelling of the underlying event, parton shower and matching of the matrix element to the parton shower are evaluated by comparing the predictions of Powheg-Box+Pythia and MC@NLO+Herwig. In the 2ℓ-DFOS channel, an uncertainty due to underlying event and parton shower modelling is assigned to top-quark production and $Z \to \tau\tau$ by comparing the expectations from Powheg-Box+Pythia and Powheg-Box+Herwig, and Alpgen+Pythia and Alpgen+Herwig, respectively. The QCD WW event yield in the 2ℓ-DFOS channel is estimated using Sherpa. The uncertainty from the underlying event, parton shower modelling and matrix element implementation is evaluated through a comparison with MadGraph+Pythia. The uncertainty on the main background in the 4ℓ channel, ZZ^*, is dominated by the statistical component; a systematic uncertainty from the different models, underlying event and parton shower is assigned through a comparison between Powheg-Box+Pythia and Sherpa.

7.2 Experimental uncertainties

One of the dominant experimental uncertainties, labelled "Jet" in table 9, derives from the propagation of the jet energy scale calibration and resolution uncertainties. They were derived from a combination of simulation, test-beam data, and in situ measurements [75]. Additional uncertainties due to differences between quark and gluon jets, and between light- and heavy-flavour jets, as well as the effect of pile-up interactions are included. For jets used in this analysis, the jet energy scale uncertainty ranges from 1% to 7%, depending on p_{T} and η. The relative uncertainty on the jet energy resolution ranges from 2% to 40%, with the largest value of the resolution and relative uncertainty occurring at the p_{T} threshold of the jet selection.

The "Muon" and "Electron" uncertainties include those from lepton reconstruction, identification and isolation, as well as lepton energy and momentum measurements. The "Trigger efficiency" uncertainty in table 9 refers to the uncertainty on the lepton trigger efficiencies. The uncertainties on the lepton and trigger efficiencies are of the order of 1% or smaller.

The changes in jet, electron and muon energy scale uncertainties due to varying them by their systematic uncertainties are propagated to the $E_{\mathrm{T}}^{\mathrm{miss}}$ evaluation and included in the "Jet", "Electron" and "Muon" rows in table 9. An additional "$E_{\mathrm{T}}^{\mathrm{miss}}$ soft term" uncertainty is associated with the contribution of calorimeter energy deposits not assigned to any reconstructed objects in the $E_{\mathrm{T}}^{\mathrm{miss}}$ reconstruction [68–70].

The "b-tagging efficiency" row refers to the uncertainties on the efficiency of tagging of b-jets and include contributions from b-jet identification and charm and light-flavour jet rejection factors [67, 76]. The uncertainties related to b-jet identification range from <1% to 8%. The uncertainties on the misidentification rate for light-quark jets depend on p_{T} and η, and have a range of 9–19%. The uncertainties on c-jets reconstructed as b-jets range between 6% and 14% depending on p_{T}.

JHEP08(2015)137

The uncertainty labelled as "Fake factor" is associated with the data-driven estimates of the W+jets and multijet backgrounds in the 2ℓ channels; it ranges between 35% and 45% depending on the sample and on categories. A "Charge mis-assignment" systematic uncertainty is estimated to account for the mismodelling of the charge flip effect by comparing the number of lepton pairs with same charge and opposite charge under the Z boson mass peak in data and MC simulation, resulting in a 16% relative uncertainty. The uncertainty is assigned to $WZ/W\gamma^*$ in the 3ℓ-0SFOS SR, and top-quark production, Z+jets and WW in the 2ℓ-SS channel.

The uncertainty labelled as "Photon conversion rate" is assigned to $W\gamma$ in the 2ℓ-SS channel, and is evaluated by comparing the yield in data and in MC simulation for events with two muons and one electron with no hit on the innermost pixel detector layer. It is relevant only for the 2ℓ-SS channel and has a size of 6.5% for $W\gamma$.

The "Pile-up" field in table 9 includes the uncertainty on the weights applied to all simulated events to match the distribution of the number of pile-up interactions to that of data. The uncertainty on the integrated luminosity for the 2012 data is $\pm$ 2.8% and it is derived following the same methodology as that detailed in ref. [77]. For the 2011 data the uncertainty on the integrated luminosity is $\pm$ 1.8% [77]. The backgrounds normalised with CR data are not affected by the luminosity uncertainty.

The dominant systematic uncertainties on the $VH(H\to WW^*)$ process in the 4ℓ and 3ℓ channels are due to uncertainties on lepton reconstruction and on the jet energy scale and resolution. In the 2ℓ channels, the jet energy scale and resolution uncertainties are the most important.

8 Results

The data collected at $\sqrt{s} = 8$ TeV and 7 TeV are analysed separately and then combined in all channels in order to search for the Higgs boson in WH and ZH production using $H\to WW^*$ decays. The analyses are optimised for a Higgs boson mass of $m_H = 125$ GeV. For this mass, the selected Higgs bosons decay mainly as $H \to WW^* \to \ell\nu + X$, but a small contamination from the VH production of Higgs bosons, from the decay chain $H \to \tau\tau \to \ell\nu\ell\nu$, is present. This contribution is treated as background and normalised to the SM expectation for the VH production cross section σ_{VH}, and the $H \to \tau\tau$ branching fraction.

This section is subdivided in five sub-sections. Section 8.1 shows the event yields in each category of the 8 TeV and 7 TeV data samples. Furthermore, distributions of some of the relevant variables are shown for the 8 TeV data sample. Section 8.2 summarises the statistical treatment used for the signal extraction. Section 8.3 quantifies the agreement with the background only hypothesis in each analysis category and evaluates the observed and expected significance in each of them. Section 8.4 reports the significance for WH, ZH and combined VH production, moreover it shows the measurement of their cross sections divided by their SM expectations (μ). The VH categories are then combined with the categories of the ggF and VBF analysis using $H \to WW^* \to \ell\nu\ell\nu$ decays described in

JHEP08(2015)137

ref. [22]. In addition the ggF and VBF yields are extracted in a consistent manner together with the VH yields. Finally, section 8.5 shows the measurement of the couplings to vector bosons and to fermions obtained from the combination of the analyses sensitive to the three production modes using $H \to WW^*$ decays.

8.1 Event yields and distributions

The number of events in each category is summarised in table 10 and in table 11 for the 8 TeV and 7 TeV data sample, respectively. In the 2ℓ-DFOS and 2ℓ-SS1jet categories the numbers of observed events are slightly larger than the expectation. The lepton flavour composition of the events in the 2ℓ-SS channel is shown in table 12, in which the high event yield of the 2ℓ-SS1jet SR mainly originates from the $\mu\mu$ and μe channels. The behaviour of the observed data yield as a function of the data period was studied. The events were uniformly distributed according to the acquired luminosity as expected, excluding temporary failures of the detector subsystems as an explanation of the excess. Moreover it was checked that known detector defects were not increasing the rate of particular background sources. Finally, the kinematic distributions of the events were analysed in order to look for striking features pointing to some particular missing background contribution. Because no particular problem was found, the data excesses were attributed to statistical fluctuations.

Distributions of some of the relevant variables after the event selection are presented for 8 TeV data in figure 6 for the 4ℓ analyses, in figure 7 for the 3ℓ analyses and in figure 8 for the 2ℓ analyses. Figures 6(a) and 6(c) show the opening angle between the leptons in the frame where the p_{T} of the Higgs boson is zero, $\Delta\phi^{\mathrm{boost}}_{\ell_0\ell_1}$, in 4ℓ-1SFOS events. Figures 6(b) and 6(d) show the $\Delta\phi^{\mathrm{boost}}_{\ell_0\ell_1}$ in 4ℓ-2SFOS events. Figures 7(a) and 7(b) present the "BDT Score" distribution in the 3ℓ-3SF and 3ℓ-1SFOS SRs, respectively, and figure 7(c) shows the distribution of ΔR between the leptons from the Higgs boson candidate, $\Delta R_{\ell_0\ell_1}$, in the 3ℓ-0SFOS SR. Figures 6(a) and 6(b) are obtained by applying the selections in table 2 only down to the cuts on the $p^{\mathrm{miss}}_{\mathrm{T}}$, in order to maximise the number of events, while the full selection is applied to produce the distributions in figures 6(c) and 6(d). The distributions in figures 7(a)–7(c) are shown with all the selections applied except for the one on the displayed variable. Figure 8(a) presents the transverse mass, m_{T}, in the 2ℓ-DFOS SR, while figure 8(b) and figure 8(c) show the smallest opening angle in the transverse plane between a lepton and a jet, $\Delta\phi^{\mathrm{min}}_{\ell_i,j}$, in the 2ℓ-SS1jet SR and the 2ℓ-SS2jet SR, respectively. The distributions in figure 8 are shown with all the selections applied except for the one on the displayed variable. No data populates figure 6(d). In all distributions, good agreement between data and the MC prediction is observed.

JHEP08(2015)137

8 TeV data sample

Process	4ℓ		3ℓ			2ℓ		
Category	2SFOS	1SFOS	3SF	1SFOS	0SFOS	DFOS	SS2jet	SS1jet
Higgs boson								
VH ($H \to WW^*$)	0.203±0.030	0.228±0.034	0.73±0.10	1.61±0.18	1.43±0.16	2.15±0.30	1.04±0.18	2.04±0.30
VH ($H \to \tau\tau$)	0.0084±0.0032	0.012±0.004	0.057±0.011	0.152±0.023	0.248±0.035	—	0.036±0.008	0.27±0.04
ggF	—	—	0.076±0.015	0.085±0.018	—	2.4±0.5	—	—
VBF	—	—	—	—	—	0.180±0.025	—	—
ttH	—	—	—	—	—	—	—	—
Background								
V	—	—	0.22±0.16	1.9±0.6	0.37±0.15	14±4	8±4	15±5
VV	1.17±0.20	0.31±0.06	19±3	28±4	4.7±0.6	10.1±1.6	11.2±2.1	26±4
VVV	0.12±0.04	0.10±0.04	0.8±0.3	2.2±0.7	2.93±0.29	—	—	0.47±0.05
Top	0.014±0.011	—	0.91±0.26	2.4±0.6	3.7±0.9	24±4	0.75±0.19	1.3±0.5
Others	—	—	—	—	—	2.3±0.9	0.71±0.30	0.60±0.24
Total	1.30±0.23	0.41±0.09	22±4	34±6	11.7±1.8	50±5	21±5	44±6
Observed events	0	3	22	38	14	63	25	62

Table 10. Number of observed and predicted events in the SRs and their composition in the 8 TeV data sample. Background processes that contribute less than 1% of the total background, and Higgs boson production modes that contribute less than 1% of the $VH(H \to WW^*)$ process, are not included in the table. The uncertainties on event yields include both the statistical and systematic components (see section 7).

7 TeV data sample

Process	4ℓ		3ℓ			2ℓ
Category	2SFOS	1SFOS	3SF	1SFOS	0SFOS	DFOS
Higgs boson						
$V(H \to WW^*)$	0.0226±0.0033	0.0208±0.0031	0.129±0.013	0.325±0.034	0.291±0.031	0.28±0.05
$V(H \to \tau\tau)$	0.0031±0.0012	0.0014±0.0008	0.0163±0.0035	0.041±0.006	0.067±0.010	0.0075±0.0032
ggF	—	—	0.0045±0.0015	0.0045±0.0019	0.0048±0.0027	0.32±0.09
VBF	—	—	—	—	—	0.021±0.004
$t\bar{t}$H	—	—	—	0.006±0.004	0.0041±0.0032	—
Background						
V	—	—	0.36±0.30	0.59±0.34	0.36±0.22	3.4±1.3
VV	0.37±0.14	0.031±0.013	4.1±0.6	5.7±1.0	1.3±0.2	0.89±0.27
VVV	0.014±0.005	0.0095±0.0033	0.082±0.028	0.21±0.07	0.338±0.031	—
Top	0.006±0.004	—	0.12±0.14	0.4±0.3	0.44±0.29	3.2±0.8
Others	—	—	—	—	—	—
Total	0.39±0.15	0.041±0.016	4.6±1.1	7.0±1.9	2.5±0.7	7.5±1.7
Observed events	1	0	5	6	2	7

Table 11. Number of observed and predicted events in the SRs and their composition in the 7 TeV data sample. Background processes that contribute less than 1% of the total background, and Higgs boson production modes that contribute less than 1% of the $VH(H \to WW^*)$ process, are not included in the table. The uncertainties on event yields include both the statistical and systematic components (see section 7).

8 TeV data sample

Process	SS 2ℓ (ee)		SS 2ℓ ($e\mu$)		SS 2ℓ (μe)		SS 2ℓ ($\mu\mu$)	
Category	SS2jet	SS1jet	SS2jet	SS1jet	SS2jet	SS1jet	SS2jet	SS1jet
Higgs boson								
VH ($H \to WW^*$)	0.15±0.07	0.39±0.08	0.36±0.08	0.50±0.12	0.24±0.08	0.69±0.14	0.28±0.06	0.46±0.11
VH ($H \to \tau\tau$)	0.009±0.004	0.063±0.013	0.012±0.004	0.081±0.018	0.0040±0.0020	0.080±0.014	0.012±0.004	0.046±0.010
ggF	0.0028±0.0021	0.0011±0.0011	—	—	—	—	—	—
VBF	—	—	—	—	—	—	—	—
$t\bar{t}$H	—	—	—	—	—	—	—	—
Background								
V	2.9±2.8	5.0±2.0	2.5±1.0	6.6±2.3	1.4±0.6	2.1±0.7	1.1±0.8	1.1±0.8
VV	2.8±0.9	6.3±1.3	4.7±1.3	10.9±1.8	2.3±0.7	5.6±1.1	1.3±0.4	3.5±0.8
VVV	—	—	—	—	—	0.13±0.02	—	0.11±0.03
Top	0.12±0.08	0.49±0.14	0.36±0.15	0.48±0.23	0.24±0.08	0.39±0.13	0.035±0.032	—
Others	0.07±0.04	—	0.26±0.12	0.44±0.17	0.32±0.15	—	0.061±0.031	0.056±0.029
Total	5.9±3.1	11.9±2.4	7.9±1.7	18.6±3.0	4.3±0.9	8.2±1.3	2.6±0.9	4.8±1.2
Observed events	4	12	8	25	7	14	6	11

Table 12. Number of observed and predicted events in the 2ℓ-SS channel in the 8 TeV data sample with different lepton flavour combinations: ee, $e\mu$, μe and $\mu\mu$. Background processes that contribute less than 1% of the total background, and Higgs boson production modes that contribute less than 1% of the $VH(H \to WW^*)$ process, are not included in the table. The uncertainties on event yields include both the statistical and systematic components (see section 7)

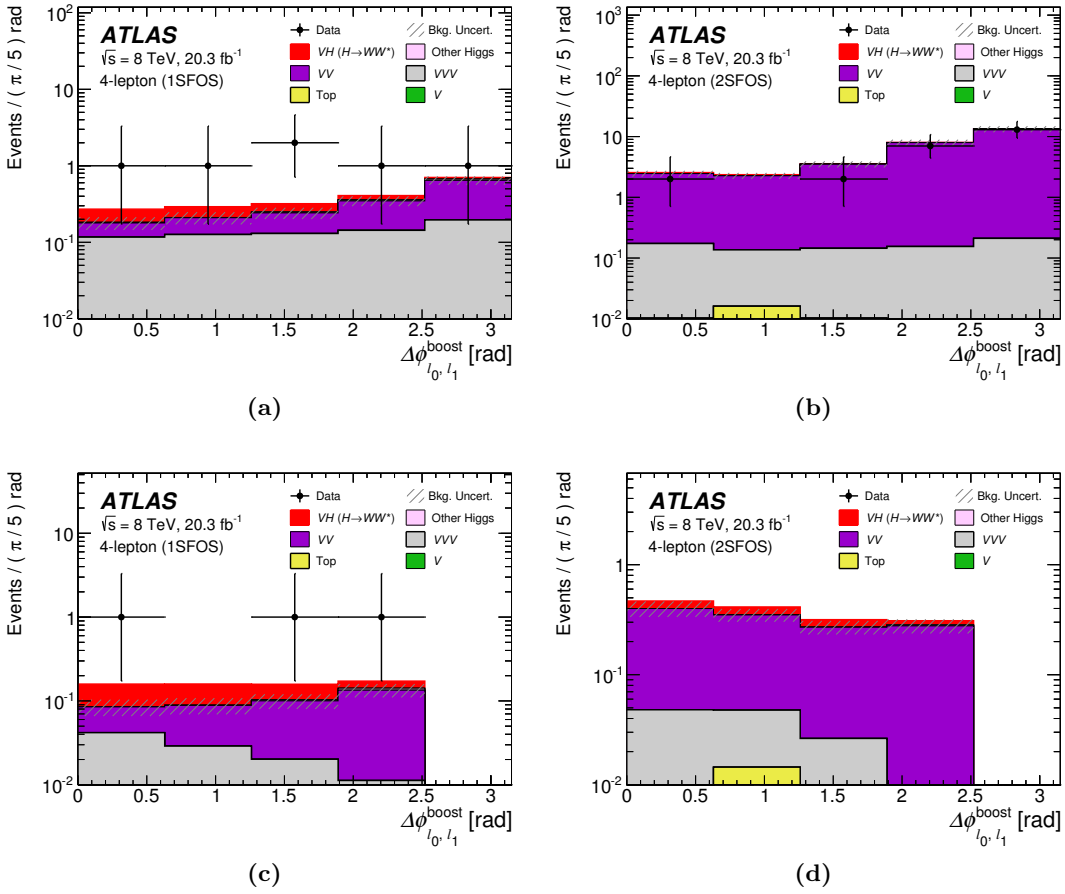

Figure 6. Distributions of the angular separation in ϕ between the opposite-sign lepton pair from the Higgs boson decay candidate in the frame where the p_{T} of the Higgs boson is zero, $\Delta\phi^{\mathrm{boost}}_{\ell_0\ell_1}$, in the 4ℓ analyses using the 8 TeV data sample: (a) and (c) with 4ℓ-1SFOS events, and (b) and (d) with 4ℓ-2SFOS events. Figures (a) and (b) are obtained by applying the cuts in table 2 down to the track missing p_{T} ($p_{\mathrm{T}}^{\mathrm{miss}}$) selection, removing the other selections in order to increase the otherwise very limited number of events, while the distributions in (c) and (d) have all the selections applied. Data (points) are compared to the background plus the $VH(H\to WW^*)$ (m_H=125 GeV) signal expectation (stacked filled histograms), where the background components are normalised by applying the normalisation factors shown in table 7. The hatched area on the histogram represents the total uncertainty on the background estimate including the statistical and systematic uncertainties added in quadrature.

JHEP08(2015)137

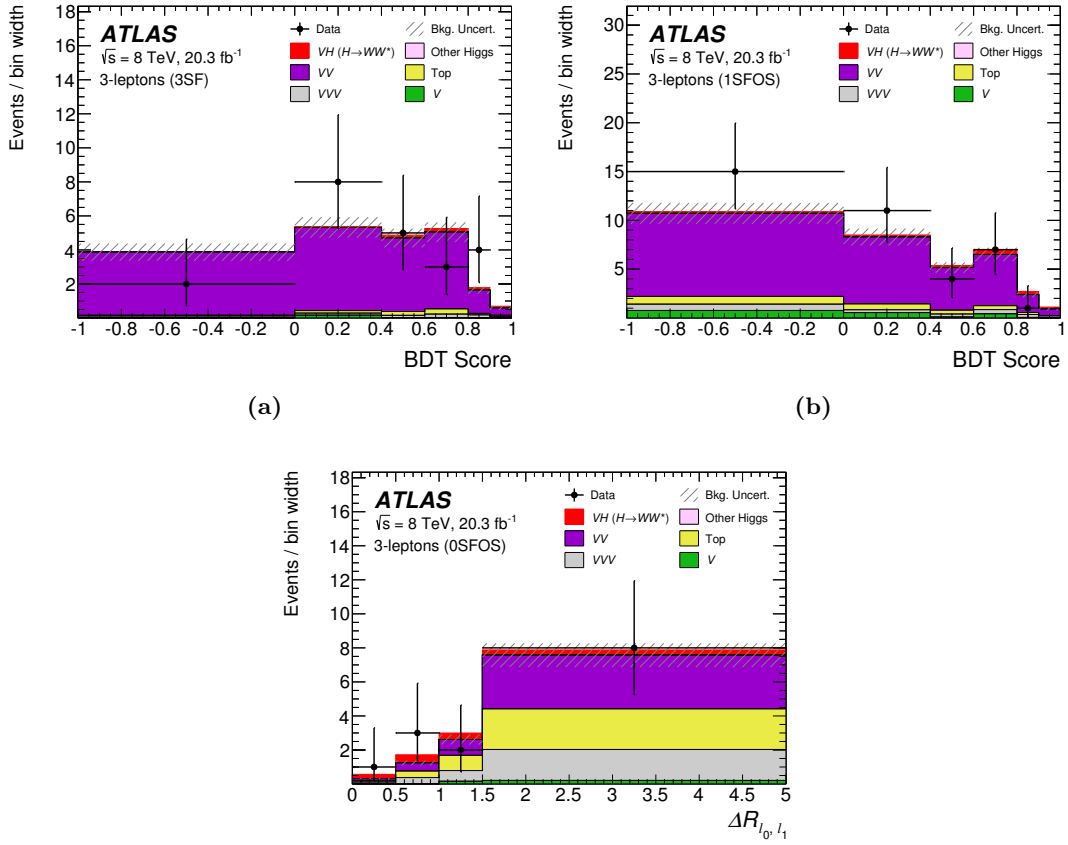

Figure 7. Distributions of relevant quantities for the 3ℓ analyses using the 8 TeV data sample: (a) "BDT Score" in the 3ℓ-3SF and (b) in the 3ℓ-1SFOS SRs, and (c) the angular separation in R of the two opposite-sign leptons with smaller ΔR distance, $\Delta R_{\ell_0\ell_1}$, in the 3ℓ-0SFOS SR. The distributions are shown with all the selections applied except for the one on the displayed variable. Data (points) are compared to the background plus the $VH(H\to WW^*)$ (m_H=125 GeV) signal expectation (stacked filled histograms), where the background components are normalised by applying the normalisation factors shown in table 7. The hatched area on the histogram represents the total uncertainty on the background estimate including the statistical and systematic uncertainties added in quadrature.

JHEP08(2015)137

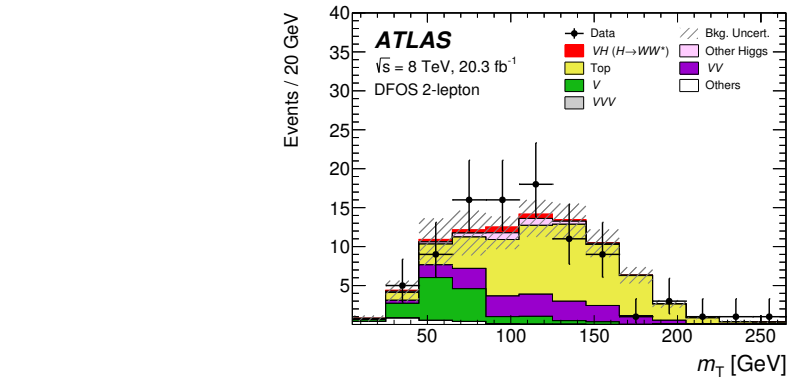

(a)

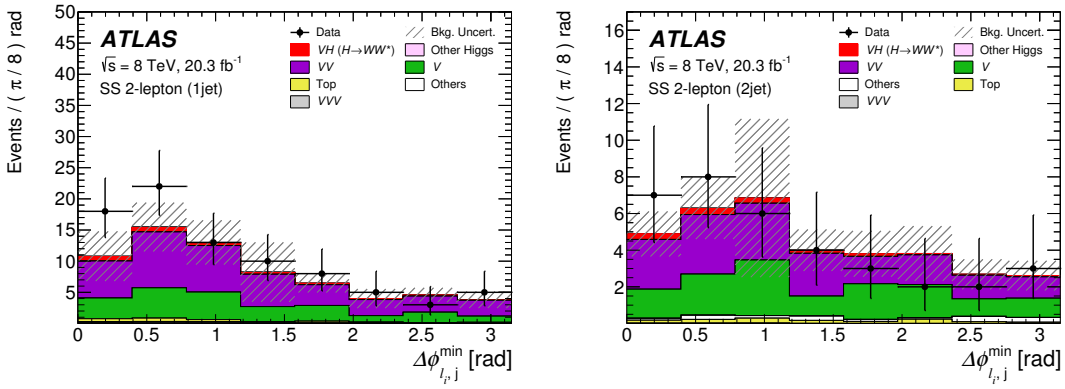

(b) (c)

Figure 8. Distributions of relevant quantities for the 2ℓ analyses using the 8 TeV data sample: (a) transverse mass m_{T} in the 2ℓ-DFOS SR, the smallest azimuthal opening angle between a lepton and a jet, $\phi^{\mathrm{min}}_{\ell_i j}$, (b) in the 2ℓ-SS1jet and (c) 2ℓ-SS2jet SRs. The distributions are shown with all the selections applied except for the one on the displayed variable. Data (points) are compared to the background plus the $VH(H\to WW^*)$ (m_H=125 GeV) signal expectation (stacked filled histograms), where the background components are normalised by applying the normalisation factors shown in table 7. The hatched area on the histogram represents the total uncertainty on the background estimate including the statistical and systematic uncertainties added in quadrature.

8.2 Statistical method

The signal extraction is performed using the profile likelihood ratio method [78], which consists of maximising a binned likelihood function $\mathcal{L}(\mu, \boldsymbol{\theta} \mid \boldsymbol{n})$. The likelihood is the product of Poisson distributions for each SR and CR. The mean values of the distributions are the sum of the expected yields of signal and background. The symbol $\boldsymbol{n}$ represents the observed events in each SR and CR. The signal and background expectations are functions of the signal-strength parameter, μ, and a set of nuisance parameters, $\boldsymbol{\theta}$. The signal strength μ multiplies the SM predicted signal event yield in all categories, while background normalisation factors, included as nuisance parameters, represent corrections for background sources normalised to data. Signal and background predictions are affected by systematic

JHEP08(2015)137

uncertainties that are described by nuisance parameters. The normalisation factors are left free in the fit, while the constraints on the systematic uncertainties are chosen to be log-normal distributions.

The test statistic q_μ is defined as

$$q_\mu = -2\ln\frac{\mathcal{L}(\mu, \hat{\boldsymbol{\theta}}_{\boldsymbol{\mu}})}{\mathcal{L}_{\max}} = -2\ln\Lambda. \tag{8.1}$$

The symbol $\hat{\boldsymbol{\theta}}_{\boldsymbol{\mu}}$ indicates the nuisance parameter values at the maximum of the likelihood function for a given μ. The denominator is the maximum value of $\mathcal{L}$ obtained with both μ and θ floating. When the denominator is maximised, μ takes the value of $\hat{\mu}$. The p_0 value is computed for the test statistic q_0 evaluated at $\mu = 0$ in eq. (8.1), and is defined to be the probability to obtain a value of q_0 larger than the observed value under the background-only hypothesis. There are no bounds on $\hat{\mu}$, although q_0 is defined to be negative if $\hat{\mu} \leq 0$. The equivalent formulation, expressed in terms of the number of standard deviations σ, is referred to as the local significance Z_0. The signal acceptance for all production modes and decays are computed assuming $m_H = 125.36$ GeV, which is the mass measured in $H \to \gamma\gamma$ and $H \to 4\ell$ decays by ATLAS [79]. The acceptance for this mass is obtained interpolating between the values computed at $m_H = 125$ and 130 GeV.

8.3 Characterisation of the excess and VH signal region splitting

Table 13 shows the expected sensitivity to the SM Higgs boson with mass $m_H = 125.36$ GeV, the observed signal significance Z_0 for $H \to WW^*$ decays and the measured μ value using the categories described in section 5. The 3ℓ-3SF and 3ℓ-1SFOS SRs are further split in the likelihood function according to the value of the "BDT Score", while the 3ℓ-0SFOS SR is split into intervals of $\Delta R_{\ell_0,\ell_1}$, as discussed in section 5.2.2. The intervals are shown in figures 7(a)–7(c). Each of the 2ℓ-SS2jet and 2ℓ-SS1jet SRs is further split into four sub-categories according to the flavour of the leading and sub-leading leptons. For the 2ℓ-DFOS a single SR is considered. The numbers in table 13 are computed by adding the contributions from the ggF and VBF production to the signal component, and the relative strengths of VH, ggF and VBF production are fixed to the SM values and constrained with their theoretical uncertainties.

8.4 Signal significance extraction and determination of signal strengths

The VH-targeted categories are then combined with the categories of the ggF and VBF analysis using $H \to WW^* \to \ell\nu\ell\nu$ decays described in ref. [22]. The combination is again performed by building a likelihood function that includes the SRs and CRs of the ggF, VBF and VH analyses. The experimental and theoretical uncertainties affecting the same sources are correlated among different production modes. The μ values for each production mode (μ_{ggF}, μ_{VBF}, μ_{VH}) are correlated in all categories and fitted together while the background NFs are uncorrelated among the different analyses as they cover different phase-space regions. Therefore, when extracting μ_{VH}, μ_{WH} and μ_{ZH}, the ggF and VBF productions are treated as background and their yields determined by the global fit.

JHEP08(2015)137

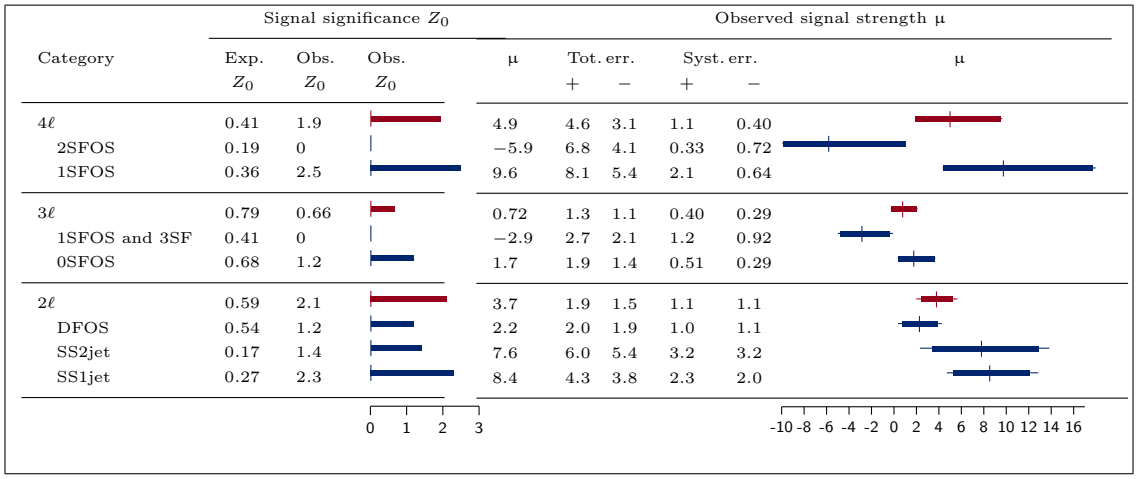

Table 13. The signal significance Z_0, and the $H \to WW^*$ signal strength μ evaluated in the signal regions, combining the 8 TeV and 7 TeV data. The expected (exp.) and observed (obs.) values are shown. The two plots represent the observed significance and the observed μ. In the μ plot the statistical uncertainty (stat.) is represented by the thick line, the total uncertainty (tot.) by the thin line. The first entry in each group (in red) indicates the combination of more than one category. All values are computed for a Higgs boson mass of 125.36 GeV.

The fit results for the μ values for the WH, ZH and VH production are:

$$\mu_{WH} = 2.1^{+1.5}_{-1.3}\,(\text{stat.})^{+1.2}_{-0.8}\,(\text{sys.}), \qquad \mu_{ZH} = 5.1^{+3.8}_{-3.0}\,(\text{stat.})^{+1.9}_{-0.9}\,(\text{sys.}),$$
$$\mu_{VH} = 3.0^{+1.3}_{-1.1}\,(\text{stat.})^{+1.0}_{-0.7}\,(\text{sys.}).$$

The uncertainties on the μ_{VH} value are shown in table 14 (see section 7 for their description). The derivative of μ_{VH} with m_H has been evaluated to be -5.8 %/GeV at $m_H = 125.36$ GeV.

Figure 9 shows the value of the test statistic as a function of μ_{WH} and μ_{ZH}; as shown, the correlation between the two parameters is weak.

Table 15 summarises the signal strengths for each production mode and their combination at a value of $m_H = 125.36$ GeV, together with the observed and the expected Z_0. The combined signal strength is $\mu = 1.16^{+0.16}_{-0.15}(\text{stat.})^{+0.18}_{-0.15}(\text{sys.})$, and the significance of the excess respect to the background only hypothesis is 6.5 σ, while the expected significance in the presence of a Higgs boson decaying to WW^* is 5.9 σ. Figure 10 shows the value of the test statistic as a function of the signal strength of each production mode $(\mu_{\text{ggF}}, \mu_{\text{VBF}}, \mu_{VH})$ and as a function of the combined signal strength μ_{HWW}.

The obtained values are all compatible with the SM expectation within 1.4 standard deviations. Figures 11(a) and 11(b) show the two-dimensional dependence of the likelihood on μ_{VH} and μ_{ggF}, and on μ_{VH} and μ_{VBF}. The μ values not displayed are kept as free unconstrained parameters in the fit. The correlation between the parameters shown in figure 11 is small. The central values obtained for μ_{ggF} and μ_{VBF} are slightly different from those reported in ref. [22]. The shift represents a few percent of the quoted errors and is pulled up by the presence of a small contamination by $VH(H \to WW^*)$ events in the 1-jet and 2-jets categories of the ggF and VBF analysis.

JHEP08(2015)137

Uncertainties on the signal strength μ_{VH} (%)

Signal theoretical uncertainties	$\Delta\mu_{VH}/\mu_{VH}$	
	+	-
VH acceptance	11	7
Higgs boson branching fraction	7	4
QCD scale	1.6	0.7
PDF and α_S	3.2	1.5
VH NLO EW corrections	2.5	1.2
Background theoretical uncertainties		
QCD scale	10	9
PDF and α_S	2.3	2.0
VVV K-factor	3.0	3.0
MC modelling	7.5	6.9
Experimental uncertainties		
Jet	14	9
E_T^{miss} soft term	3.4	2.3
Electron	4.8	2.9
Muon	4.8	3.2
Trigger efficiency	1.7	0.9
b-tagging efficiency	4.7	3.2
Fake factor	14	12
Charge mis-assignment	1.1	1.0
Photon conversion rate	0.8	0.7
Pile-up	3.0	1.9
Luminosity	5.4	3.3
MC statistics	8	8
CR statistics	18	15
ggF SR statistics	5.5	4.4
VBF SR statistics	1.9	1.5
ggF+VBF CR statistics	10	9

Table 14. Percentage theoretical and experimental uncertainties on the observed VH signal strength μ_{VH}. The contributions from signal-related and background-related theoretical uncertainties are specified. The "VH acceptance" is evaluated using both the $qq \to (W/Z)H$ and the $gg \to ZH$ production. The statistical uncertainty due to the ggF and VBF subtraction measured in the categories of the ggF and VBF analysis are indicated with "ggF SR statistics" and "VBF SR statistics", for the contribution from the signal regions, and "ggF+VBF CR statistics" for the contribution from the control regions. The row "MC statistics" shows the uncertainty due to the statistics of the simulated samples. The values are obtained from the combination of the 8 TeV and 7 TeV data samples.

JHEP08(2015)137

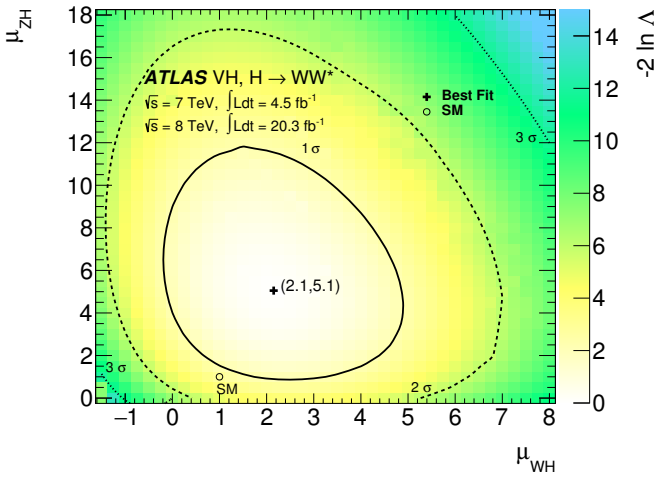

Figure 9. The value of the test statistic as a function of μ_{WH} and μ_{ZH}, for $m_H = 125.36$ GeV. The contours correspond to the values of (μ_{WH}, μ_{ZH}) associated with the 68%, 90% and 95% confidence levels. The black cross indicates the best fit to the data and the open circle represents the SM expectation (μ_{WH}, μ_{ZH})=(1,1).

Category	Signal significance Z_0 Exp. Z_0	Obs. Z_0	Obs. Z_0	Observed signal strength μ μ	Tot. err. +	Tot. err. −	Syst. err. +	Syst. err. −	μ
ggF	4.4	4.2		0.98	0.29	0.26	0.22	0.18	
VBF	2.6	3.2		1.28	0.55	0.47	0.32	0.25	
VH	0.93	2.5		3.0	1.6	1.3	0.95	0.65	
WH only	0.77	1.4		2.1	1.9	1.6	1.2	0.79	
ZH only	0.30	2.0		5.1	4.3	3.1	1.9	0.89	
ggF+VBF+VH	5.9	6.5		1.16	0.24	0.21	0.18	0.15	

Table 15. The signal significance Z_0, and the signal strength μ evaluated for the different production modes: ggF, VBF and VH for $m_H = 125.36$ GeV, for the 8 TeV and 7 TeV data combined. The two plots represent the observed significance and the observed μ. In the μ plot the statistical uncertainty (stat.) is represented by the thick line, the total uncertainty (tot.) by the thin line. Combinations of different categories (in red) are shown too. All values are computed for a Higgs boson mass of 125.36 GeV.

8.5 Measurement of the couplings to vector bosons and fermions

The values of μ_{ggF}, μ_{VBF} and μ_{VH} can be used to test the compatibility of the bosonic and fermionic couplings of the Higgs boson with the SM prediction using the formalism developed in ref. [21]. Assuming the validity of the SU(2) custodial symmetry and a universal scaling of the fermion couplings relative to the SM prediction, two parameters are defined: the scale factor for the SM coupling to the vector bosons (κ_V) and the scale factor for the coupling to the fermions (κ_F). Loop-induced processes are assumed to scale as in the SM. The $H \to \tau\tau$ contribution is treated as signal and its yield is parameterised as a function of κ_V and κ_F. The total width of the Higgs boson can be expressed as the

JHEP08(2015)137

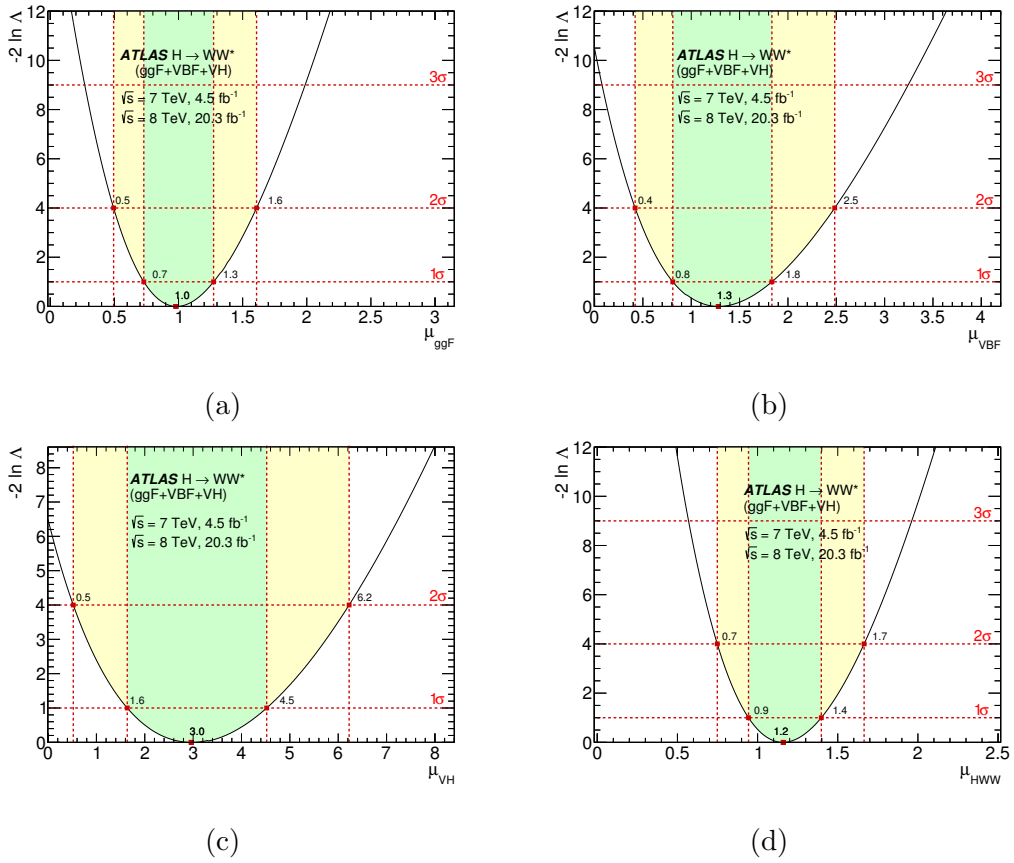

Figure 10. The value of the test statistic as a function of the μ value from the different production modes (a) ggF, (b) VBF, (c) VH and (d) all combined. All values are extracted from the combined fit. The best fit values are represented by the markers at the likelihood minima, with the $\pm 1\sigma$ and $\pm 2\sigma$ uncertainties given by the green and yellow shaded bands.

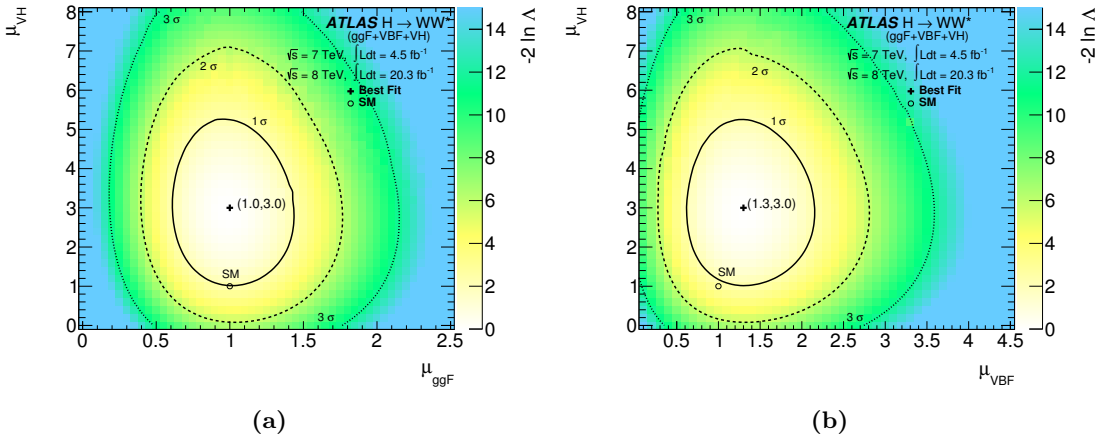

Figure 11. Likelihood as a function of the production mode signal strengths in two-dimensional planes of (a) μ_{VH} vs μ_{ggF} and (b) μ_{VH} vs μ_{VBF}. The black cross indicates the best fit to the data and the open circle represents the SM expectation (1,1).

JHEP08(2015)137

sum of the different partial widths, each one rescaled by the square of the appropriate scaling factor. Neglecting the small contribution from $\Gamma(H \to \gamma\gamma)$ and rarer decay modes, the $H \to WW^*$ decay branching fraction is expressed as:

$$\mathrm{Br}(H \to WW^*) = \frac{\kappa_V^2 \Gamma_{\mathrm{SM}}(H \to WW^*)}{\kappa_F^2 \Gamma_{\mathrm{SM}}(H \to f\bar{f}) + \kappa_F^2 \Gamma_{\mathrm{SM}}(H \to gg) + \kappa_V^2 \Gamma_{\mathrm{SM}}(H \to VV)},$$

where $\Gamma_{\mathrm{SM}}(H \to f\bar{f})$, $\Gamma_{\mathrm{SM}}(H \to gg)$ and $\Gamma_{\mathrm{SM}}(H \to VV)$ are the SM partial decay widths to fermions, gluons and weak bosons, respectively.

The ggF ($gg \to H$) process depends directly on the fermion scale factor κ_F^2 through the top and bottom quark loops, while the VBF ($qq \to Hqq$) and $VH(qq \to VH)$ production cross sections are proportional to κ_V^2, as expressed by the following relations:

$$\sigma(gg \to H) = \kappa_F^2 \sigma_{\mathrm{SM}}(gg \to H), \quad \sigma(qq \to Hqq) = \kappa_V^2 \sigma_{\mathrm{SM}}(qq \to Hqq),$$
$$\sigma(qq \to WH, ZH) = \kappa_V^2 \sigma_{\mathrm{SM}}(qq \to WH, ZH).$$

where the σ without subscript indicates the (κ_V, κ_F)-dependent cross sections and σ_{SM} represents the SM cross sections. The $gg \to ZH$ production cross sections are more complex functions of both κ_V and κ_F [80]:

$$\sigma(gg \to ZH)_{8\ \mathrm{TeV}} = (0.37 \times \kappa_F^2 - 1.64 \times \kappa_F \times \kappa_V + 2.27 \times \kappa_V^2)\, \sigma_{\mathrm{SM}}(gg \to ZH)_{8\ \mathrm{TeV}},$$
$$\sigma(gg \to ZH)_{7\ \mathrm{TeV}} = (0.35 \times \kappa_F^2 - 1.58 \times \kappa_F \times \kappa_V + 2.24 \times \kappa_V^2)\, \sigma_{\mathrm{SM}}(gg \to ZH)_{7\ \mathrm{TeV}},$$

The signal event yield is expressed as $\sigma \cdot \mathrm{Br}(H \to WW^*)$ using the narrow-width approximation. Only the relative sign between κ_V and κ_F is observable and hence in the following only $\kappa_V > 0$ is considered, without loss of generality.

Sensitivity to the sign results from negative interference, in the $gg \to ZH$ process, between the box diagram in which both the Z and H bosons are produced directly from the heavy-quark loop and the triangle diagram in which only the Z^* is produced and subsequently radiates a Higgs boson [81]. Because the relative weights of such processes depend on the $\sqrt{s}$ of the interaction, different coefficients appear in the expression for 8 and 7 TeV.

The likelihood dependence on κ_V and κ_F is shown in figure 12. The product $\sigma(gg \to H) \cdot \mathrm{Br}(H \to WW^*)$, which is measured with good accuracy, does not depend on $|\kappa_F|$ in the limit $|\kappa_F| \gg \kappa_V$. This explains the low sensitivity to high values of κ_F.

On the other hand μ_{VBF} and μ_{VH}, as measured for the $H \to WW^*$ decay, should vanish in the limit $|\kappa_F| \gg \kappa_V$ due to the increased value of the Higgs boson total width and the consequent reduction of the $H \to WW^*$ branching fraction. The observation of significant excesses in the VBF and VH production modes therefore leads to an exclusion of the $|\kappa_F| \gg \kappa_V$ region.

The fit to the data results in two local minima and, although the negative κ_F solution is preferred to the positive solution at 0.5σ, the observed results are compatible with the SM expectation, and the best fit values are:

$$|\kappa_F| = 0.85^{+0.26}_{-0.20}, \quad |\kappa_V| = 1.06^{+0.10}_{-0.10},$$

and their correlation is $\rho = 0.54$.

JHEP08(2015)137

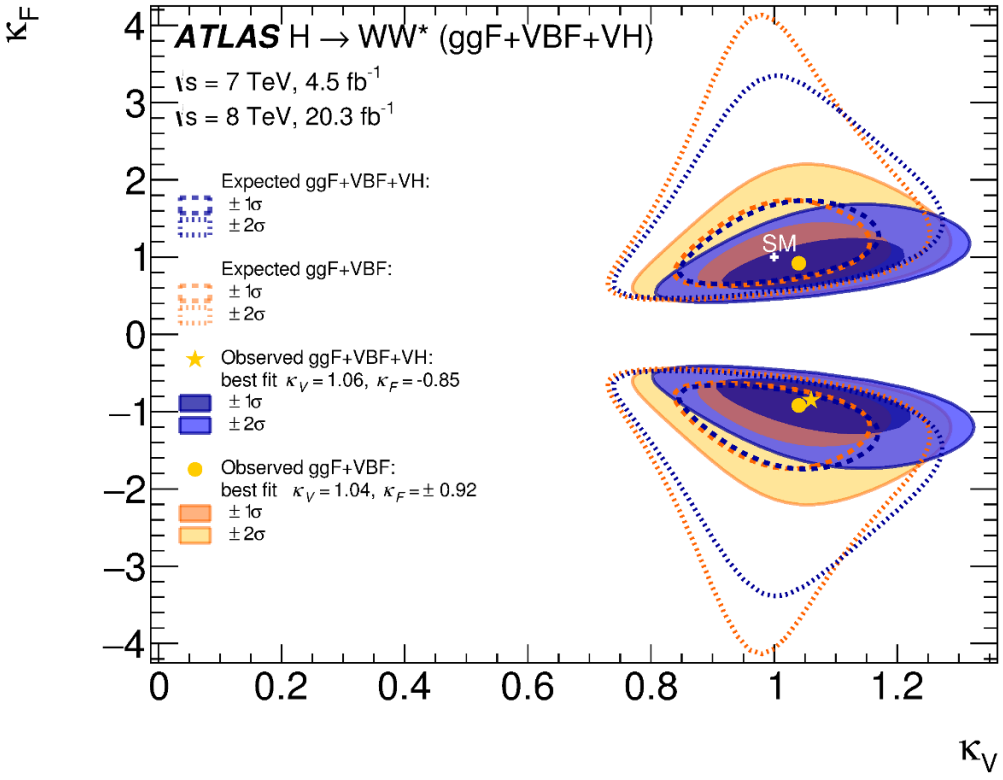

Figure 12. The likelihood scan as a function of κ_V and κ_F both with and without the $VH(H\to WW^*)$ contribution. Both the expected and observed contours corresponding to the 68%, and 95% C.L. are shown. The yellow star and circles indicate the best fit values to the data, and the white cross represents the SM expectation (κ_V, κ_F)=(1,1).

9 Conclusions

A search for the Standard Model Higgs boson produced in association with a W or Z boson and decaying into WW^* is presented. Associated WH production is studied in the final states in which the three W bosons decay to leptons or where one W boson decays to hadrons while the others decay leptonically. The two-lepton and four-lepton final states are used to search for ZH production. The dataset corresponds to integrated luminosities of $4.5\,\text{fb}^{-1}$ and $20.3\,\text{fb}^{-1}$ recorded by the ATLAS experiment with LHC proton-proton collisions at $\sqrt{s} = 7$ TeV and 8 TeV, respectively. For the Higgs boson mass of 125.36 GeV, the observed (expected) deviation from the background-only hypothesis, which includes the Standard Model expectation for $H \to \tau\tau$, corresponds to a significance of 2.5 (0.9) standard deviations. The ratio of the measured signal yield to its Standard Model expectation for the VH production is found to be $\mu_{\text{VH}} = 3.0^{+1.3}_{-1.1}\,(\text{stat.})^{+1.0}_{-0.7}\,(\text{sys.})$. A combination with the gluon fusion and vector boson fusion analyses using the $H \to WW^* \to \ell\nu\ell\nu$ decay is also presented. Including VH production the observed significance for a Higgs boson decaying to WW^* is 6.5 σ with an expectation of 5.9 σ for a Standard Model Higgs boson of mass

JHEP08(2015)137

$m_H = 125.36$ GeV. The combined signal strength is $\mu = 1.16^{+0.16}_{-0.15}(\text{stat.})^{+0.18}_{-0.15}(\text{sys.})$. The data were analysed using a model where all Higgs boson couplings to the vector bosons are scaled by a common factor κ_V and those to the fermions by a factor κ_F. They are measured as $|\kappa_V| = 1.06^{+0.10}_{-0.10}$ and $|\kappa_F| = 0.85^{+0.26}_{-0.20}$.

Acknowledgments

We thank CERN for the very successful operation of the LHC, as well as the support staff from our institutions without whom ATLAS could not be operated efficiently.

We acknowledge the support of ANPCyT, Argentina; YerPhI, Armenia; ARC, Australia; BMWFW and FWF, Austria; ANAS, Azerbaijan; SSTC, Belarus; CNPq and FAPESP, Brazil; NSERC, NRC and CFI, Canada; CERN; CONICYT, Chile; CAS, MOST and NSFC, China; COLCIENCIAS, Colombia; MSMT CR, MPO CR and VSC CR, Czech Republic; DNRF, DNSRC and Lundbeck Foundation, Denmark; EPLANET, ERC and NSRF, European Union; IN2P3-CNRS, CEA-DSM/IRFU, France; GNSF, Georgia; BMBF, DFG, HGF, MPG and AvH Foundation, Germany; GSRT and NSRF, Greece; RGC, Hong Kong SAR, China; ISF, MINERVA, GIF, I-CORE and Benoziyo Center, Israel; INFN, Italy; MEXT and JSPS, Japan; CNRST, Morocco; FOM and NWO, Netherlands; BRF and RCN, Norway; MNiSW and NCN, Poland; GRICES and FCT, Portugal; MNE/IFA, Romania; MES of Russia and NRC KI, Russian Federation; JINR; MSTD, Serbia; MSSR, Slovakia; ARRS and MIZŠ, Slovenia; DST/NRF, South Africa; MINECO, Spain; SRC and Wallenberg Foundation, Sweden; SER, SNSF and Cantons of Bern and Geneva, Switzerland; NSC, Taiwan; TAEK, Turkey; STFC, the Royal Society and Leverhulme Trust, United Kingdom; DOE and NSF, United States of America.

The crucial computing support from all WLCG partners is acknowledged gratefully, in particular from CERN and the ATLAS Tier-1 facilities at TRIUMF (Canada), NDGF (Denmark, Norway, Sweden), CC-IN2P3 (France), KIT/GridKA (Germany), INFN-CNAF (Italy), NL-T1 (Netherlands), PIC (Spain), ASGC (Taiwan), RAL (U.K.) and BNL (U.S.A.) and in the Tier-2 facilities worldwide.

References

[1] F. Englert and R. Brout, *Broken symmetry and the mass of gauge vector mesons*, *Phys. Rev. Lett.* **13** (1964) 321 [INSPIRE].

[2] P.W. Higgs, *Broken symmetries and the masses of gauge bosons*, *Phys. Rev. Lett.* **13** (1964) 508 [INSPIRE].

[3] G.S. Guralnik, C.R. Hagen and T.W.B. Kibble, *Global conservation laws and massless particles*, *Phys. Rev. Lett.* **13** (1964) 585 [INSPIRE].

JHEP08(2015)137

[4] ATLAS collaboration, *Observation of a new particle in the search for the Standard Model Higgs boson with the ATLAS detector at the LHC*, *Phys. Lett.* **B 716** (2012) 1 [arXiv:1207.7214] [INSPIRE].

[5] CMS collaboration, *Observation of a new boson at a mass of* 125 *GeV with the CMS experiment at the LHC*, *Phys. Lett.* **B 716** (2012) 30 [arXiv:1207.7235] [INSPIRE].

[6] ATLAS collaboration, *Measurements of Higgs boson production and couplings in diboson final states with the ATLAS detector at the LHC*, *Phys. Lett.* **B 726** (2013) 88 [*Erratum ibid.* **B 734** (2014) 406] [arXiv:1307.1427] [INSPIRE].

[7] ATLAS collaboration, *Evidence for the spin-*0 *nature of the Higgs boson using ATLAS data*, *Phys. Lett.* **B 726** (2013) 120 [arXiv:1307.1432] [INSPIRE].

[8] ATLAS collaboration, *Measurements of fiducial and differential cross sections for Higgs boson production in the diphoton decay channel at* $\sqrt{s} = 8$ *TeV with ATLAS*, *JHEP* **09** (2014) 112 [arXiv:1407.4222] [INSPIRE].

[9] ATLAS collaboration, *Fiducial and differential cross sections of Higgs boson production measured in the four-lepton decay channel in pp collisions at* $\sqrt{s} = 8$ *TeV with the ATLAS detector*, *Phys. Lett.* **B 738** (2014) 234 [arXiv:1408.3226] [INSPIRE].

[10] CMS collaboration, *Observation of a new boson with mass near* 125 *GeV in pp collisions at* $\sqrt{s} = 7$ *and* 8 *TeV*, *JHEP* **06** (2013) 081 [arXiv:1303.4571] [INSPIRE].

[11] CMS collaboration, *Precise determination of the mass of the Higgs boson and tests of compatibility of its couplings with the standard model predictions using proton collisions at* 7 *and* 8 *TeV*, *Eur. Phys. J.* **C 75** (2015) 212 [arXiv:1412.8662] [INSPIRE].

[12] CMS collaboration, *Constraints on the spin-parity and anomalous HVV couplings of the Higgs boson in proton collisions at* 7 *and* 8 *TeV*, *Phys. Rev.* **D 92** (2015) 012004 [arXiv:1411.3441] [INSPIRE].

[13] CDF and D0 collaborations, T. Aaltonen et al., *Evidence for a particle produced in association with weak bosons and decaying to a bottom-antibottom quark pair in Higgs boson searches at the Tevatron*, *Phys. Rev. Lett.* **109** (2012) 071804 [arXiv:1207.6436] [INSPIRE].

[14] CMS collaboration, *Search for the standard model Higgs boson produced in association with a W or a Z boson and decaying to bottom quarks*, *Phys. Rev.* **D 89** (2014) 012003 [arXiv:1310.3687] [INSPIRE].

[15] ATLAS collaboration, *Search for the* $b\bar{b}$ *decay of the Standard Model Higgs boson in associated* $(W/Z)H$ *production with the ATLAS detector*, *JHEP* **01** (2015) 069 [arXiv:1409.6212] [INSPIRE].

[16] ATLAS collaboration, *Measurement of Higgs boson production in the diphoton decay channel in pp collisions at center-of-mass energies of* 7 *and* 8 *TeV with the ATLAS detector*, *Phys. Rev.* **D 90** (2014) 112015 [arXiv:1408.7084] [INSPIRE].

[17] ATLAS collaboration, *Measurements of Higgs boson production and couplings in the four-lepton channel in pp collisions at center-of-mass energies of* 7 *and* 8 *TeV with the ATLAS detector*, *Phys. Rev.* **D 91** (2015) 012006 [arXiv:1408.5191] [INSPIRE].

[18] CMS collaboration, *Observation of the diphoton decay of the Higgs boson and measurement of its properties*, *Eur. Phys. J.* **C 74** (2014) 3076 [arXiv:1407.0558] [INSPIRE].

[19] CMS collaboration, *Measurement of the properties of a Higgs boson in the four-lepton final state*, *Phys. Rev.* **D 89** (2014) 092007 [arXiv:1312.5353] [INSPIRE].

JHEP08(2015)137

[20] CMS collaboration, *Measurement of Higgs boson production and properties in the WW decay channel with leptonic final states*, *JHEP* **01** (2014) 096 [arXiv:1312.1129] [INSPIRE].

[21] LHC Higgs Cross section Working Group collaboration, S. Heinemeyer et al., *Handbook of LHC Higgs cross sections: 3. Higgs properties*, arXiv:1307.1347 [INSPIRE].

[22] ATLAS collaboration, *Observation and measurement of Higgs boson decays to WW^* with the ATLAS detector*, *Phys. Rev.* **D 92** (2015) 012006 [arXiv:1412.2641] [INSPIRE].

[23] ATLAS collaboration, *The ATLAS experiment at the CERN Large Hadron Collider*, 2008 *JINST* **3** S08003 [INSPIRE].

[24] ATLAS collaboration, *Pile-up corrections for jets from proton-proton collisions at $\sqrt{s} = 7$ TeV in ATLAS in* 2011, ATLAS-CONF-2012-064, CERN, Geneva Switzerland (2012).

[25] T. Sjöstrand, S. Mrenna and P.Z. Skands, *PYTHIA* 6.4 *physics and manual*, *JHEP* **05** (2006) 026 [hep-ph/0603175] [INSPIRE].

[26] T. Sjöstrand, S. Mrenna and P.Z. Skands, *A brief introduction to PYTHIA* 8.1, *Comput. Phys. Commun.* **178** (2008) 852 [arXiv:0710.3820] [INSPIRE].

[27] P. Nason, *A new method for combining NLO QCD with shower Monte Carlo algorithms*, *JHEP* **11** (2004) 040 [hep-ph/0409146] [INSPIRE].

[28] S. Frixione, P. Nason and C. Oleari, *Matching NLO QCD computations with parton shower simulations: the POWHEG method*, *JHEP* **11** (2007) 070 [arXiv:0709.2092] [INSPIRE].

[29] S. Alioli, P. Nason, C. Oleari and E. Re, *A general framework for implementing NLO calculations in shower Monte Carlo programs: the POWHEG BOX*, *JHEP* **06** (2010) 043 [arXiv:1002.2581] [INSPIRE].

[30] E. Bagnaschi, G. Degrassi, P. Slavich and A. Vicini, *Higgs production via gluon fusion in the POWHEG approach in the SM and in the MSSM*, *JHEP* **02** (2012) 088 [arXiv:1111.2854] [INSPIRE].

[31] P. Nason and C. Oleari, *NLO Higgs boson production via vector-boson fusion matched with shower in POWHEG*, *JHEP* **02** (2010) 037 [arXiv:0911.5299] [INSPIRE].

[32] M.L. Mangano, M. Moretti, F. Piccinini, R. Pittau and A.D. Polosa, *ALPGEN, a generator for hard multiparton processes in hadronic collisions*, *JHEP* **07** (2003) 001 [hep-ph/0206293] [INSPIRE].

[33] G. Corcella et al., *HERWIG* 6*: an event generator for hadron emission reactions with interfering gluons (including supersymmetric processes)*, *JHEP* **01** (2001) 010 [hep-ph/0011363] [INSPIRE].

[34] T. Gleisberg et al., *Event generation with SHERPA* 1.1, *JHEP* **02** (2009) 007 [arXiv:0811.4622] [INSPIRE].

[35] S. Frixione, P. Nason and G. Ridolfi, *A positive-weight next-to-leading-order Monte Carlo for heavy flavour hadroproduction*, *JHEP* **09** (2007) 126 [arXiv:0707.3088] [INSPIRE].

[36] S. Frixione and B.R. Webber, *Matching NLO QCD computations and parton shower simulations*, *JHEP* **06** (2002) 029 [hep-ph/0204244] [INSPIRE].

[37] J. Alwall, M. Herquet, F. Maltoni, O. Mattelaer and T. Stelzer, *MadGraph* 5*: going beyond*, *JHEP* **06** (2011) 128 [arXiv:1106.0522] [INSPIRE].

JHEP08(2015)137

[38] B.P. Kersevan and E. Richter-Was, *The Monte Carlo event generator AcerMC versions* 2.0 *to* 3.8 *with interfaces to PYTHIA* 6.4*, HERWIG* 6.5 *and ARIADNE* 4.1, *Comput. Phys. Commun.* **184** (2013) 919 [hep-ph/0405247] [INSPIRE].

[39] S. Alioli, P. Nason, C. Oleari and E. Re, *NLO single-top production matched with shower in POWHEG: s- and t-channel contributions*, *JHEP* **09** (2009) 111 [*Erratum ibid.* **02** (2010) 011] [arXiv:0907.4076] [INSPIRE].

[40] E. Re, *Single-top Wt-channel production matched with parton showers using the POWHEG method*, *Eur. Phys. J.* **C 71** (2011) 1547 [arXiv:1009.2450] [INSPIRE].

[41] T. Melia, P. Nason, R. Rontsch and G. Zanderighi, W^+W^-*,* WZ *and* ZZ *production in the POWHEG BOX*, *JHEP* **11** (2011) 078 [arXiv:1107.5051] [INSPIRE].

[42] T. Binoth, N. Kauer and P. Mertsch, *Gluon-induced QCD corrections to* $pp \to ZZ \to \ell\bar{\ell}\ell'\bar{\ell}'$, arXiv:0807.0024 [INSPIRE].

[43] T. Binoth, M. Ciccolini, N. Kauer and M. Krämer, *Gluon-induced W-boson pair production at the LHC*, *JHEP* **12** (2006) 046 [hep-ph/0611170] [INSPIRE].

[44] LHC Higgs Cross section Working Group collaboration, S. Dittmaier et al., *Handbook of LHC Higgs cross sections:* 1*. Inclusive observables*, arXiv:1101.0593 [INSPIRE].

[45] S. Dittmaier et al., *Handbook of LHC Higgs cross sections:* 2*. Differential distributions*, arXiv:1201.3084 [INSPIRE].

[46] M.L. Ciccolini, S. Dittmaier and M. Krämer, *Electroweak radiative corrections to associated* WH *and* ZH *production at hadron colliders*, *Phys. Rev.* **D 68** (2003) 073003 [hep-ph/0306234] [INSPIRE].

[47] O. Brein, A. Djouadi and R. Harlander, *NNLO QCD corrections to the Higgs-strahlung processes at hadron colliders*, *Phys. Lett.* **B 579** (2004) 149 [hep-ph/0307206] [INSPIRE].

[48] A. Denner, S. Dittmaier, S. Kallweit and A. Muck, *EW corrections to Higgs strahlung at the Tevatron and the LHC with HAWK*, PoS(EPS-HEP2011)235 [arXiv:1112.5258] [INSPIRE].

[49] J.M. Butterworth, J.R. Forshaw and M.H. Seymour, *Multiparton interactions in photoproduction at HERA*, *Z. Phys.* **C 72** (1996) 637 [hep-ph/9601371] [INSPIRE].

[50] H.-L. Lai et al., *New parton distributions for collider physics*, *Phys. Rev.* **D 82** (2010) 074024 [arXiv:1007.2241] [INSPIRE].

[51] P.M. Nadolsky et al., *Implications of CTEQ global analysis for collider observables*, *Phys. Rev.* **D 78** (2008) 013004 [arXiv:0802.0007] [INSPIRE].

[52] A. Sherstnev and R.S. Thorne, *Parton distributions for LO generators*, *Eur. Phys. J.* **C 55** (2008) 553 [arXiv:0711.2473] [INSPIRE].

[53] S. Catani, L. Cieri, G. Ferrera, D. de Florian and M. Grazzini, *Vector boson production at hadron colliders: a fully exclusive QCD calculation at NNLO*, *Phys. Rev. Lett.* **103** (2009) 082001 [arXiv:0903.2120] [INSPIRE].

[54] S. Catani and M. Grazzini, *An NNLO subtraction formalism in hadron collisions and its application to Higgs boson production at the LHC*, *Phys. Rev. Lett.* **98** (2007) 222002 [hep-ph/0703012] [INSPIRE].

[55] J.M. Campbell and R.K. Ellis, *MCFM for the Tevatron and the LHC*, *Nucl. Phys. Proc. Suppl.* **205-206** (2010) 10 [arXiv:1007.3492] [INSPIRE].

JHEP08(2015)137

[56] T. Binoth, G. Ossola, C.G. Papadopoulos and R. Pittau, *NLO QCD corrections to tri-boson production*, *JHEP* **06** (2008) 082 [arXiv:0804.0350] [INSPIRE].

[57] ATLAS collaboration, *The ATLAS simulation infrastructure*, *Eur. Phys. J.* **C 70** (2010) 823 [arXiv:1005.4568] [INSPIRE].

[58] GEANT4 collaboration, S. Agostinelli et al., *GEANT4: a simulation toolkit*, *Nucl. Instrum. Meth.* **A 506** (2003) 250 [INSPIRE].

[59] ATLAS collaboration, *The simulation principle and performance of the ATLAS fast calorimeter simulation FastCaloSim*, ATL-PHYS-PUB-2010-013, CERN, Geneva Switzerland (2010).

[60] ATLAS collaboration, *Measurement of the muon reconstruction performance of the ATLAS detector using* 2011 *and* 2012 *LHC proton-proton collision data*, *Eur. Phys. J.* **C 74** (2014) 3130 [arXiv:1407.3935] [INSPIRE].

[61] ATLAS collaboration, *Electron reconstruction and identification efficiency measurements with the ATLAS detector using the* 2011 *LHC proton-proton collision data*, *Eur. Phys. J.* **C 74** (2014) 2941 [arXiv:1404.2240] [INSPIRE].

[62] ATLAS collaboration, *Electron efficiency measurements with the ATLAS detector using the* 2012 *LHC proton-proton collision data*, ATLAS-CONF-2014-032, CERN, Geneva Switzerland (2014).

[63] ATLAS collaboration, *Properties of jets and inputs to jet reconstruction and calibration with the ATLAS detector using proton-proton collisions at* $\sqrt{s} = 7$ *TeV*, ATLAS-CONF-2010-053, CERN, Geneva Switzerland (2010).

[64] M. Cacciari, G.P. Salam and G. Soyez, *The anti-k_t jet clustering algorithm*, *JHEP* **04** (2008) 063 [arXiv:0802.1189] [INSPIRE].

[65] ATLAS collaboration, *Commissioning of the ATLAS high-performance b-tagging algorithms in the* 7 *TeV collision data*, ATLAS-CONF-2011-102, CERN, Geneva Switzerland (2011).

[66] ATLAS collaboration, *Calibration of the b-tagging efficiency for c jets with the ATLAS detector using events with a W boson produced in association with a single c quark*, ATLAS-CONF-2013-109, CERN, Geneva Switzerland (2013).

[67] ATLAS collaboration, *Calibration of the performance of b-tagging for c and light-flavour jets in the* 2012 *ATLAS data*, ATLAS-CONF-2014-046, CERN, Geneva Switzerland (2014).

[68] ATLAS collaboration, *Performance of missing transverse momentum reconstruction in proton-proton collisions at* 7 *TeV with ATLAS*, *Eur. Phys. J.* **C 72** (2012) 1844 [arXiv:1108.5602] [INSPIRE].

[69] ATLAS collaboration, *Pile-up suppression in missing transverse momentum reconstruction in the ATLAS experiment in proton-proton collisions at* $\sqrt{s} = 8$ *TeV*, ATLAS-CONF-2014-019, CERN, Geneva Switzerland (2014).

[70] ATLAS collaboration, *Measurement of the missing transverse momentum based on tracks in proton-proton collisions at* $\sqrt{s} = 900$ *GeV centre-of-mass energy with the ATLAS detector*, ATLAS-CONF-2010-020, CERN, Geneva Switzerland (2010).

[71] A. Höcker et al., *TMVA — Toolkit for MultiVariate data Analysis*, PoS(ACAT)040 [physics/0703039] [INSPIRE].

JHEP08(2015)137

[72] G. Luisoni, P. Nason, C. Oleari and F. Tramontano, *$HW^{\pm}/HZ + 0$ and 1 jet at NLO with the POWHEG BOX interfaced to GoSam and their merging within MiNLO*, *JHEP* **10** (2013) 083 [arXiv:1306.2542] [INSPIRE].

[73] F. Campanario, V. Hankele, C. Oleari, S. Prestel and D. Zeppenfeld, *QCD corrections to charged triple vector boson production with leptonic decay*, *Phys. Rev.* **D 78** (2008) 094012 [arXiv:0809.0790] [INSPIRE].

[74] M. Botje et al., *The PDF4LHC working group interim recommendations*, arXiv:1101.0538 [INSPIRE].

[75] ATLAS collaboration, *Jet energy measurement and its systematic uncertainty in proton-proton collisions at $\sqrt{s} = 7$ TeV with the ATLAS detector*, *Eur. Phys. J.* **C 75** (2015) 17 [arXiv:1406.0076] [INSPIRE].

[76] ATLAS collaboration, *Calibration of b-tagging using dileptonic top pair events in a combinatorial likelihood approach with the ATLAS experiment*, ATLAS-CONF-2014-004, CERN, Geneva Switzerland (2014).

[77] ATLAS collaboration, *Improved luminosity determination in pp collisions at $\sqrt{s} = 7$ TeV using the ATLAS detector at the LHC*, *Eur. Phys. J.* **C 73** (2013) 2518 [arXiv:1302.4393] [INSPIRE].

[78] G. Cowan, K. Cranmer, E. Gross and O. Vitells, *Asymptotic formulae for likelihood-based tests of new physics*, *Eur. Phys. J.* **C 71** (2011) 1554 [*Erratum ibid.* **C 73** (2013) 2501] [arXiv:1007.1727] [INSPIRE].

[79] ATLAS collaboration, *Measurement of the Higgs boson mass from the $H \to \gamma\gamma$ and $H \to ZZ^* \to 4\ell$ channels with the ATLAS detector using 25 fb^{-1} of pp collision data*, *Phys. Rev.* **D 90** (2014) 052004 [arXiv:1406.3827] [INSPIRE].

[80] ATLAS collaboration, *Measurements of the Higgs boson production and decay rates and coupling strengths using pp collision data at $\sqrt{s} = 7$ and 8 TeV in the ATLAS experiment*, arXiv:1507.04548 [INSPIRE].

[81] C. Englert, M. McCullough and M. Spannowsky, *Gluon-initiated associated production boosts Higgs physics*, *Phys. Rev.* **D 89** (2014) 013013 [arXiv:1310.4828] [INSPIRE].

JHEP08(2015)137

The ATLAS collaboration

G. Aad[85], B. Abbott[113], J. Abdallah[151], O. Abdinov[11], R. Aben[107], M. Abolins[90], O.S. AbouZeid[158], H. Abramowicz[153], H. Abreu[152], R. Abreu[30], Y. Abulaiti[146a,146b], B.S. Acharya[164a,164b,a], L. Adamczyk[38a], D.L. Adams[25], J. Adelman[108], S. Adomeit[100], T. Adye[131], A.A. Affolder[74], T. Agatonovic-Jovin[13], J.A. Aguilar-Saavedra[126a,126f], S.P. Ahlen[22], F. Ahmadov[65,b], G. Aielli[133a,133b], H. Akerstedt[146a,146b], T.P.A. Åkesson[81], G. Akimoto[155], A.V. Akimov[96], G.L. Alberghi[20a,20b], J. Albert[169], S. Albrand[55], M.J. Alconada Verzini[71], M. Aleksa[30], I.N. Aleksandrov[65], C. Alexa[26a], G. Alexander[153], T. Alexopoulos[10], M. Alhroob[113], G. Alimonti[91a], L. Alio[85], J. Alison[31], S.P. Alkire[35], B.M.M. Allbrooke[18], P.P. Allport[74], A. Aloisio[104a,104b], A. Alonso[36], F. Alonso[71], C. Alpigiani[76], A. Altheimer[35], B. Alvarez Gonzalez[30], D. Álvarez Piqueras[167], M.G. Alviggi[104a,104b], B.T. Amadio[15], K. Amako[66], Y. Amaral Coutinho[24a], C. Amelung[23], D. Amidei[89], S.P. Amor Dos Santos[126a,126c], A. Amorim[126a,126b], S. Amoroso[48], N. Amram[153], G. Amundsen[23], C. Anastopoulos[139], L.S. Ancu[49], N. Andari[30], T. Andeen[35], C.F. Anders[58b], G. Anders[30], J.K. Anders[74], K.J. Anderson[31], A. Andreazza[91a,91b], V. Andrei[58a], S. Angelidakis[9], I. Angelozzi[107], P. Anger[44], A. Angerami[35], F. Anghinolfi[30], A.V. Anisenkov[109,c], N. Anjos[12], A. Annovi[124a,124b], M. Antonelli[47], A. Antonov[98], J. Antos[144b], F. Anulli[132a], M. Aoki[66], L. Aperio Bella[18], G. Arabidze[90], Y. Arai[66], J.P. Araque[126a], A.T.H. Arce[45], F.A. Arduh[71], J-F. Arguin[95], S. Argyropoulos[42], M. Arik[19a], A.J. Armbruster[30], O. Arnaez[30], V. Arnal[82], H. Arnold[48], M. Arratia[28], O. Arslan[21], A. Artamonov[97], G. Artoni[23], S. Asai[155], N. Asbah[42], A. Ashkenazi[153], B. Åsman[146a,146b], L. Asquith[149], K. Assamagan[25], R. Astalos[144a], M. Atkinson[165], N.B. Atlay[141], B. Auerbach[6], K. Augsten[128], M. Aurousseau[145b], G. Avolio[30], B. Axen[15], M.K. Ayoub[117], G. Azuelos[95,d], M.A. Baak[30], A.E. Baas[58a], C. Bacci[134a,134b], H. Bachacou[136], K. Bachas[154], M. Backes[30], M. Backhaus[30], P. Bagiacchi[132a,132b], P. Bagnaia[132a,132b], Y. Bai[33a], T. Bain[35], J.T. Baines[131], O.K. Baker[176], P. Balek[129], T. Balestri[148], F. Balli[84], E. Banas[39], Sw. Banerjee[173], A.A.E. Bannoura[175], H.S. Bansil[18], L. Barak[30], E.L. Barberio[88], D. Barberis[50a,50b], M. Barbero[85], T. Barillari[101], M. Barisonzi[164a,164b], T. Barklow[143], N. Barlow[28], S.L. Barnes[84], B.M. Barnett[131], R.M. Barnett[15], Z. Barnovska[5], A. Baroncelli[134a], G. Barone[49], A.J. Barr[120], F. Barreiro[82], J. Barreiro Guimarães da Costa[57], R. Bartoldus[143], A.E. Barton[72], P. Bartos[144a], A. Basalaev[123], A. Bassalat[117], A. Basye[165], R.L. Bates[53], S.J. Batista[158], J.R. Batley[28], M. Battaglia[137], M. Bauce[132a,132b], F. Bauer[136], H.S. Bawa[143,e], J.B. Beacham[111], M.D. Beattie[72], T. Beau[80], P.H. Beauchemin[161], R. Beccherle[124a,124b], P. Bechtle[21], H.P. Beck[17,f], K. Becker[120], M. Becker[83], S. Becker[100], M. Beckingham[170], C. Becot[117], A.J. Beddall[19c], A. Beddall[19c], V.A. Bednyakov[65], C.P. Bee[148], L.J. Beemster[107], T.A. Beermann[175], M. Begel[25], J.K. Behr[120], C. Belanger-Champagne[87], W.H. Bell[49], G. Bella[153], L. Bellagamba[20a], A. Bellerive[29], M. Bellomo[86], K. Belotskiy[98], O. Beltramello[30], O. Benary[153], D. Benchekroun[135a], M. Bender[100], K. Bendtz[146a,146b], N. Benekos[10], Y. Benhammou[153], E. Benhar Noccioli[49], J.A. Benitez Garcia[159b], D.P. Benjamin[45], J.R. Bensinger[23], S. Bentvelsen[107], L. Beresford[120], M. Beretta[47], D. Berge[107], E. Bergeaas Kuutmann[166], N. Berger[5], F. Berghaus[169], J. Beringer[15], C. Bernard[22], N.R. Bernard[86], C. Bernius[110], F.U. Bernlochner[21], T. Berry[77], P. Berta[129], C. Bertella[83], G. Bertoli[146a,146b], F. Bertolucci[124a,124b], C. Bertsche[113], D. Bertsche[113], M.I. Besana[91a], G.J. Besjes[106], O. Bessidskaia Bylund[146a,146b], M. Bessner[42], N. Besson[136], C. Betancourt[48], S. Bethke[101], A.J. Bevan[76], W. Bhimji[46], R.M. Bianchi[125], L. Bianchini[23], M. Bianco[30], O. Biebel[100], S.P. Bieniek[78], M. Biglietti[134a], J. Bilbao De Mendizabal[49], H. Bilokon[47], M. Bindi[54], S. Binet[117], A. Bingul[19c], C. Bini[132a,132b], C.W. Black[150], J.E. Black[143], K.M. Black[22], D. Blackburn[138], R.E. Blair[6], J.-B. Blanchard[136], J.E. Blanco[77], T. Blazek[144a], I. Bloch[42], C. Blocker[23], W. Blum[83,*], U. Blumenschein[54], G.J. Bobbink[107],

JHEP08(2015)137

V.S. Bobrovnikov[109,c], S.S. Bocchetta[81], A. Bocci[45], C. Bock[100], M. Boehler[48], J.A. Bogaerts[30], A.G. Bogdanchikov[109], C. Bohm[146a], V. Boisvert[77], T. Bold[38a], V. Boldea[26a], A.S. Boldyrev[99], M. Bomben[80], M. Bona[76], M. Boonekamp[136], A. Borisov[130], G. Borissov[72], S. Borroni[42], J. Bortfeldt[100], V. Bortolotto[60a,60b,60c], K. Bos[107], D. Boscherini[20a], M. Bosman[12], J. Boudreau[125], J. Bouffard[2], E.V. Bouhova-Thacker[72], D. Boumediene[34], C. Bourdarios[117], N. Bousson[114], A. Boveia[30], J. Boyd[30], I.R. Boyko[65], I. Bozic[13], J. Bracinik[18], A. Brandt[8], G. Brandt[54], O. Brandt[58a], U. Bratzler[156], B. Brau[86], J.E. Brau[116], H.M. Braun[175,*], S.F. Brazzale[164a,164c], K. Brendlinger[122], A.J. Brennan[88], L. Brenner[107], R. Brenner[166], S. Bressler[172], K. Bristow[145c], T.M. Bristow[46], D. Britton[53], D. Britzger[42], F.M. Brochu[28], I. Brock[21], R. Brock[90], J. Bronner[101], G. Brooijmans[35], T. Brooks[77], W.K. Brooks[32b], J. Brosamer[15], E. Brost[116], J. Brown[55], P.A. Bruckman de Renstrom[39], D. Bruncko[144b], R. Bruneliere[48], A. Bruni[20a], G. Bruni[20a], M. Bruschi[20a], L. Bryngemark[81], T. Buanes[14], Q. Buat[142], P. Buchholz[141], A.G. Buckley[53], S.I. Buda[26a], I.A. Budagov[65], F. Buehrer[48], L. Bugge[119], M.K. Bugge[119], O. Bulekov[98], D. Bullock[8], H. Burckhart[30], S. Burdin[74], B. Burghgrave[108], S. Burke[131], I. Burmeister[43], E. Busato[34], D. Büscher[48], V. Büscher[83], P. Bussey[53], J.M. Butler[22], A.I. Butt[3], C.M. Buttar[53], J.M. Butterworth[78], P. Butti[107], W. Buttinger[25], A. Buzatu[53], A.R. Buzykaev[109,c], S. Cabrera Urbán[167], D. Caforio[128], V.M. Cairo[37a,37b], O. Cakir[4a], P. Calafiura[15], A. Calandri[136], G. Calderini[80], P. Calfayan[100], L.P. Caloba[24a], D. Calvet[34], S. Calvet[34], R. Camacho Toro[49], S. Camarda[42], P. Camarri[133a,133b], D. Cameron[119], L.M. Caminada[15], R. Caminal Armadans[12], S. Campana[30], M. Campanelli[78], A. Campoverde[148], V. Canale[104a,104b], A. Canepa[159a], M. Cano Bret[76], J. Cantero[82], R. Cantrill[126a], T. Cao[40], M.D.M. Capeans Garrido[30], I. Caprini[26a], M. Caprini[26a], M. Capua[37a,37b], R. Caputo[83], R. Cardarelli[133a], T. Carli[30], G. Carlino[104a], L. Carminati[91a,91b], S. Caron[106], E. Carquin[32a], G.D. Carrillo-Montoya[8], J.R. Carter[28], J. Carvalho[126a,126c], D. Casadei[78], M.P. Casado[12], M. Casolino[12], E. Castaneda-Miranda[145b], A. Castelli[107], V. Castillo Gimenez[167], N.F. Castro[126a,g], P. Catastini[57], A. Catinaccio[30], J.R. Catmore[119], A. Cattai[30], J. Caudron[83], V. Cavaliere[165], D. Cavalli[91a], M. Cavalli-Sforza[12], V. Cavasinni[124a,124b], F. Ceradini[134a,134b], B.C. Cerio[45], K. Cerny[129], A.S. Cerqueira[24b], A. Cerri[149], L. Cerrito[76], F. Cerutti[15], M. Cerv[30], A. Cervelli[17], S.A. Cetin[19b], A. Chafaq[135a], D. Chakraborty[108], I. Chalupkova[129], P. Chang[165], B. Chapleau[87], J.D. Chapman[28], D.G. Charlton[18], C.C. Chau[158], C.A. Chavez Barajas[149], S. Cheatham[152], A. Chegwidden[90], S. Chekanov[6], S.V. Chekulaev[159a], G.A. Chelkov[65,h], M.A. Chelstowska[89], C. Chen[64], H. Chen[25], K. Chen[148], L. Chen[33d,i], S. Chen[33c], X. Chen[33f], Y. Chen[67], H.C. Cheng[89], Y. Cheng[31], A. Cheplakov[65], E. Cheremushkina[130], R. Cherkaoui El Moursli[135e], V. Chernyatin[25,*], E. Cheu[7], L. Chevalier[136], V. Chiarella[47], J.T. Childers[6], G. Chiodini[73a], A.S. Chisholm[18], R.T. Chislett[78], A. Chitan[26a], M.V. Chizhov[65], K. Choi[61], S. Chouridou[9], B.K.B. Chow[100], V. Christodoulou[78], D. Chromek-Burckhart[30], M.L. Chu[151], J. Chudoba[127], A.J. Chuinard[87], J.J. Chwastowski[39], L. Chytka[115], G. Ciapetti[132a,132b], A.K. Ciftci[4a], D. Cinca[53], V. Cindro[75], I.A. Cioara[21], A. Ciocio[15], Z.H. Citron[172], M. Ciubancan[26a], A. Clark[49], B.L. Clark[57], P.J. Clark[46], R.N. Clarke[15], W. Cleland[125], C. Clement[146a,146b], Y. Coadou[85], M. Cobal[164a,164c], A. Coccaro[138], J. Cochran[64], L. Coffey[23], J.G. Cogan[143], B. Cole[35], S. Cole[108], A.P. Colijn[107], J. Collot[55], T. Colombo[58c], G. Compostella[101], P. Conde Muiño[126a,126b], E. Coniavitis[48], S.H. Connell[145b], I.A. Connelly[77], S.M. Consonni[91a,91b], V. Consorti[48], S. Constantinescu[26a], C. Conta[121a,121b], G. Conti[30], F. Conventi[104a,j], M. Cooke[15], B.D. Cooper[78], A.M. Cooper-Sarkar[120], T. Cornelissen[175], M. Corradi[20a], F. Corriveau[87,k], A. Corso-Radu[163], A. Cortes-Gonzalez[12], G. Cortiana[101], G. Costa[91a], M.J. Costa[167], D. Costanzo[139], D. Côté[8], G. Cottin[28], G. Cowan[77], B.E. Cox[84], K. Cranmer[110], G. Cree[29], S. Crépé-Renaudin[55], F. Crescioli[80], W.A. Cribbs[146a,146b], M. Crispin Ortuzar[120], M. Cristinziani[21], V. Croft[106],

JHEP08(2015)137

G. Crosetti[37a,37b], T. Cuhadar Donszelmann[139], J. Cummings[176], M. Curatolo[47], C. Cuthbert[150], H. Czirr[141], P. Czodrowski[3], S. D'Auria[53], M. D'Onofrio[74], M.J. Da Cunha Sargedas De Sousa[126a,126b], C. Da Via[84], W. Dabrowski[38a], A. Dafinca[120], T. Dai[89], O. Dale[14], F. Dallaire[95], C. Dallapiccola[86], M. Dam[36], J.R. Dandoy[31], N.P. Dang[48], A.C. Daniells[18], M. Danninger[168], M. Dano Hoffmann[136], V. Dao[48], G. Darbo[50a], S. Darmora[8], J. Dassoulas[3], A. Dattagupta[61], W. Davey[21], C. David[169], T. Davidek[129], E. Davies[120,l], M. Davies[153], P. Davison[78], Y. Davygora[58a], E. Dawe[88], I. Dawson[139], R.K. Daya-Ishmukhametova[86], K. De[8], R. de Asmundis[104a], S. De Castro[20a,20b], S. De Cecco[80], N. De Groot[106], P. de Jong[107], H. De la Torre[82], F. De Lorenzi[64], L. De Nooij[107], D. De Pedis[132a], A. De Salvo[132a], U. De Sanctis[149], A. De Santo[149], J.B. De Vivie De Regie[117], W.J. Dearnaley[72], R. Debbe[25], C. Debenedetti[137], D.V. Dedovich[65], I. Deigaard[107], J. Del Peso[82], T. Del Prete[124a,124b], D. Delgove[117], F. Deliot[136], C.M. Delitzsch[49], M. Deliyergiyev[75], A. Dell'Acqua[30], L. Dell'Asta[22], M. Dell'Orso[124a,124b], M. Della Pietra[104a,j], D. della Volpe[49], M. Delmastro[5], P.A. Delsart[55], C. Deluca[107], D.A. DeMarco[158], S. Demers[176], M. Demichev[65], A. Demilly[80], S.P. Denisov[130], D. Derendarz[39], J.E. Derkaoui[135d], F. Derue[80], P. Dervan[74], K. Desch[21], C. Deterre[42], P.O. Deviveiros[30], A. Dewhurst[131], S. Dhaliwal[23], A. Di Ciaccio[133a,133b], L. Di Ciaccio[5], A. Di Domenico[132a,132b], C. Di Donato[104a,104b], A. Di Girolamo[30], B. Di Girolamo[30], A. Di Mattia[152], B. Di Micco[134a,134b], R. Di Nardo[47], A. Di Simone[48], R. Di Sipio[158], D. Di Valentino[29], C. Diaconu[85], M. Diamond[158], F.A. Dias[46], M.A. Diaz[32a], E.B. Diehl[89], J. Dietrich[16], S. Diglio[85], A. Dimitrievska[13], J. Dingfelder[21], P. Dita[26a], S. Dita[26a], F. Dittus[30], F. Djama[85], T. Djobava[51b], J.I. Djuvsland[58a], M.A.B. do Vale[24c], D. Dobos[30], M. Dobre[26a], C. Doglioni[49], T. Dohmae[155], J. Dolejsi[129], Z. Dolezal[129], B.A. Dolgoshein[98,*], M. Donadelli[24d], S. Donati[124a,124b], P. Dondero[121a,121b], J. Donini[34], J. Dopke[131], A. Doria[104a], M.T. Dova[71], A.T. Doyle[53], E. Drechsler[54], M. Dris[10], E. Dubreuil[34], E. Duchovni[172], G. Duckeck[100], O.A. Ducu[26a,85], D. Duda[175], A. Dudarev[30], L. Duflot[117], L. Duguid[77], M. Dührssen[30], M. Dunford[58a], H. Duran Yildiz[4a], M. Düren[52], A. Durglishvili[51b], D. Duschinger[44], M. Dyndal[38a], C. Eckardt[42], K.M. Ecker[101], R.C. Edgar[89], W. Edson[2], N.C. Edwards[46], W. Ehrenfeld[21], T. Eifert[30], G. Eigen[14], K. Einsweiler[15], T. Ekelof[166], M. El Kacimi[135c], M. Ellert[166], S. Elles[5], F. Ellinghaus[83], A.A. Elliot[169], N. Ellis[30], J. Elmsheuser[100], M. Elsing[30], D. Emeliyanov[131], Y. Enari[155], O.C. Endner[83], M. Endo[118], J. Erdmann[43], A. Ereditato[17], G. Ernis[175], J. Ernst[2], M. Ernst[25], S. Errede[165], E. Ertel[83], M. Escalier[117], H. Esch[43], C. Escobar[125], B. Esposito[47], A.I. Etienvre[136], E. Etzion[153], H. Evans[61], A. Ezhilov[123], L. Fabbri[20a,20b], G. Facini[31], R.M. Fakhrutdinov[130], S. Falciano[132a], R.J. Falla[78], J. Faltova[129], Y. Fang[33a], M. Fanti[91a,91b], A. Farbin[8], A. Farilla[134a], T. Farooque[12], S. Farrell[15], S.M. Farrington[170], P. Farthouat[30], F. Fassi[135e], P. Fassnacht[30], D. Fassouliotis[9], M. Faucci Giannelli[77], A. Favareto[50a,50b], L. Fayard[117], P. Federic[144a], O.L. Fedin[123,m], W. Fedorko[168], S. Feigl[30], L. Feligioni[85], C. Feng[33d], E.J. Feng[6], H. Feng[89], A.B. Fenyuk[130], P. Fernandez Martinez[167], S. Fernandez Perez[30], J. Ferrando[53], A. Ferrari[166], P. Ferrari[107], R. Ferrari[121a], D.E. Ferreira de Lima[53], A. Ferrer[167], D. Ferrere[49], C. Ferretti[89], A. Ferretto Parodi[50a,50b], M. Fiascaris[31], F. Fiedler[83], A. Filipčič[75], M. Filipuzzi[42], F. Filthaut[106], M. Fincke-Keeler[169], K.D. Finelli[150], M.C.N. Fiolhais[126a,126c], L. Fiorini[167], A. Firan[40], A. Fischer[2], C. Fischer[12], J. Fischer[175], W.C. Fisher[90], E.A. Fitzgerald[23], M. Flechl[48], I. Fleck[141], P. Fleischmann[89], S. Fleischmann[175], G.T. Fletcher[139], G. Fletcher[76], T. Flick[175], A. Floderus[81], L.R. Flores Castillo[60a], M.J. Flowerdew[101], A. Formica[136], A. Forti[84], D. Fournier[117], H. Fox[72], S. Fracchia[12], P. Francavilla[80], M. Franchini[20a,20b], D. Francis[30], L. Franconi[119], M. Franklin[57], M. Fraternali[121a,121b], D. Freeborn[78], S.T. French[28], F. Friedrich[44], D. Froidevaux[30], J.A. Frost[120], C. Fukunaga[156], E. Fullana Torregrosa[83], B.G. Fulsom[143], J. Fuster[167], C. Gabaldon[55], O. Gabizon[175], A. Gabrielli[20a,20b], A. Gabrielli[132a,132b], S. Gadatsch[107],

JHEP08(2015)137

S. Gadomski[49], G. Gagliardi[50a,50b], P. Gagnon[61], C. Galea[106], B. Galhardo[126a,126c], E.J. Gallas[120], B.J. Gallop[131], P. Gallus[128], G. Galster[36], K.K. Gan[111], J. Gao[33b,85], Y. Gao[46], Y.S. Gao[143,e], F.M. Garay Walls[46], F. Garberson[176], C. García[167], J.E. García Navarro[167], M. Garcia-Sciveres[15], R.W. Gardner[31], N. Garelli[143], V. Garonne[119], C. Gatti[47], A. Gaudiello[50a,50b], G. Gaudio[121a], B. Gaur[141], L. Gauthier[95], P. Gauzzi[132a,132b], I.L. Gavrilenko[96], C. Gay[168], G. Gaycken[21], E.N. Gazis[10], P. Ge[33d], Z. Gecse[168], C.N.P. Gee[131], D.A.A. Geerts[107], Ch. Geich-Gimbel[21], M.P. Geisler[58a], C. Gemme[50a], M.H. Genest[55], S. Gentile[132a,132b], M. George[54], S. George[77], D. Gerbaudo[163], A. Gershon[153], H. Ghazlane[135b], B. Giacobbe[20a], S. Giagu[132a,132b], V. Giangiobbe[12], P. Giannetti[124a,124b], B. Gibbard[25], S.M. Gibson[77], M. Gilchriese[15], T.P.S. Gillam[28], D. Gillberg[30], G. Gilles[34], D.M. Gingrich[3,d], N. Giokaris[9], M.P. Giordani[164a,164c], F.M. Giorgi[20a], F.M. Giorgi[16], P.F. Giraud[136], P. Giromini[47], D. Giugni[91a], C. Giuliani[48], M. Giulini[58b], B.K. Gjelsten[119], S. Gkaitatzis[154], I. Gkialas[154], E.L. Gkougkousis[117], L.K. Gladilin[99], C. Glasman[82], J. Glatzer[30], P.C.F. Glaysher[46], A. Glazov[42], M. Goblirsch-Kolb[101], J.R. Goddard[76], J. Godlewski[39], S. Goldfarb[89], T. Golling[49], D. Golubkov[130], A. Gomes[126a,126b,126d], R. Gonçalo[126a], J. Goncalves Pinto Firmino Da Costa[136], L. Gonella[21], S. González de la Hoz[167], G. Gonzalez Parra[12], S. Gonzalez-Sevilla[49], L. Goossens[30], P.A. Gorbounov[97], H.A. Gordon[25], I. Gorelov[105], B. Gorini[30], E. Gorini[73a,73b], A. Gorišek[75], E. Gornicki[39], A.T. Goshaw[45], C. Gössling[43], M.I. Gostkin[65], D. Goujdami[135c], A.G. Goussiou[138], N. Govender[145b], H.M.X. Grabas[137], L. Graber[54], I. Grabowska-Bold[38a], P. Grafström[20a,20b], K-J. Grahn[42], J. Gramling[49], E. Gramstad[119], S. Grancagnolo[16], V. Grassi[148], V. Gratchev[123], H.M. Gray[30], E. Graziani[134a], Z.D. Greenwood[79,n], K. Gregersen[78], I.M. Gregor[42], P. Grenier[143], J. Griffiths[8], A.A. Grillo[137], K. Grimm[72], S. Grinstein[12,o], Ph. Gris[34], J.-F. Grivaz[117], J.P. Grohs[44], A. Grohsjean[42], E. Gross[172], J. Grosse-Knetter[54], G.C. Grossi[79], Z.J. Grout[149], L. Guan[33b], J. Guenther[128], F. Guescini[49], D. Guest[176], O. Gueta[153], E. Guido[50a,50b], T. Guillemin[117], S. Guindon[2], U. Gul[53], C. Gumpert[44], J. Guo[33e], S. Gupta[120], P. Gutierrez[113], N.G. Gutierrez Ortiz[53], C. Gutschow[44], C. Guyot[136], C. Gwenlan[120], C.B. Gwilliam[74], A. Haas[110], C. Haber[15], H.K. Hadavand[8], N. Haddad[135e], P. Haefner[21], S. Hageböck[21], Z. Hajduk[39], H. Hakobyan[177], M. Haleem[42], J. Haley[114], D. Hall[120], G. Halladjian[90], G.D. Hallewell[85], K. Hamacher[175], P. Hamal[115], K. Hamano[169], M. Hamer[54], A. Hamilton[145a], S. Hamilton[161], G.N. Hamity[145c], P.G. Hamnett[42], L. Han[33b], K. Hanagaki[118], K. Hanawa[155], M. Hance[15], P. Hanke[58a], R. Hanna[136], J.B. Hansen[36], J.D. Hansen[36], M.C. Hansen[21], P.H. Hansen[36], K. Hara[160], A.S. Hard[173], T. Harenberg[175], F. Hariri[117], S. Harkusha[92], R.D. Harrington[46], P.F. Harrison[170], F. Hartjes[107], M. Hasegawa[67], S. Hasegawa[103], Y. Hasegawa[140], A. Hasib[113], S. Hassani[136], S. Haug[17], R. Hauser[90], L. Hauswald[44], M. Havranek[127], C.M. Hawkes[18], R.J. Hawkings[30], A.D. Hawkins[81], T. Hayashi[160], D. Hayden[90], C.P. Hays[120], J.M. Hays[76], H.S. Hayward[74], S.J. Haywood[131], S.J. Head[18], T. Heck[83], V. Hedberg[81], L. Heelan[8], S. Heim[122], T. Heim[175], B. Heinemann[15], L. Heinrich[110], J. Hejbal[127], L. Helary[22], S. Hellman[146a,146b], D. Hellmich[21], C. Helsens[30], J. Henderson[120], R.C.W. Henderson[72], Y. Heng[173], C. Hengler[42], A. Henrichs[176], A.M. Henriques Correia[30], S. Henrot-Versille[117], G.H. Herbert[16], Y. Hernández Jiménez[167], R. Herrberg-Schubert[16], G. Herten[48], R. Hertenberger[100], L. Hervas[30], G.G. Hesketh[78], N.P. Hessey[107], J.W. Hetherly[40], R. Hickling[76], E. Higón-Rodriguez[167], E. Hill[169], J.C. Hill[28], K.H. Hiller[42], S.J. Hillier[18], I. Hinchliffe[15], E. Hines[122], R.R. Hinman[15], M. Hirose[157], D. Hirschbuehl[175], J. Hobbs[148], N. Hod[107], M.C. Hodgkinson[139], P. Hodgson[139], A. Hoecker[30], M.R. Hoeferkamp[105], F. Hoenig[100], M. Hohlfeld[83], D. Hohn[21], T.R. Holmes[15], M. Homann[43], T.M. Hong[125], L. Hooft van Huysduynen[110], W.H. Hopkins[116], Y. Horii[103], A.J. Horton[142], J-Y. Hostachy[55], S. Hou[151], A. Hoummada[135a], J. Howard[120], J. Howarth[42], M. Hrabovsky[115], I. Hristova[16], J. Hrivnac[117], T. Hryn'ova[5], A. Hrynevich[93], C. Hsu[145c], P.J. Hsu[151,p], S.-C. Hsu[138], D. Hu[35],

JHEP08(2015)137

Q. Hu[33b], X. Hu[89], Y. Huang[42], Z. Hubacek[30], F. Hubaut[85], F. Huegging[21], T.B. Huffman[120], E.W. Hughes[35], G. Hughes[72], M. Huhtinen[30], T.A. Hülsing[83], N. Huseynov[65,b], J. Huston[90], J. Huth[57], G. Iacobucci[49], G. Iakovidis[25], I. Ibragimov[141], L. Iconomidou-Fayard[117], E. Ideal[176], Z. Idrissi[135e], P. Iengo[30], O. Igonkina[107], T. Iizawa[171], Y. Ikegami[66], K. Ikematsu[141], M. Ikeno[66], Y. Ilchenko[31,q], D. Iliadis[154], N. Ilic[158], Y. Inamaru[67], T. Ince[101], P. Ioannou[9], M. Iodice[134a], K. Iordanidou[35], V. Ippolito[57], A. Irles Quiles[167], C. Isaksson[166], M. Ishino[68], M. Ishitsuka[157], R. Ishmukhametov[111], C. Issever[120], S. Istin[19a], J.M. Iturbe Ponce[84], R. Iuppa[133a,133b], J. Ivarsson[81], W. Iwanski[39], H. Iwasaki[66], J.M. Izen[41], V. Izzo[104a], S. Jabbar[3], B. Jackson[122], M. Jackson[74], P. Jackson[1], M.R. Jaekel[30], V. Jain[2], K. Jakobs[48], S. Jakobsen[30], T. Jakoubek[127], J. Jakubek[128], D.O. Jamin[151], D.K. Jana[79], E. Jansen[78], R.W. Jansky[62], J. Janssen[21], M. Janus[170], G. Jarlskog[81], N. Javadov[65,b], T. Javůrek[48], L. Jeanty[15], J. Jejelava[51a,r], G.-Y. Jeng[150], D. Jennens[88], P. Jenni[48,s], J. Jentzsch[43], C. Jeske[170], S. Jézéquel[5], H. Ji[173], J. Jia[148], Y. Jiang[33b], S. Jiggins[78], J. Jimenez Pena[167], S. Jin[33a], A. Jinaru[26a], O. Jinnouchi[157], M.D. Joergensen[36], P. Johansson[139], K.A. Johns[7], K. Jon-And[146a,146b], G. Jones[170], R.W.L. Jones[72], T.J. Jones[74], J. Jongmanns[58a], P.M. Jorge[126a,126b], K.D. Joshi[84], J. Jovicevic[159a], X. Ju[173], C.A. Jung[43], P. Jussel[62], A. Juste Rozas[12,o], M. Kaci[167], A. Kaczmarska[39], M. Kado[117], H. Kagan[111], M. Kagan[143], S.J. Kahn[85], E. Kajomovitz[45], C.W. Kalderon[120], S. Kama[40], A. Kamenshchikov[130], N. Kanaya[155], M. Kaneda[30], S. Kaneti[28], V.A. Kantserov[98], J. Kanzaki[66], B. Kaplan[110], A. Kapliy[31], D. Kar[53], K. Karakostas[10], A. Karamaoun[3], N. Karastathis[10,107], M.J. Kareem[54], M. Karnevskiy[83], S.N. Karpov[65], Z.M. Karpova[65], K. Karthik[110], V. Kartvelishvili[72], A.N. Karyukhin[130], L. Kashif[173], R.D. Kass[111], A. Kastanas[14], Y. Kataoka[155], A. Katre[49], J. Katzy[42], K. Kawagoe[70], T. Kawamoto[155], G. Kawamura[54], S. Kazama[155], V.F. Kazanin[109,c], M.Y. Kazarinov[65], R. Keeler[169], R. Kehoe[40], J.S. Keller[42], J.J. Kempster[77], H. Keoshkerian[84], O. Kepka[127], B.P. Kerševan[75], S. Kersten[175], R.A. Keyes[87], F. Khalil-zada[11], H. Khandanyan[146a,146b], A. Khanov[114], A.G. Kharlamov[109,c], T.J. Khoo[28], V. Khovanskiy[97], E. Khramov[65], J. Khubua[51b,t], H.Y. Kim[8], H. Kim[146a,146b], S.H. Kim[160], Y. Kim[31], N. Kimura[154], O.M. Kind[16], B.T. King[74], M. King[167], R.S.B. King[120], S.B. King[168], J. Kirk[131], A.E. Kiryunin[101], T. Kishimoto[67], D. Kisielewska[38a], F. Kiss[48], K. Kiuchi[160], O. Kivernyk[136], E. Kladiva[144b], M.H. Klein[35], M. Klein[74], U. Klein[74], K. Kleinknecht[83], P. Klimek[146a,146b], A. Klimentov[25], R. Klingenberg[43], J.A. Klinger[84], T. Klioutchnikova[30], E.-E. Kluge[58a], P. Kluit[107], S. Kluth[101], E. Kneringer[62], E.B.F.G. Knoops[85], A. Knue[53], A. Kobayashi[155], D. Kobayashi[157], T. Kobayashi[155], M. Kobel[44], M. Kocian[143], P. Kodys[129], T. Koffas[29], E. Koffeman[107], L.A. Kogan[120], S. Kohlmann[175], Z. Kohout[128], T. Kohriki[66], T. Koi[143], H. Kolanoski[16], I. Koletsou[5], A.A. Komar[96,*], Y. Komori[155], T. Kondo[66], N. Kondrashova[42], K. Köneke[48], A.C. König[106], S. König[83], T. Kono[66,u], R. Konoplich[110,v], N. Konstantinidis[78], R. Kopeliansky[152], S. Koperny[38a], L. Köpke[83], A.K. Kopp[48], K. Korcyl[39], K. Kordas[154], A. Korn[78], A.A. Korol[109,c], I. Korolkov[12], E.V. Korolkova[139], O. Kortner[101], S. Kortner[101], T. Kosek[129], V.V. Kostyukhin[21], V.M. Kotov[65], A. Kotwal[45], A. Kourkoumeli-Charalampidi[154], C. Kourkoumelis[9], V. Kouskoura[25], A. Koutsman[159a], R. Kowalewski[169], T.Z. Kowalski[38a], W. Kozanecki[136], A.S. Kozhin[130], V.A. Kramarenko[99], G. Kramberger[75], D. Krasnopevtsev[98], M.W. Krasny[80], A. Krasznahorkay[30], J.K. Kraus[21], A. Kravchenko[25], S. Kreiss[110], M. Kretz[58c], J. Kretzschmar[74], K. Kreutzfeldt[52], P. Krieger[158], K. Krizka[31], K. Kroeninger[43], H. Kroha[101], J. Kroll[122], J. Kroseberg[21], J. Krstic[13], U. Kruchonak[65], H. Krüger[21], N. Krumnack[64], Z.V. Krumshteyn[65], A. Kruse[173], M.C. Kruse[45], M. Kruskal[22], T. Kubota[88], H. Kucuk[78], S. Kuday[4c], S. Kuehn[48], A. Kugel[58c], F. Kuger[174], A. Kuhl[137], T. Kuhl[42], V. Kukhtin[65], Y. Kulchitsky[92], S. Kuleshov[32b], M. Kuna[132a,132b], T. Kunigo[68], A. Kupco[127], H. Kurashige[67], Y.A. Kurochkin[92], R. Kurumida[67], V. Kus[127], E.S. Kuwertz[169], M. Kuze[157], J. Kvita[115], T. Kwan[169], D. Kyriazopoulos[139], A. La Rosa[49], J.L. La Rosa Navarro[24d], L. La Rotonda[37a,37b],

JHEP08(2015)137

C. Lacasta[167], F. Lacava[132a,132b], J. Lacey[29], H. Lacker[16], D. Lacour[80], V.R. Lacuesta[167], E. Ladygin[65], R. Lafaye[5], B. Laforge[80], T. Lagouri[176], S. Lai[48], L. Lambourne[78], S. Lammers[61], C.L. Lampen[7], W. Lampl[7], E. Lançon[136], U. Landgraf[48], M.P.J. Landon[76], V.S. Lang[58a], J.C. Lange[12], A.J. Lankford[163], F. Lanni[25], K. Lantzsch[30], S. Laplace[80], C. Lapoire[30], J.F. Laporte[136], T. Lari[91a], F. Lasagni Manghi[20a,20b], M. Lassnig[30], P. Laurelli[47], W. Lavrijsen[15], A.T. Law[137], P. Laycock[74], O. Le Dortz[80], E. Le Guirriec[85], E. Le Menedeu[12], M. LeBlanc[169], T. LeCompte[6], F. Ledroit-Guillon[55], C.A. Lee[145b], S.C. Lee[151], L. Lee[1], G. Lefebvre[80], M. Lefebvre[169], F. Legger[100], C. Leggett[15], A. Lehan[74], G. Lehmann Miotto[30], X. Lei[7], W.A. Leight[29], A. Leisos[154,w], A.G. Leister[176], M.A.L. Leite[24d], R. Leitner[129], D. Lellouch[172], B. Lemmer[54], K.J.C. Leney[78], T. Lenz[21], B. Lenzi[30], R. Leone[7], S. Leone[124a,124b], C. Leonidopoulos[46], S. Leontsinis[10], C. Leroy[95], C.G. Lester[28], M. Levchenko[123], J. Levêque[5], D. Levin[89], L.J. Levinson[172], M. Levy[18], A. Lewis[120], A.M. Leyko[21], M. Leyton[41], B. Li[33b,x], H. Li[148], H.L. Li[31], L. Li[45], L. Li[33e], S. Li[45], Y. Li[33c,y], Z. Liang[137], H. Liao[34], B. Liberti[133a], A. Liblong[158], P. Lichard[30], K. Lie[165], J. Liebal[21], W. Liebig[14], C. Limbach[21], A. Limosani[150], S.C. Lin[151,z], T.H. Lin[83], F. Linde[107], B.E. Lindquist[148], J.T. Linnemann[90], E. Lipeles[122], A. Lipniacka[14], M. Lisovyi[42], T.M. Liss[165], D. Lissauer[25], A. Lister[168], A.M. Litke[137], B. Liu[151,aa], D. Liu[151], J. Liu[85], J.B. Liu[33b], K. Liu[85], L. Liu[165], M. Liu[45], M. Liu[33b], Y. Liu[33b], M. Livan[121a,121b], A. Lleres[55], J. Llorente Merino[82], S.L. Lloyd[76], F. Lo Sterzo[151], E. Lobodzinska[42], P. Loch[7], W.S. Lockman[137], F.K. Loebinger[84], A.E. Loevschall-Jensen[36], A. Loginov[176], T. Lohse[16], K. Lohwasser[42], M. Lokajicek[127], B.A. Long[22], J.D. Long[89], R.E. Long[72], K.A. Looper[111], L. Lopes[126a], D. Lopez Mateos[57], B. Lopez Paredes[139], I. Lopez Paz[12], J. Lorenz[100], N. Lorenzo Martinez[61], M. Losada[162], P. Loscutoff[15], P.J. Lösel[100], X. Lou[33a], A. Lounis[117], J. Love[6], P.A. Love[72], N. Lu[89], H.J. Lubatti[138], C. Luci[132a,132b], A. Lucotte[55], F. Luehring[61], W. Lukas[62], L. Luminari[132a], O. Lundberg[146a,146b], B. Lund-Jensen[147], D. Lynn[25], R. Lysak[127], E. Lytken[81], H. Ma[25], L.L. Ma[33d], G. Maccarrone[47], A. Macchiolo[101], C.M. Macdonald[139], J. Machado Miguens[122,126b], D. Macina[30], D. Madaffari[85], R. Madar[34], H.J. Maddocks[72], W.F. Mader[44], A. Madsen[166], S. Maeland[14], T. Maeno[25], A. Maevskiy[99], E. Magradze[54], K. Mahboubi[48], J. Mahlstedt[107], C. Maiani[136], C. Maidantchik[24a], A.A. Maier[101], T. Maier[100], A. Maio[126a,126b,126d], S. Majewski[116], Y. Makida[66], N. Makovec[117], B. Malaescu[80], Pa. Malecki[39], V.P. Maleev[123], F. Malek[55], U. Mallik[63], D. Malon[6], C. Malone[143], S. Maltezos[10], V.M. Malyshev[109], S. Malyukov[30], J. Mamuzic[42], G. Mancini[47], B. Mandelli[30], L. Mandelli[91a], I. Mandić[75], R. Mandrysch[63], J. Maneira[126a,126b], A. Manfredini[101], L. Manhaes de Andrade Filho[24b], J. Manjarres Ramos[159b], A. Mann[100], P.M. Manning[137], A. Manousakis-Katsikakis[9], B. Mansoulie[136], R. Mantifel[87], M. Mantoani[54], L. Mapelli[30], L. March[145c], G. Marchiori[80], M. Marcisovsky[127], C.P. Marino[169], M. Marjanovic[13], F. Marroquim[24a], S.P. Marsden[84], Z. Marshall[15], L.F. Marti[17], S. Marti-Garcia[167], B. Martin[90], T.A. Martin[170], V.J. Martin[46], B. Martin dit Latour[14], M. Martinez[12,o], S. Martin-Haugh[131], V.S. Martoiu[26a], A.C. Martyniuk[78], M. Marx[138], F. Marzano[132a], A. Marzin[30], L. Masetti[83], T. Mashimo[155], R. Mashinistov[96], J. Masik[84], A.L. Maslennikov[109,c], I. Massa[20a,20b], L. Massa[20a,20b], N. Massol[5], P. Mastrandrea[148], A. Mastroberardino[37a,37b], T. Masubuchi[155], P. Mättig[175], J. Mattmann[83], J. Maurer[26a], S.J. Maxfield[74], D.A. Maximov[109,c], R. Mazini[151], S.M. Mazza[91a,91b], L. Mazzaferro[133a,133b], G. Mc Goldrick[158], S.P. Mc Kee[89], A. McCarn[89], R.L. McCarthy[148], T.G. McCarthy[29], N.A. McCubbin[131], K.W. McFarlane[56,*], J.A. Mcfayden[78], G. Mchedlidze[54], S.J. McMahon[131], R.A. McPherson[169,k], M. Medinnis[42], S. Meehan[145a], S. Mehlhase[100], A. Mehta[74], K. Meier[58a], C. Meineck[100], B. Meirose[41], B.R. Mellado Garcia[145c], F. Meloni[17], A. Mengarelli[20a,20b], S. Menke[101], E. Meoni[161], K.M. Mercurio[57], S. Mergelmeyer[21], P. Mermod[49], L. Merola[104a,104b], C. Meroni[91a], F.S. Merritt[31], A. Messina[132a,132b], J. Metcalfe[25], A.S. Mete[163], C. Meyer[83], C. Meyer[122], J-P. Meyer[136], J. Meyer[107], R.P. Middleton[131],

JHEP08(2015)137

S. Miglioranzi[164a,164c], L. Mijović[21], G. Mikenberg[172], M. Mikestikova[127], M. Mikuž[75], M. Milesi[88], A. Milic[30], D.W. Miller[31], C. Mills[46], A. Milov[172], D.A. Milstead[146a,146b], A.A. Minaenko[130], Y. Minami[155], I.A. Minashvili[65], A.I. Mincer[110], B. Mindur[38a], M. Mineev[65], Y. Ming[173], L.M. Mir[12], T. Mitani[171], J. Mitrevski[100], V.A. Mitsou[167], A. Miucci[49], P.S. Miyagawa[139], J.U. Mjörnmark[81], T. Moa[146a,146b], K. Mochizuki[85], S. Mohapatra[35], W. Mohr[48], S. Molander[146a,146b], R. Moles-Valls[167], K. Mönig[42], C. Monini[55], J. Monk[36], E. Monnier[85], J. Montejo Berlingen[12], F. Monticelli[71], S. Monzani[132a,132b], R.W. Moore[3], N. Morange[117], D. Moreno[162], M. Moreno Llácer[54], P. Morettini[50a], M. Morgenstern[44], M. Morii[57], M. Morinaga[155], V. Morisbak[119], S. Moritz[83], A.K. Morley[147], G. Mornacchi[30], J.D. Morris[76], S.S. Mortensen[36], A. Morton[53], L. Morvaj[103], M. Mosidze[51b], J. Moss[111], K. Motohashi[157], R. Mount[143], E. Mountricha[25], S.V. Mouraviev[96,*], E.J.W. Moyse[86], S. Muanza[85], R.D. Mudd[18], F. Mueller[101], J. Mueller[125], K. Mueller[21], R.S.P. Mueller[100], T. Mueller[28], D. Muenstermann[49], P. Mullen[53], Y. Munwes[153], J.A. Murillo Quijada[18], W.J. Murray[170,131], H. Musheghyan[54], E. Musto[152], A.G. Myagkov[130,ab], M. Myska[128], O. Nackenhorst[54], J. Nadal[54], K. Nagai[120], R. Nagai[157], Y. Nagai[85], K. Nagano[66], A. Nagarkar[111], Y. Nagasaka[59], K. Nagata[160], M. Nagel[101], E. Nagy[85], A.M. Nairz[30], Y. Nakahama[30], K. Nakamura[66], T. Nakamura[155], I. Nakano[112], H. Namasivayam[41], R.F. Naranjo Garcia[42], R. Narayan[31], T. Naumann[42], G. Navarro[162], R. Nayyar[7], H.A. Neal[89], P.Yu. Nechaeva[96], T.J. Neep[84], P.D. Nef[143], A. Negri[121a,121b], M. Negrini[20a], S. Nektarijevic[106], C. Nellist[117], A. Nelson[163], S. Nemecek[127], P. Nemethy[110], A.A. Nepomuceno[24a], M. Nessi[30,ac], M.S. Neubauer[165], M. Neumann[175], R.M. Neves[110], P. Nevski[25], P.R. Newman[18], D.H. Nguyen[6], R.B. Nickerson[120], R. Nicolaidou[136], B. Nicquevert[30], J. Nielsen[137], N. Nikiforou[35], A. Nikiforov[16], V. Nikolaenko[130,ab], I. Nikolic-Audit[80], K. Nikolopoulos[18], J.K. Nilsen[119], P. Nilsson[25], Y. Ninomiya[155], A. Nisati[132a], R. Nisius[101], T. Nobe[157], M. Nomachi[118], I. Nomidis[29], T. Nooney[76], S. Norberg[113], M. Nordberg[30], O. Novgorodova[44], S. Nowak[101], M. Nozaki[66], L. Nozka[115], K. Ntekas[10], G. Nunes Hanninger[88], T. Nunnemann[100], E. Nurse[78], F. Nuti[88], B.J. O'Brien[46], F. O'grady[7], D.C. O'Neil[142], V. O'Shea[53], F.G. Oakham[29,d], H. Oberlack[101], T. Obermann[21], J. Ocariz[80], A. Ochi[67], I. Ochoa[78], J.P. Ochoa-Ricoux[32a], S. Oda[70], S. Odaka[66], H. Ogren[61], A. Oh[84], S.H. Oh[45], C.C. Ohm[15], H. Ohman[166], H. Oide[30], W. Okamura[118], H. Okawa[160], Y. Okumura[31], T. Okuyama[155], A. Olariu[26a], S.A. Olivares Pino[46], D. Oliveira Damazio[25], E. Oliver Garcia[167], A. Olszewski[39], J. Olszowska[39], A. Onofre[126a,126e], P.U.E. Onyisi[31,q], C.J. Oram[159a], M.J. Oreglia[31], Y. Oren[153], D. Orestano[134a,134b], N. Orlando[154], C. Oropeza Barrera[53], R.S. Orr[158], B. Osculati[50a,50b], R. Ospanov[84], G. Otero y Garzon[27], H. Otono[70], M. Ouchrif[135d], E.A. Ouellette[169], F. Ould-Saada[119], A. Ouraou[136], K.P. Oussoren[107], Q. Ouyang[33a], A. Ovcharova[15], M. Owen[53], R.E. Owen[18], V.E. Ozcan[19a], N. Ozturk[8], K. Pachal[142], A. Pacheco Pages[12], C. Padilla Aranda[12], M. Pagáčová[48], S. Pagan Griso[15], E. Paganis[139], C. Pahl[101], F. Paige[25], P. Pais[86], K. Pajchel[119], G. Palacino[159b], S. Palestini[30], M. Palka[38b], D. Pallin[34], A. Palma[126a,126b], Y.B. Pan[173], E. Panagiotopoulou[10], C.E. Pandini[80], J.G. Panduro Vazquez[77], P. Pani[146a,146b], S. Panitkin[25], D. Pantea[26a], L. Paolozzi[49], Th.D. Papadopoulou[10], K. Papageorgiou[154], A. Paramonov[6], D. Paredes Hernandez[154], M.A. Parker[28], K.A. Parker[139], F. Parodi[50a,50b], J.A. Parsons[35], U. Parzefall[48], E. Pasqualucci[132a], S. Passaggio[50a], F. Pastore[134a,134b,*], Fr. Pastore[77], G. Pásztor[29], S. Pataraia[175], N.D. Patel[150], J.R. Pater[84], T. Pauly[30], J. Pearce[169], B. Pearson[113], L.E. Pedersen[36], M. Pedersen[119], S. Pedraza Lopez[167], R. Pedro[126a,126b], S.V. Peleganchuk[109,c], D. Pelikan[166], H. Peng[33b], B. Penning[31], J. Penwell[61], D.V. Perepelitsa[25], E. Perez Codina[159a], M.T. Pérez García-Estañ[167], L. Perini[91a,91b], H. Pernegger[30], S. Perrella[104a,104b], R. Peschke[42], V.D. Peshekhonov[65], K. Peters[30], R.F.Y. Peters[84], B.A. Petersen[30], T.C. Petersen[36], E. Petit[42], A. Petridis[146a,146b], C. Petridou[154], E. Petrolo[132a], F. Petrucci[134a,134b], N.E. Pettersson[157],

JHEP08(2015)137

R. Pezoa[32b], P.W. Phillips[131], G. Piacquadio[143], E. Pianori[170], A. Picazio[49], E. Piccaro[76], M. Piccinini[20a,20b], M.A. Pickering[120], R. Piegaia[27], D.T. Pignotti[111], J.E. Pilcher[31], A.D. Pilkington[84], J. Pina[126a,126b,126d], M. Pinamonti[164a,164c,ad], J.L. Pinfold[3], A. Pingel[36], B. Pinto[126a], S. Pires[80], M. Pitt[172], C. Pizio[91a,91b], L. Plazak[144a], M.-A. Pleier[25], V. Pleskot[129], E. Plotnikova[65], P. Plucinski[146a,146b], D. Pluth[64], R. Poettgen[83], L. Poggioli[117], D. Pohl[21], G. Polesello[121a], A. Policicchio[37a,37b], R. Polifka[158], A. Polini[20a], C.S. Pollard[53], V. Polychronakos[25], K. Pommès[30], L. Pontecorvo[132a], B.G. Pope[90], G.A. Popeneciu[26b], D.S. Popovic[13], A. Poppleton[30], S. Pospisil[128], K. Potamianos[15], I.N. Potrap[65], C.J. Potter[149], C.T. Potter[116], G. Poulard[30], J. Poveda[30], V. Pozdnyakov[65], P. Pralavorio[85], A. Pranko[15], S. Prasad[30], S. Prell[64], D. Price[84], L.E. Price[6], M. Primavera[73a], S. Prince[87], M. Proissl[46], K. Prokofiev[60c], F. Prokoshin[32b], E. Protopapadaki[136], S. Protopopescu[25], J. Proudfoot[6], M. Przybycien[38a], E. Ptacek[116], D. Puddu[134a,134b], E. Pueschel[86], D. Puldon[148], M. Purohit[25,ae], P. Puzo[117], J. Qian[89], G. Qin[53], Y. Qin[84], A. Quadt[54], D.R. Quarrie[15], W.B. Quayle[164a,164b], M. Queitsch-Maitland[84], D. Quilty[53], S. Raddum[119], V. Radeka[25], V. Radescu[42], S.K. Radhakrishnan[148], P. Radloff[116], P. Rados[88], F. Ragusa[91a,91b], G. Rahal[178], S. Rajagopalan[25], M. Rammensee[30], C. Rangel-Smith[166], F. Rauscher[100], S. Rave[83], T. Ravenscroft[53], M. Raymond[30], A.L. Read[119], N.P. Readioff[74], D.M. Rebuzzi[121a,121b], A. Redelbach[174], G. Redlinger[25], R. Reece[137], K. Reeves[41], L. Rehnisch[16], H. Reisin[27], M. Relich[163], C. Rembser[30], H. Ren[33a], A. Renaud[117], M. Rescigno[132a], S. Resconi[91a], O.L. Rezanova[109,c], P. Reznicek[129], R. Rezvani[95], R. Richter[101], S. Richter[78], E. Richter-Was[38b], O. Ricken[21], M. Ridel[80], P. Rieck[16], C.J. Riegel[175], J. Rieger[54], M. Rijssenbeek[148], A. Rimoldi[121a,121b], L. Rinaldi[20a], B. Ristić[49], E. Ritsch[62], I. Riu[12], F. Rizatdinova[114], E. Rizvi[76], S.H. Robertson[87,k], A. Robichaud-Veronneau[87], D. Robinson[28], J.E.M. Robinson[84], A. Robson[53], C. Roda[124a,124b], S. Roe[30], O. Røhne[119], S. Rolli[161], A. Romaniouk[98], M. Romano[20a,20b], S.M. Romano Saez[34], E. Romero Adam[167], N. Rompotis[138], M. Ronzani[48], L. Roos[80], E. Ros[167], S. Rosati[132a], K. Rosbach[48], P. Rose[137], P.L. Rosendahl[14], O. Rosenthal[141], V. Rossetti[146a,146b], E. Rossi[104a,104b], L.P. Rossi[50a], R. Rosten[138], M. Rotaru[26a], I. Roth[172], J. Rothberg[138], D. Rousseau[117], C.R. Royon[136], A. Rozanov[85], Y. Rozen[152], X. Ruan[145c], F. Rubbo[143], I. Rubinskiy[42], V.I. Rud[99], C. Rudolph[44], M.S. Rudolph[158], F. Rühr[48], A. Ruiz-Martinez[30], Z. Rurikova[48], N.A. Rusakovich[65], A. Ruschke[100], H.L. Russell[138], J.P. Rutherfoord[7], N. Ruthmann[48], Y.F. Ryabov[123], M. Rybar[129], G. Rybkin[117], N.C. Ryder[120], A.F. Saavedra[150], G. Sabato[107], S. Sacerdoti[27], A. Saddique[3], H.F-W. Sadrozinski[137], R. Sadykov[65], F. Safai Tehrani[132a], M. Saimpert[136], H. Sakamoto[155], Y. Sakurai[171], G. Salamanna[134a,134b], A. Salamon[133a], M. Saleem[113], D. Salek[107], P.H. Sales De Bruin[138], D. Salihagic[101], A. Salnikov[143], J. Salt[167], D. Salvatore[37a,37b], F. Salvatore[149], A. Salvucci[106], A. Salzburger[30], D. Sampsonidis[154], A. Sanchez[104a,104b], J. Sánchez[167], V. Sanchez Martinez[167], H. Sandaker[14], R.L. Sandbach[76], H.G. Sander[83], M.P. Sanders[100], M. Sandhoff[175], C. Sandoval[162], R. Sandstroem[101], D.P.C. Sankey[131], M. Sannino[50a,50b], A. Sansoni[47], C. Santoni[34], R. Santonico[133a,133b], H. Santos[126a], I. Santoyo Castillo[149], K. Sapp[125], A. Sapronov[65], J.G. Saraiva[126a,126d], B. Sarrazin[21], O. Sasaki[66], Y. Sasaki[155], K. Sato[160], G. Sauvage[5,*], E. Sauvan[5], G. Savage[77], P. Savard[158,d], C. Sawyer[120], L. Sawyer[79,n], J. Saxon[31], C. Sbarra[20a], A. Sbrizzi[20a,20b], T. Scanlon[78], D.A. Scannicchio[163], M. Scarcella[150], V. Scarfone[37a,37b], J. Schaarschmidt[172], P. Schacht[101], D. Schaefer[30], R. Schaefer[42], J. Schaeffer[83], S. Schaepe[21], S. Schaetzel[58b], U. Schäfer[83], A.C. Schaffer[117], D. Schaile[100], R.D. Schamberger[148], V. Scharf[58a], V.A. Schegelsky[123], D. Scheirich[129], M. Schernau[163], C. Schiavi[50a,50b], C. Schillo[48], M. Schioppa[37a,37b], S. Schlenker[30], E. Schmidt[48], K. Schmieden[30], C. Schmitt[83], S. Schmitt[58b], S. Schmitt[42], B. Schneider[159a], Y.J. Schnellbach[74], U. Schnoor[44], L. Schoeffel[136], A. Schoening[58b], B.D. Schoenrock[90], E. Schopf[21], A.L.S. Schorlemmer[54], M. Schott[83], D. Schouten[159a],

JHEP08(2015)137

J. Schovancova[8], S. Schramm[158], M. Schreyer[174], C. Schroeder[83], N. Schuh[83], M.J. Schultens[21], H.-C. Schultz-Coulon[58a], H. Schulz[16], M. Schumacher[48], B.A. Schumm[137], Ph. Schune[136], C. Schwanenberger[84], A. Schwartzman[143], T.A. Schwarz[89], Ph. Schwegler[101], Ph. Schwemling[136], R. Schwienhorst[90], J. Schwindling[136], T. Schwindt[21], M. Schwoerer[5], F.G. Sciacca[17], E. Scifo[117], G. Sciolla[23], F. Scuri[124a,124b], F. Scutti[21], J. Searcy[89], G. Sedov[42], E. Sedykh[123], P. Seema[21], S.C. Seidel[105], A. Seiden[137], F. Seifert[128], J.M. Seixas[24a], G. Sekhniaidze[104a], K. Sekhon[89], S.J. Sekula[40], K.E. Selbach[46], D.M. Seliverstov[123,*], N. Semprini-Cesari[20a,20b], C. Serfon[30], L. Serin[117], L. Serkin[164a,164b], T. Serre[85], M. Sessa[134a,134b], R. Seuster[159a], H. Severini[113], T. Sfiligoj[75], F. Sforza[101], A. Sfyrla[30], E. Shabalina[54], M. Shamim[116], L.Y. Shan[33a], R. Shang[165], J.T. Shank[22], M. Shapiro[15], P.B. Shatalov[97], K. Shaw[164a,164b], S.M. Shaw[84], A. Shcherbakova[146a,146b], C.Y. Shehu[149], P. Sherwood[78], L. Shi[151,af], S. Shimizu[67], C.O. Shimmin[163], M. Shimojima[102], M. Shiyakova[65], A. Shmeleva[96], D. Shoaleh Saadi[95], M.J. Shochet[31], S. Shojaii[91a,91b], S. Shrestha[111], E. Shulga[98], M.A. Shupe[7], S. Shushkevich[42], P. Sicho[127], O. Sidiropoulou[174], D. Sidorov[114], A. Sidoti[20a,20b], F. Siegert[44], Dj. Sijacki[13], J. Silva[126a,126d], Y. Silver[153], S.B. Silverstein[146a], V. Simak[128], O. Simard[5], Lj. Simic[13], S. Simion[117], E. Simioni[83], B. Simmons[78], D. Simon[34], R. Simoniello[91a,91b], P. Sinervo[158], N.B. Sinev[116], G. Siragusa[174], A.N. Sisakyan[65,*], S.Yu. Sivoklokov[99], J. Sjölin[146a,146b], T.B. Sjursen[14], M.B. Skinner[72], H.P. Skottowe[57], P. Skubic[113], M. Slater[18], T. Slavicek[128], M. Slawinska[107], K. Sliwa[161], V. Smakhtin[172], B.H. Smart[46], L. Smestad[14], S.Yu. Smirnov[98], Y. Smirnov[98], L.N. Smirnova[99,ag], O. Smirnova[81], M.N.K. Smith[35], M. Smizanska[72], K. Smolek[128], A.A. Snesarev[96], G. Snidero[76], S. Snyder[25], R. Sobie[169,k], F. Socher[44], A. Soffer[153], D.A. Soh[151,af], C.A. Solans[30], M. Solar[128], J. Solc[128], E.Yu. Soldatov[98], U. Soldevila[167], A.A. Solodkov[130], A. Soloshenko[65], O.V. Solovyanov[130], V. Solovyev[123], P. Sommer[48], H.Y. Song[33b], N. Soni[1], A. Sood[15], A. Sopczak[128], B. Sopko[128], V. Sopko[128], V. Sorin[12], D. Sosa[58b], M. Sosebee[8], C.L. Sotiropoulou[124a,124b], R. Soualah[164a,164c], P. Soueid[95], A.M. Soukharev[109,c], D. South[42], S. Spagnolo[73a,73b], M. Spalla[124a,124b], F. Spanò[77], W.R. Spearman[57], F. Spettel[101], R. Spighi[20a], G. Spigo[30], L.A. Spiller[88], M. Spousta[129], T. Spreitzer[158], R.D. St. Denis[53,*], S. Staerz[44], J. Stahlman[122], R. Stamen[58a], S. Stamm[16], E. Stanecka[39], C. Stanescu[134a], M. Stanescu-Bellu[42], M.M. Stanitzki[42], S. Stapnes[119], E.A. Starchenko[130], J. Stark[55], P. Staroba[127], P. Starovoitov[42], R. Staszewski[39], P. Stavina[144a,*], P. Steinberg[25], B. Stelzer[142], H.J. Stelzer[30], O. Stelzer-Chilton[159a], H. Stenzel[52], S. Stern[101], G.A. Stewart[53], J.A. Stillings[21], M.C. Stockton[87], M. Stoebe[87], G. Stoicea[26a], P. Stolte[54], S. Stonjek[101], A.R. Stradling[8], A. Straessner[44], M.E. Stramaglia[17], J. Strandberg[147], S. Strandberg[146a,146b], A. Strandlie[119], E. Strauss[143], M. Strauss[113], P. Strizenec[144b], R. Ströhmer[174], D.M. Strom[116], R. Stroynowski[40], A. Strubig[106], S.A. Stucci[17], B. Stugu[14], N.A. Styles[42], D. Su[143], J. Su[125], R. Subramaniam[79], A. Succurro[12], Y. Sugaya[118], C. Suhr[108], M. Suk[128], V.V. Sulin[96], S. Sultansoy[4d], T. Sumida[68], S. Sun[57], X. Sun[33a], J.E. Sundermann[48], K. Suruliz[149], G. Susinno[37a,37b], M.R. Sutton[149], S. Suzuki[66], Y. Suzuki[66], M. Svatos[127], S. Swedish[168], M. Swiatlowski[143], I. Sykora[144a], T. Sykora[129], D. Ta[90], C. Taccini[134a,134b], K. Tackmann[42], J. Taenzer[158], A. Taffard[163], R. Tafirout[159a], N. Taiblum[153], H. Takai[25], R. Takashima[69], H. Takeda[67], T. Takeshita[140], Y. Takubo[66], M. Talby[85], A.A. Talyshev[109,c], J.Y.C. Tam[174], K.G. Tan[88], J. Tanaka[155], R. Tanaka[117], S. Tanaka[66], B.B. Tannenwald[111], N. Tannoury[21], S. Tapprogge[83], S. Tarem[152], F. Tarrade[29], G.F. Tartarelli[91a], P. Tas[129], M. Tasevsky[127], T. Tashiro[68], E. Tassi[37a,37b], A. Tavares Delgado[126a,126b], Y. Tayalati[135d], F.E. Taylor[94], G.N. Taylor[88], W. Taylor[159b], F.A. Teischinger[30], M. Teixeira Dias Castanheira[76], P. Teixeira-Dias[77], K.K. Temming[48], H. Ten Kate[30], P.K. Teng[151], J.J. Teoh[118], F. Tepel[175], S. Terada[66], K. Terashi[155], J. Terron[82], S. Terzo[101], M. Testa[47], R.J. Teuscher[158,k], J. Therhaag[21], T. Theveneaux-Pelzer[34], J.P. Thomas[18], J. Thomas-Wilsker[77], E.N. Thompson[35],

JHEP08(2015)137

P.D. Thompson[18], R.J. Thompson[84], A.S. Thompson[53], L.A. Thomsen[176], E. Thomson[122], M. Thomson[28], R.P. Thun[89,*], M.J. Tibbetts[15], R.E. Ticse Torres[85], V.O. Tikhomirov[96,ah], Yu.A. Tikhonov[109,c], S. Timoshenko[98], E. Tiouchichine[85], P. Tipton[176], S. Tisserant[85], T. Todorov[5,*], S. Todorova-Nova[129], J. Tojo[70], S. Tokár[144a], K. Tokushuku[66], K. Tollefson[90], E. Tolley[57], L. Tomlinson[84], M. Tomoto[103], L. Tompkins[143,ai], K. Toms[105], E. Torrence[116], H. Torres[142], E. Torró Pastor[167], J. Toth[85,aj], F. Touchard[85], D.R. Tovey[139], T. Trefzger[174], L. Tremblet[30], A. Tricoli[30], I.M. Trigger[159a], S. Trincaz-Duvoid[80], M.F. Tripiana[12], W. Trischuk[158], B. Trocmé[55], C. Troncon[91a], M. Trottier-McDonald[15], M. Trovatelli[134a,134b], P. True[90], L. Truong[164a,164c], M. Trzebinski[39], A. Trzupek[39], C. Tsarouchas[30], J.C-L. Tseng[120], P.V. Tsiareshka[92], D. Tsionou[154], G. Tsipolitis[10], N. Tsirintanis[9], S. Tsiskaridze[12], V. Tsiskaridze[48], E.G. Tskhadadze[51a], I.I. Tsukerman[97], V. Tsulaia[15], S. Tsuno[66], D. Tsybychev[148], A. Tudorache[26a], V. Tudorache[26a], A.N. Tuna[122], S.A. Tupputi[20a,20b], S. Turchikhin[99,ag], D. Turecek[128], R. Turra[91a,91b], A.J. Turvey[40], P.M. Tuts[35], A. Tykhonov[49], M. Tylmad[146a,146b], M. Tyndel[131], I. Ueda[155], R. Ueno[29], M. Ughetto[146a,146b], M. Ugland[14], M. Uhlenbrock[21], F. Ukegawa[160], G. Unal[30], A. Undrus[25], G. Unel[163], F.C. Ungaro[48], Y. Unno[66], C. Unverdorben[100], J. Urban[144b], P. Urquijo[88], P. Urrejola[83], G. Usai[8], A. Usanova[62], L. Vacavant[85], V. Vacek[128], B. Vachon[87], C. Valderanis[83], N. Valencic[107], S. Valentinetti[20a,20b], A. Valero[167], L. Valery[12], S. Valkar[129], E. Valladolid Gallego[167], S. Vallecorsa[49], J.A. Valls Ferrer[167], W. Van Den Wollenberg[107], P.C. Van Der Deijl[107], R. van der Geer[107], H. van der Graaf[107], R. Van Der Leeuw[107], N. van Eldik[152], P. van Gemmeren[6], J. Van Nieuwkoop[142], I. van Vulpen[107], M.C. van Woerden[30], M. Vanadia[132a,132b], W. Vandelli[30], R. Vanguri[122], A. Vaniachine[6], F. Vannucci[80], G. Vardanyan[177], R. Vari[132a], E.W. Varnes[7], T. Varol[40], D. Varouchas[80], A. Vartapetian[8], K.E. Varvell[150], F. Vazeille[34], T. Vazquez Schroeder[87], J. Veatch[7], F. Veloso[126a,126c], T. Velz[21], S. Veneziano[132a], A. Ventura[73a,73b], D. Ventura[86], M. Venturi[169], N. Venturi[158], A. Venturini[23], V. Vercesi[121a], M. Verducci[132a,132b], W. Verkerke[107], J.C. Vermeulen[107], A. Vest[44], M.C. Vetterli[142,d], O. Viazlo[81], I. Vichou[165], T. Vickey[139], O.E. Vickey Boeriu[139], G.H.A. Viehhauser[120], S. Viel[15], R. Vigne[30], M. Villa[20a,20b], M. Villaplana Perez[91a,91b], E. Vilucchi[47], M.G. Vincter[29], V.B. Vinogradov[65], I. Vivarelli[149], F. Vives Vaque[3], S. Vlachos[10], D. Vladoiu[100], M. Vlasak[128], M. Vogel[32a], P. Vokac[128], G. Volpi[124a,124b], M. Volpi[88], H. von der Schmitt[101], H. von Radziewski[48], E. von Toerne[21], V. Vorobel[129], K. Vorobev[98], M. Vos[167], R. Voss[30], J.H. Vossebeld[74], N. Vranjes[13], M. Vranjes Milosavljevic[13], V. Vrba[127], M. Vreeswijk[107], R. Vuillermet[30], I. Vukotic[31], Z. Vykydal[128], P. Wagner[21], W. Wagner[175], H. Wahlberg[71], S. Wahrmund[44], J. Wakabayashi[103], J. Walder[72], R. Walker[100], W. Walkowiak[141], C. Wang[33c], F. Wang[173], H. Wang[15], H. Wang[40], J. Wang[42], J. Wang[33a], K. Wang[87], R. Wang[6], S.M. Wang[151], T. Wang[21], X. Wang[176], C. Wanotayaroj[116], A. Warburton[87], C.P. Ward[28], D.R. Wardrope[78], M. Warsinsky[48], A. Washbrook[46], C. Wasicki[42], P.M. Watkins[18], A.T. Watson[18], I.J. Watson[150], M.F. Watson[18], G. Watts[138], S. Watts[84], B.M. Waugh[78], S. Webb[84], M.S. Weber[17], S.W. Weber[174], J.S. Webster[31], A.R. Weidberg[120], B. Weinert[61], J. Weingarten[54], C. Weiser[48], H. Weits[107], P.S. Wells[30], T. Wenaus[25], T. Wengler[30], S. Wenig[30], N. Wermes[21], M. Werner[48], P. Werner[30], M. Wessels[58a], J. Wetter[161], K. Whalen[29], A.M. Wharton[72], A. White[8], M.J. White[1], R. White[32b], S. White[124a,124b], D. Whiteson[163], F.J. Wickens[131], W. Wiedenmann[173], M. Wielers[131], P. Wienemann[21], C. Wiglesworth[36], L.A.M. Wiik-Fuchs[21], A. Wildauer[101], H.G. Wilkens[30], H.H. Williams[122], S. Williams[107], C. Willis[90], S. Willocq[86], A. Wilson[89], J.A. Wilson[18], I. Wingerter-Seez[5], F. Winklmeier[116], B.T. Winter[21], M. Wittgen[143], J. Wittkowski[100], S.J. Wollstadt[83], M.W. Wolter[39], H. Wolters[126a,126c], B.K. Wosiek[39], J. Wotschack[30], M.J. Woudstra[84], K.W. Wozniak[39], M. Wu[55], M. Wu[31], S.L. Wu[173], X. Wu[49], Y. Wu[89], T.R. Wyatt[84], B.M. Wynne[46], S. Xella[36], D. Xu[33a],

JHEP08(2015)137

L. Xu[33b,ak], B. Yabsley[150], S. Yacoob[145b,al], R. Yakabe[67], M. Yamada[66], Y. Yamaguchi[118], A. Yamamoto[66], S. Yamamoto[155], T. Yamanaka[155], K. Yamauchi[103], Y. Yamazaki[67], Z. Yan[22], H. Yang[33e], H. Yang[173], Y. Yang[151], L. Yao[33a], W-M. Yao[15], Y. Yasu[66], E. Yatsenko[5], K.H. Yau Wong[21], J. Ye[40], S. Ye[25], I. Yeletskikh[65], A.L. Yen[57], E. Yildirim[42], K. Yorita[171], R. Yoshida[6], K. Yoshihara[122], C. Young[143], C.J.S. Young[30], S. Youssef[22], D.R. Yu[15], J. Yu[8], J.M. Yu[89], J. Yu[114], L. Yuan[67], A. Yurkewicz[108], I. Yusuff[28,am], B. Zabinski[39], R. Zaidan[63], A.M. Zaitsev[130,ab], J. Zalieckas[14], A. Zaman[148], S. Zambito[57], L. Zanello[132a,132b], D. Zanzi[88], C. Zeitnitz[175], M. Zeman[128], A. Zemla[38a], K. Zengel[23], O. Zenin[130], T. Ženiš[144a], D. Zerwas[117], D. Zhang[89], F. Zhang[173], J. Zhang[6], L. Zhang[48], R. Zhang[33b], X. Zhang[33d], Z. Zhang[117], X. Zhao[40], Y. Zhao[33d,117], Z. Zhao[33b], A. Zhemchugov[65], J. Zhong[120], B. Zhou[89], C. Zhou[45], L. Zhou[35], L. Zhou[40], N. Zhou[163], C.G. Zhu[33d], H. Zhu[33a], J. Zhu[89], Y. Zhu[33b], X. Zhuang[33a], K. Zhukov[96], A. Zibell[174], D. Zieminska[61], N.I. Zimine[65], C. Zimmermann[83], S. Zimmermann[48], Z. Zinonos[54], M. Zinser[83], M. Ziolkowski[141], L. Živković[13], G. Zobernig[173], A. Zoccoli[20a,20b], M. zur Nedden[16], G. Zurzolo[104a,104b] and L. Zwalinski[30].

[1] *Department of Physics, University of Adelaide, Adelaide, Australia*
[2] *Physics Department, SUNY Albany, Albany NY, United States of America*
[3] *Department of Physics, University of Alberta, Edmonton AB, Canada*
[4] [(a)] *Department of Physics, Ankara University, Ankara;* [(c)] *Istanbul Aydin University, Istanbul;* [(d)] *Division of Physics, TOBB University of Economics and Technology, Ankara, Turkey*
[5] *LAPP, CNRS/IN2P3 and Université Savoie Mont Blanc, Annecy-le-Vieux, France*
[6] *High Energy Physics Division, Argonne National Laboratory, Argonne IL, United States of America*
[7] *Department of Physics, University of Arizona, Tucson AZ, United States of America*
[8] *Department of Physics, The University of Texas at Arlington, Arlington TX, United States of America*
[9] *Physics Department, University of Athens, Athens, Greece*
[10] *Physics Department, National Technical University of Athens, Zografou, Greece*
[11] *Institute of Physics, Azerbaijan Academy of Sciences, Baku, Azerbaijan*
[12] *Institut de Física d'Altes Energies and Departament de Física de la Universitat Autònoma de Barcelona, Barcelona, Spain*
[13] *Institute of Physics, University of Belgrade, Belgrade, Serbia*
[14] *Department for Physics and Technology, University of Bergen, Bergen, Norway*
[15] *Physics Division, Lawrence Berkeley National Laboratory and University of California, Berkeley CA, United States of America*
[16] *Department of Physics, Humboldt University, Berlin, Germany*
[17] *Albert Einstein Center for Fundamental Physics and Laboratory for High Energy Physics, University of Bern, Bern, Switzerland*
[18] *School of Physics and Astronomy, University of Birmingham, Birmingham, United Kingdom*
[19] [(a)] *Department of Physics, Bogazici University, Istanbul;* [(b)] *Department of Physics, Dogus University, Istanbul;* [(c)] *Department of Physics Engineering, Gaziantep University, Gaziantep, Turkey*
[20] [(a)] *INFN Sezione di Bologna;* [(b)] *Dipartimento di Fisica e Astronomia, Università di Bologna, Bologna, Italy*
[21] *Physikalisches Institut, University of Bonn, Bonn, Germany*
[22] *Department of Physics, Boston University, Boston MA, United States of America*
[23] *Department of Physics, Brandeis University, Waltham MA, United States of America*
[24] [(a)] *Universidade Federal do Rio De Janeiro COPPE/EE/IF, Rio de Janeiro;* [(b)] *Electrical Circuits Department, Federal University of Juiz de Fora (UFJF), Juiz de Fora;* [(c)] *Federal University of Sao Joao del Rei (UFSJ), Sao Joao del Rei;* [(d)] *Instituto de Fisica, Universidade de Sao Paulo, Sao Paulo, Brazil*
[25] *Physics Department, Brookhaven National Laboratory, Upton NY, United States of America*

JHEP08(2015)137

[26] [(a)] National Institute of Physics and Nuclear Engineering, Bucharest; [(b)] National Institute for Research and Development of Isotopic and Molecular Technologies, Physics Department, Cluj Napoca; [(c)] University Politehnica Bucharest, Bucharest; [(d)] West University in Timisoara, Timisoara, Romania
[27] Departamento de Física, Universidad de Buenos Aires, Buenos Aires, Argentina
[28] Cavendish Laboratory, University of Cambridge, Cambridge, United Kingdom
[29] Department of Physics, Carleton University, Ottawa ON, Canada
[30] CERN, Geneva, Switzerland
[31] Enrico Fermi Institute, University of Chicago, Chicago IL, United States of America
[32] [(a)] Departamento de Física, Pontificia Universidad Católica de Chile, Santiago; [(b)] Departamento de Física, Universidad Técnica Federico Santa María, Valparaíso, Chile
[33] [(a)] Institute of High Energy Physics, Chinese Academy of Sciences, Beijing; [(b)] Department of Modern Physics, University of Science and Technology of China, Anhui; [(c)] Department of Physics, Nanjing University, Jiangsu; [(d)] School of Physics, Shandong University, Shandong; [(e)] Department of Physics and Astronomy, Shanghai Key Laboratory for Particle Physics and Cosmology, Shanghai Jiao Tong University, Shanghai; [(f)] Physics Department, Tsinghua University, Beijing 100084, China
[34] Laboratoire de Physique Corpusculaire, Clermont Université and Université Blaise Pascal and CNRS/IN2P3, Clermont-Ferrand, France
[35] Nevis Laboratory, Columbia University, Irvington NY, United States of America
[36] Niels Bohr Institute, University of Copenhagen, Kobenhavn, Denmark
[37] [(a)] INFN Gruppo Collegato di Cosenza, Laboratori Nazionali di Frascati; [(b)] Dipartimento di Fisica, Università della Calabria, Rende, Italy
[38] [(a)] AGH University of Science and Technology, Faculty of Physics and Applied Computer Science, Krakow; [(b)] Marian Smoluchowski Institute of Physics, Jagiellonian University, Krakow, Poland
[39] Institute of Nuclear Physics Polish Academy of Sciences, Krakow, Poland
[40] Physics Department, Southern Methodist University, Dallas TX, United States of America
[41] Physics Department, University of Texas at Dallas, Richardson TX, United States of America
[42] DESY, Hamburg and Zeuthen, Germany
[43] Institut für Experimentelle Physik IV, Technische Universität Dortmund, Dortmund, Germany
[44] Institut für Kern- und Teilchenphysik, Technische Universität Dresden, Dresden, Germany
[45] Department of Physics, Duke University, Durham NC, United States of America
[46] SUPA - School of Physics and Astronomy, University of Edinburgh, Edinburgh, United Kingdom
[47] INFN Laboratori Nazionali di Frascati, Frascati, Italy
[48] Fakultät für Mathematik und Physik, Albert-Ludwigs-Universität, Freiburg, Germany
[49] Section de Physique, Université de Genève, Geneva, Switzerland
[50] [(a)] INFN Sezione di Genova; [(b)] Dipartimento di Fisica, Università di Genova, Genova, Italy
[51] [(a)] E. Andronikashvili Institute of Physics, Iv. Javakhishvili Tbilisi State University, Tbilisi; [(b)] High Energy Physics Institute, Tbilisi State University, Tbilisi, Georgia
[52] II Physikalisches Institut, Justus-Liebig-Universität Giessen, Giessen, Germany
[53] SUPA - School of Physics and Astronomy, University of Glasgow, Glasgow, United Kingdom
[54] II Physikalisches Institut, Georg-August-Universität, Göttingen, Germany
[55] Laboratoire de Physique Subatomique et de Cosmologie, Université Grenoble-Alpes, CNRS/IN2P3, Grenoble, France
[56] Department of Physics, Hampton University, Hampton VA, United States of America
[57] Laboratory for Particle Physics and Cosmology, Harvard University, Cambridge MA, United States of America
[58] [(a)] Kirchhoff-Institut für Physik, Ruprecht-Karls-Universität Heidelberg, Heidelberg; [(b)] Physikalisches Institut, Ruprecht-Karls-Universität Heidelberg, Heidelberg; [(c)] ZITI Institut für technische Informatik, Ruprecht-Karls-Universität Heidelberg, Mannheim, Germany
[59] Faculty of Applied Information Science, Hiroshima Institute of Technology, Hiroshima, Japan
[60] [(a)] Department of Physics, The Chinese University of Hong Kong, Shatin, N.T., Hong Kong; [(b)]

JHEP08(2015)137

Department of Physics, The University of Hong Kong, Hong Kong; [(c)] *Department of Physics, The Hong Kong University of Science and Technology, Clear Water Bay, Kowloon, Hong Kong, China*
[61] *Department of Physics, Indiana University, Bloomington IN, United States of America*
[62] *Institut für Astro- und Teilchenphysik, Leopold-Franzens-Universität, Innsbruck, Austria*
[63] *University of Iowa, Iowa City IA, United States of America*
[64] *Department of Physics and Astronomy, Iowa State University, Ames IA, United States of America*
[65] *Joint Institute for Nuclear Research, JINR Dubna, Dubna, Russia*
[66] *KEK, High Energy Accelerator Research Organization, Tsukuba, Japan*
[67] *Graduate School of Science, Kobe University, Kobe, Japan*
[68] *Faculty of Science, Kyoto University, Kyoto, Japan*
[69] *Kyoto University of Education, Kyoto, Japan*
[70] *Department of Physics, Kyushu University, Fukuoka, Japan*
[71] *Instituto de Física La Plata, Universidad Nacional de La Plata and CONICET, La Plata, Argentina*
[72] *Physics Department, Lancaster University, Lancaster, United Kingdom*
[73] [(a)] *INFN Sezione di Lecce;* [(b)] *Dipartimento di Matematica e Fisica, Università del Salento, Lecce, Italy*
[74] *Oliver Lodge Laboratory, University of Liverpool, Liverpool, United Kingdom*
[75] *Department of Physics, Jožef Stefan Institute and University of Ljubljana, Ljubljana, Slovenia*
[76] *School of Physics and Astronomy, Queen Mary University of London, London, United Kingdom*
[77] *Department of Physics, Royal Holloway University of London, Surrey, United Kingdom*
[78] *Department of Physics and Astronomy, University College London, London, United Kingdom*
[79] *Louisiana Tech University, Ruston LA, United States of America*
[80] *Laboratoire de Physique Nucléaire et de Hautes Energies, UPMC and Université Paris-Diderot and CNRS/IN2P3, Paris, France*
[81] *Fysiska institutionen, Lunds universitet, Lund, Sweden*
[82] *Departamento de Fisica Teorica C-15, Universidad Autonoma de Madrid, Madrid, Spain*
[83] *Institut für Physik, Universität Mainz, Mainz, Germany*
[84] *School of Physics and Astronomy, University of Manchester, Manchester, United Kingdom*
[85] *CPPM, Aix-Marseille Université and CNRS/IN2P3, Marseille, France*
[86] *Department of Physics, University of Massachusetts, Amherst MA, United States of America*
[87] *Department of Physics, McGill University, Montreal QC, Canada*
[88] *School of Physics, University of Melbourne, Victoria, Australia*
[89] *Department of Physics, The University of Michigan, Ann Arbor MI, United States of America*
[90] *Department of Physics and Astronomy, Michigan State University, East Lansing MI, United States of America*
[91] [(a)] *INFN Sezione di Milano;* [(b)] *Dipartimento di Fisica, Università di Milano, Milano, Italy*
[92] *B.I. Stepanov Institute of Physics, National Academy of Sciences of Belarus, Minsk, Republic of Belarus*
[93] *National Scientific and Educational Centre for Particle and High Energy Physics, Minsk, Republic of Belarus*
[94] *Department of Physics, Massachusetts Institute of Technology, Cambridge MA, United States of America*
[95] *Group of Particle Physics, University of Montreal, Montreal QC, Canada*
[96] *P.N. Lebedev Institute of Physics, Academy of Sciences, Moscow, Russia*
[97] *Institute for Theoretical and Experimental Physics (ITEP), Moscow, Russia*
[98] *National Research Nuclear University MEPhI, Moscow, Russia*
[99] *D.V. Skobeltsyn Institute of Nuclear Physics, M.V. Lomonosov Moscow State University, Moscow, Russia*
[100] *Fakultät für Physik, Ludwig-Maximilians-Universität München, München, Germany*
[101] *Max-Planck-Institut für Physik (Werner-Heisenberg-Institut), München, Germany*
[102] *Nagasaki Institute of Applied Science, Nagasaki, Japan*
[103] *Graduate School of Science and Kobayashi-Maskawa Institute, Nagoya University, Nagoya, Japan*

JHEP08(2015)137

[104] [(a)] INFN Sezione di Napoli; [(b)] Dipartimento di Fisica, Università di Napoli, Napoli, Italy
[105] Department of Physics and Astronomy, University of New Mexico, Albuquerque NM, United States of America
[106] Institute for Mathematics, Astrophysics and Particle Physics, Radboud University Nijmegen/Nikhef, Nijmegen, Netherlands
[107] Nikhef National Institute for Subatomic Physics and University of Amsterdam, Amsterdam, Netherlands
[108] Department of Physics, Northern Illinois University, DeKalb IL, United States of America
[109] Budker Institute of Nuclear Physics, SB RAS, Novosibirsk, Russia
[110] Department of Physics, New York University, New York NY, United States of America
[111] Ohio State University, Columbus OH, United States of America
[112] Faculty of Science, Okayama University, Okayama, Japan
[113] Homer L. Dodge Department of Physics and Astronomy, University of Oklahoma, Norman OK, United States of America
[114] Department of Physics, Oklahoma State University, Stillwater OK, United States of America
[115] Palacký University, RCPTM, Olomouc, Czech Republic
[116] Center for High Energy Physics, University of Oregon, Eugene OR, United States of America
[117] LAL, Université Paris-Sud and CNRS/IN2P3, Orsay, France
[118] Graduate School of Science, Osaka University, Osaka, Japan
[119] Department of Physics, University of Oslo, Oslo, Norway
[120] Department of Physics, Oxford University, Oxford, United Kingdom
[121] [(a)] INFN Sezione di Pavia; [(b)] Dipartimento di Fisica, Università di Pavia, Pavia, Italy
[122] Department of Physics, University of Pennsylvania, Philadelphia PA, United States of America
[123] National Research Centre "Kurchatov Institute" B.P.Konstantinov Petersburg Nuclear Physics Institute, St. Petersburg, Russia
[124] [(a)] INFN Sezione di Pisa; [(b)] Dipartimento di Fisica E. Fermi, Università di Pisa, Pisa, Italy
[125] Department of Physics and Astronomy, University of Pittsburgh, Pittsburgh PA, United States of America
[126] [(a)] Laboratorio de Instrumentacao e Fisica Experimental de Particulas - LIP, Lisboa; [(b)] Faculdade de Ciências, Universidade de Lisboa, Lisboa; [(c)] Department of Physics, University of Coimbra, Coimbra; [(d)] Centro de Física Nuclear da Universidade de Lisboa, Lisboa; [(e)] Departamento de Fisica, Universidade do Minho, Braga; [(f)] Departamento de Fisica Teorica y del Cosmos and CAFPE, Universidad de Granada, Granada (Spain); [(g)] Dep Fisica and CEFITEC of Faculdade de Ciencias e Tecnologia, Universidade Nova de Lisboa, Caparica, Portugal
[127] Institute of Physics, Academy of Sciences of the Czech Republic, Praha, Czech Republic
[128] Czech Technical University in Prague, Praha, Czech Republic
[129] Faculty of Mathematics and Physics, Charles University in Prague, Praha, Czech Republic
[130] State Research Center Institute for High Energy Physics, Protvino, Russia
[131] Particle Physics Department, Rutherford Appleton Laboratory, Didcot, United Kingdom
[132] [(a)] INFN Sezione di Roma; [(b)] Dipartimento di Fisica, Sapienza Università di Roma, Roma, Italy
[133] [(a)] INFN Sezione di Roma Tor Vergata; [(b)] Dipartimento di Fisica, Università di Roma Tor Vergata, Roma, Italy
[134] [(a)] INFN Sezione di Roma Tre; [(b)] Dipartimento di Matematica e Fisica, Università Roma Tre, Roma, Italy
[135] [(a)] Faculté des Sciences Ain Chock, Réseau Universitaire de Physique des Hautes Energies - Université Hassan II, Casablanca; [(b)] Centre National de l'Energie des Sciences Techniques Nucleaires, Rabat; [(c)] Faculté des Sciences Semlalia, Université Cadi Ayyad, LPHEA-Marrakech; [(d)] Faculté des Sciences, Université Mohamed Premier and LPTPM, Oujda; [(e)] Faculté des sciences, Université Mohammed V-Agdal, Rabat, Morocco
[136] DSM/IRFU (Institut de Recherches sur les Lois Fondamentales de l'Univers), CEA Saclay (Commissariat à l'Energie Atomique et aux Energies Alternatives), Gif-sur-Yvette, France
[137] Santa Cruz Institute for Particle Physics, University of California Santa Cruz, Santa Cruz CA,

JHEP08(2015)137

United States of America
[138] *Department of Physics, University of Washington, Seattle WA, United States of America*
[139] *Department of Physics and Astronomy, University of Sheffield, Sheffield, United Kingdom*
[140] *Department of Physics, Shinshu University, Nagano, Japan*
[141] *Fachbereich Physik, Universität Siegen, Siegen, Germany*
[142] *Department of Physics, Simon Fraser University, Burnaby BC, Canada*
[143] *SLAC National Accelerator Laboratory, Stanford CA, United States of America*
[144] [(a)] *Faculty of Mathematics, Physics & Informatics, Comenius University, Bratislava;* [(b)] *Department of Subnuclear Physics, Institute of Experimental Physics of the Slovak Academy of Sciences, Kosice, Slovak Republic*
[145] [(a)] *Department of Physics, University of Cape Town, Cape Town;* [(b)] *Department of Physics, University of Johannesburg, Johannesburg;* [(c)] *School of Physics, University of the Witwatersrand, Johannesburg, South Africa*
[146] [(a)] *Department of Physics, Stockholm University;* [(b)] *The Oskar Klein Centre, Stockholm, Sweden*
[147] *Physics Department, Royal Institute of Technology, Stockholm, Sweden*
[148] *Departments of Physics & Astronomy and Chemistry, Stony Brook University, Stony Brook NY, United States of America*
[149] *Department of Physics and Astronomy, University of Sussex, Brighton, United Kingdom*
[150] *School of Physics, University of Sydney, Sydney, Australia*
[151] *Institute of Physics, Academia Sinica, Taipei, Taiwan*
[152] *Department of Physics, Technion: Israel Institute of Technology, Haifa, Israel*
[153] *Raymond and Beverly Sackler School of Physics and Astronomy, Tel Aviv University, Tel Aviv, Israel*
[154] *Department of Physics, Aristotle University of Thessaloniki, Thessaloniki, Greece*
[155] *International Center for Elementary Particle Physics and Department of Physics, The University of Tokyo, Tokyo, Japan*
[156] *Graduate School of Science and Technology, Tokyo Metropolitan University, Tokyo, Japan*
[157] *Department of Physics, Tokyo Institute of Technology, Tokyo, Japan*
[158] *Department of Physics, University of Toronto, Toronto ON, Canada*
[159] [(a)] *TRIUMF, Vancouver BC;* [(b)] *Department of Physics and Astronomy, York University, Toronto ON, Canada*
[160] *Faculty of Pure and Applied Sciences, University of Tsukuba, Tsukuba, Japan*
[161] *Department of Physics and Astronomy, Tufts University, Medford MA, United States of America*
[162] *Centro de Investigaciones, Universidad Antonio Narino, Bogota, Colombia*
[163] *Department of Physics and Astronomy, University of California Irvine, Irvine CA, United States of America*
[164] [(a)] *INFN Gruppo Collegato di Udine, Sezione di Trieste, Udine;* [(b)] *ICTP, Trieste;* [(c)] *Dipartimento di Chimica, Fisica e Ambiente, Università di Udine, Udine, Italy*
[165] *Department of Physics, University of Illinois, Urbana IL, United States of America*
[166] *Department of Physics and Astronomy, University of Uppsala, Uppsala, Sweden*
[167] *Instituto de Física Corpuscular (IFIC) and Departamento de Física Atómica, Molecular y Nuclear and Departamento de Ingeniería Electrónica and Instituto de Microelectrónica de Barcelona (IMB-CNM), University of Valencia and CSIC, Valencia, Spain*
[168] *Department of Physics, University of British Columbia, Vancouver BC, Canada*
[169] *Department of Physics and Astronomy, University of Victoria, Victoria BC, Canada*
[170] *Department of Physics, University of Warwick, Coventry, United Kingdom*
[171] *Waseda University, Tokyo, Japan*
[172] *Department of Particle Physics, The Weizmann Institute of Science, Rehovot, Israel*
[173] *Department of Physics, University of Wisconsin, Madison WI, United States of America*
[174] *Fakultät für Physik und Astronomie, Julius-Maximilians-Universität, Würzburg, Germany*
[175] *Fachbereich C Physik, Bergische Universität Wuppertal, Wuppertal, Germany*
[176] *Department of Physics, Yale University, New Haven CT, United States of America*

JHEP08(2015)137

[177] *Yerevan Physics Institute, Yerevan, Armenia*
[178] *Centre de Calcul de l'Institut National de Physique Nucléaire et de Physique des Particules (IN2P3), Villeurbanne, France*

[a] *Also at Department of Physics, King's College London, London, United Kingdom*
[b] *Also at Institute of Physics, Azerbaijan Academy of Sciences, Baku, Azerbaijan*
[c] *Also at Novosibirsk State University, Novosibirsk, Russia*
[d] *Also at TRIUMF, Vancouver BC, Canada*
[e] *Also at Department of Physics, California State University, Fresno CA, United States of America*
[f] *Also at Department of Physics, University of Fribourg, Fribourg, Switzerland*
[g] *Also at Departamento de Fisica e Astronomia, Faculdade de Ciencias, Universidade do Porto, Portugal*
[h] *Also at Tomsk State University, Tomsk, Russia*
[i] *Also at CPPM, Aix-Marseille Université and CNRS/IN2P3, Marseille, France*
[j] *Also at Universita di Napoli Parthenope, Napoli, Italy*
[k] *Also at Institute of Particle Physics (IPP), Canada*
[l] *Also at Particle Physics Department, Rutherford Appleton Laboratory, Didcot, United Kingdom*
[m] *Also at Department of Physics, St. Petersburg State Polytechnical University, St. Petersburg, Russia*
[n] *Also at Louisiana Tech University, Ruston LA, United States of America*
[o] *Also at Institucio Catalana de Recerca i Estudis Avancats, ICREA, Barcelona, Spain*
[p] *Also at Department of Physics, National Tsing Hua University, Taiwan*
[q] *Also at Department of Physics, The University of Texas at Austin, Austin TX, United States of America*
[r] *Also at Institute of Theoretical Physics, Ilia State University, Tbilisi, Georgia*
[s] *Also at CERN, Geneva, Switzerland*
[t] *Also at Georgian Technical University (GTU),Tbilisi, Georgia*
[u] *Also at Ochadai Academic Production, Ochanomizu University, Tokyo, Japan*
[v] *Also at Manhattan College, New York NY, United States of America*
[w] *Also at Hellenic Open University, Patras, Greece*
[x] *Also at Institute of Physics, Academia Sinica, Taipei, Taiwan*
[y] *Also at LAL, Université Paris-Sud and CNRS/IN2P3, Orsay, France*
[z] *Also at Academia Sinica Grid Computing, Institute of Physics, Academia Sinica, Taipei, Taiwan*
[aa] *Also at School of Physics, Shandong University, Shandong, China*
[ab] *Also at Moscow Institute of Physics and Technology State University, Dolgoprudny, Russia*
[ac] *Also at section de Physique, Université de Genève, Geneva, Switzerland*
[ad] *Also at International School for Advanced Studies (SISSA), Trieste, Italy*
[ae] *Also at Department of Physics and Astronomy, University of South Carolina, Columbia SC, United States of America*
[af] *Also at School of Physics and Engineering, Sun Yat-sen University, Guangzhou, China*
[ag] *Also at Faculty of Physics, M.V.Lomonosov Moscow State University, Moscow, Russia*
[ah] *Also at National Research Nuclear University MEPhI, Moscow, Russia*
[ai] *Also at Department of Physics, Stanford University, Stanford CA, United States of America*
[aj] *Also at Institute for Particle and Nuclear Physics, Wigner Research Centre for Physics, Budapest, Hungary*
[ak] *Also at Department of Physics, The University of Michigan, Ann Arbor MI, United States of America*
[al] *Also at Discipline of Physics, University of KwaZulu-Natal, Durban, South Africa*
[am] *Also at University of Malaya, Department of Physics, Kuala Lumpur, Malaysia*
[*] *Deceased*

JHEP08(2015)137